PHOTOGRAPH THIS SHEET

DTIC FILE COPY

AD-A227 036

DTIC ACCESSION NUMBER

LEVEL

1

INVENTORY

AFOSR-TR 90 1022

DOCUMENT IDENTIFICATION

3 APR 1986

DISTRIBUTION STATEMENT A

Approved for public release;
Distribution Unlimited

DISTRIBUTION STATEMENT

ACCESSION FOR

NTIS GRA&I

DTIC TRAC

UNANNOUNCED

JUSTIFICATION

BY

DISTRIBUTION/

AVAILABILITY CODES

DISTRIBUTION	AVAILABILITY AND/OR SPECIAL	
A-1		

DISTRIBUTION STAMP

DTIC
ELECTE
SEP 21 1990
S E D

DATE ACCESSIONED

DTIC COPY INSPECTED

DATE RETURNED

2

DATE RECEIVED IN DTIC

REGISTERED OR CERTIFIED NUMBER

PHOTOGRAPH THIS SHEET AND RETURN TO DTIC-FDAC

DTIC FORM 70A APR 87

DOCUMENT PROCESSING SHEET

PREVIOUS EDITIONS MAY BE USED UNTIL STOCK IS EXHAUSTED

1 Sep 85 to 31 MAY 86

MERGED BEAM STUDIES OF THE DISSOCIATIVE RECOMBINATION OF H_3^+ IONS WITH LOW INTERNAL ENERGY.

by

JBA MITCHELL.

PHYSICS

The University of Western Ontario

UNCLASSIFIED

SECURITY CLASSIFICATION OF THIS PAGE

REPORT DOCUMENTATION PAGE

1a. REPORT SECURITY CLASSIFICATION Unclassified	1b. RESTRICTIVE MARKINGS
2a. SECURITY CLASSIFICATION AUTHORITY	3. DISTRIBUTION/AVAILABILITY OF REPORT Approved for public release, distribution unlimited
2b. DECLASSIFICATION/DOWNGRADING SCHEDULE	
4. PERFORMING ORGANIZATION REPORT NUMBER(S)	5. MONITORING ORGANIZATION REPORT NUMBER(S) AFOSR-TR- 00 1022
6a. NAME OF PERFORMING ORGANIZATION University of Western Ontario 6b. OFFICE SYMBOL (If applicable)	7a. NAME OF MONITORING ORGANIZATION AFOSR
6c. ADDRESS (City, State and ZIP Code) University of Western Ontario Department of Physics London, Ontario, Canada, N6A 3K7	7b. ADDRESS (City, State and ZIP Code) Building 410 Bolling AFB, D.C. 20332-6448
8a. NAME OF FUNDING/SPONSORING ORGANIZATION AFOSR 8b. OFFICE SYMBOL (If applicable) NP	9. PROCUREMENT INSTRUMENT IDENTIFICATION NUMBER AFOSR-85-0279
8c. ADDRESS (City, State and ZIP Code) Building 410 Bolling AFB, D.C. 20332-6448	10. SOURCE OF FUNDING NOS. PROGRAM ELEMENT NO. 61102F; PROJECT NO. 2301; TASK NO. A7; WORK UNIT NO.
11. TITLE (Include Security Classification) "MERGED BEAM STUDIES OF THE DISSOCIATIVE RECOMBINATION OF H+3 IONS WITH LOW INTERNAL ENERGY"	
PERSONAL AUTHOR(S) J.B.A. Mitchell	
13a. TYPE OF REPORT FINAL 13b. TIME COVERED FROM 85/09/01 TO 86/05/31	14. DATE OF REPORT (Yr., Mo., Day) 30 Apr 86 15. PAGE COUNT
16. SUPPLEMENTARY NOTATION	
17. COSATI CODES FIELD / GROUP / SUB. GR.	18. SUBJECT TERMS (Continue on reverse if necessary and identify by block number)

19. ABSTRACT (Continue on reverse if necessary and identify by block number)

Dissociative recombination and excitation measurements have been performed for H+3 ions formed under a variety of Source pressures and gas mixtures. At low pressures, an r.f. trap ion source results are lower than previous measurements from a conventional source by a factor of eight. Similar reasurements are made for H+3 formed in an rf trap source using a he-ium hydrogen mixture. Ions used for there measurements had an internal energy of lev.

20. DISTRIBUTION/AVAILABILITY OF ABSTRACT CLASSIFIED/UNLIMITED ☒ SAME AS RPT. ☒ DTIC USERS ☐	21. ABSTRACT SECURITY CLASSIFICATION UNCLASSIFIED
22a. NAME OF RESPONSIBLE INDIVIDUAL BRUCE L. SMITH	22b TELEPHONE NUMBER (Include Area Code) 202/767-4906 22c OFFICE SYMBOL NP

DD FORM 1473, 83 APR EDITION OF 1 JAN 73 IS OBSOLETE.

Unclassified

SECURITY CLASSIFICATION OF THIS PAGE

MERGED BEAM STUDIES OF THE DISSOCIATIVE RECOMBINATION OF H_3^+ IONS WITH LOW INTERNAL ENERGY

J.B.A. MITCHELL

PRINCIPAL INVESTIGATOR

DEPARTMENT OF PHYSICS

THE UNIVERSITY OF WESTERN ONTARIO

LONDON, ONTARIO, CANADA. N6A 3K7

SCIENTIFIC REPORT

ON

AFOSR GRANT NUMBER

AFOSR-85-0279

30 APRIL 1986

PRINCIPAL INVESTIGATOR:	J.B.A. MITCHELL
GRADUATE STUDENTS:	H. HUS
	J. MILLER
	C. NOREN
TECHNICIAN:	P. PERQUIN

INTRODUCTION

The development of negative hydrogen ion sources for neutral beam production has been an area of very active research over the last few years. Two main approaches to the problem have been pursued involving cesium catalyzed H^- production on one hand and volume production on the other. The latter approach is much favoured for routine H^- production as it obviates the difficulties involved in handling cesium in the source. The physics of volume production of H^- is not really well understood however. Currently it is believed that the primary process leading to H^- production is the dissociative attachment of electrons to vibrationally excited hydrogen molecules i.e.

$$e + H_2\ (v) \rightarrow (H_2^-)^{**} \rightarrow H^- + H \qquad --$$

The rate coefficient for this process is several orders of magnitude greater than for attachment to vibrationally cold H_2 molecules.

The problem is to explain the presence of vibrationally excited H_2 in the source plasma. Hiskes[1] has suggested that electronic excitation of H_2 by fast electrons followed by a transition to a lower, vibrationally excited state might be the major pumping process. Multistage ion sources designed to exploit the high energy and low energy electron components needed for the vibrational pumping and attachment processes have been constructed and tested. One of the problems with this mechanism

is that theoretical modelling predicts that H^- ions should account for 1-2% of the total plasma ions whilst actual measurements show that H^- ions account for more than 10% of the total ion content[1]. The reasons for this discrepancy may be due to a lack of understanding of the electron energy distribution in the source plasma. At the pressures at which H^- ion sources generally operate, (2-5 x 10^{-2} Torr) H_3^+ is the dominant ion. In addition H_3^+ is formed with several eV of internal energy. It must be expected, therefore, to play an important role in the ion chemistry of the source. Unfortunately, there is a serious lack of detailed experimental information concerning the atomic processes involving H_3^+ and so its role is not well understood.

The dissociative recombination of H_3^+ namely: -

$$e + H_3^+ \rightarrow H_3^{**} \rightarrow H + H + H \quad \text{-- I}$$

$$\rightarrow H_2(v) + H \quad \text{-- II}$$

has been implicated[2] as a possible source of vibrationally excited H_2 molecules. Measurements of the branching ratio[3] for this reaction, made in this laboratory, indicated that channel I dominated over channel II by a factor of 2:1. These measurements were made using H_3^+ ions, 60% of which were vibrationally excited. These findings qualitatively agree with theoretical studies of Kulander[4] which implied that ground state H_3^+ ions could not recombine via channel II, although ions with more than 1eV of internal energy could.

In the last two years some very significant results concerning H_3^+ recombination have been published. Theoretical studies by Michels and Hobbs[5] have indicated that H_3^+ recombination should have a very small probability for ground state ions. This finding was quickly followed by experimental work by Smith and co-workers[6,7] who found that indeed the rate coefficient for H_3^+ recombination measured in a Flowing Afterglow Langmuir Probe (FALP) apparatus was very small ($\alpha < 10^{-11} cm^3 sec^{-1}$, Smith, Private Communication 1986).

Previous measurements of H_3^+ recombination involving a variety of techniques indicated that the recombination rate coefficient was large ($2.3 \times 10^{-7} cm^3 s^{-1}$ at 300°K). Some of these measurements certainly involved excited ions, although Biondi's afterglow and Peart and Dolder's inclined beam experiments were believed to involve ground state vibrationally cold ions. Smith et al have suggested that perhaps the conditions present in Biondi's afterglow allowed H_3^+ ions to have a significant population within the plasma which would artificially raise the measured recombination rate. Clearly there is a need for an unequivocal remeasurement of this process using mass identified ions with measured internal energies.

If indeed ground state H_3^+ does not recombine then this implies that the recombination coefficient for vibrationally excited ions is larger than previously believed. These levels give rise to dissociation via channel II and hence would produce more vibrationally excited H_2 molecules.

EXPERIMENT AND METHOD

Over the past ten years dissociative recombination cross sections for more than thirty molecular species have been measured in this laboratory using the Merged Electron Ion Beam Experiment (MEIBE). In this apparatus, a beam of 400 KeV ions, produced in a Van de Graaff accelerator is merged with a beam of electrons having velocities close to the ion velocity. since both beams intersect at zero degrees and travel in the samc direction, their relative velocities can be made very small. This means that atomic collisions can be studied at very low energies (<10 meV) in the centre of mass energy frame. A major advantage of the technique is that the neutral particles formed as a result of electron ion recombination are moving at high velocities in the laboratory frame and so they can be detected using nuclear detectors such as the surface barrier detector. A detailed description of the merged beam technique is given in Appendix A.

Up until now all the measurements made with the MEIBE apparatus have used ions prepared in a conventional radio-frequency ion source which is standard equipment on a Van de Graaff accelerator. It has been calculated however, that this source is not capable of producing hydrogen molecular ions with low vibrational states[8]. The reason for this is that the residence time for ions in the source is too short to allow sufficient numbers of de-exciting collisions to occur.

An alternative source, based upon a design by Teloy in West Germany[9], has been constructed in our laboratory. This source uses an inhomogeneous radiofrequency field to trap ions, formed by electron impact, for several milliseconds before extraction. A schematic diagram of the source is shown in Fig. 1. Collision Induced Dissociation studies have been performed using ions from this source and these have shown that the source is capable of producing H_2^+ ions with $v \leq 1$ only and H_3^+ ions with less than 0.5eV of internal energy. These measurements are discussed further in Appendix B. In the past few months this source has been mounted in the terminal of the 400 KeV Van de Graaff accelerator used for the MEIBE experiments. It has been found to operate well for several weeks without requiring filament changes and ion currents up to 1×10^{-9} A have been obtained in the MEIBE apparatus. This is the current that has been used in all previous measurements. Two main measurements are being made using this source. These are dissociative recombination studies of H_3^+, namely: -

$$e + H_3^+ \rightarrow H + H + H \quad \text{---} \quad 1a$$

$$\rightarrow H_2 + H \quad \text{---} \quad 1b$$

and Dissociative Excitation Studies: -

$$e + H_3^+ \rightarrow H + H_2^+ + e \quad \text{---} \quad 2a$$

$$\rightarrow (H + H) + H^+ + e \quad \text{---} \quad 2b$$

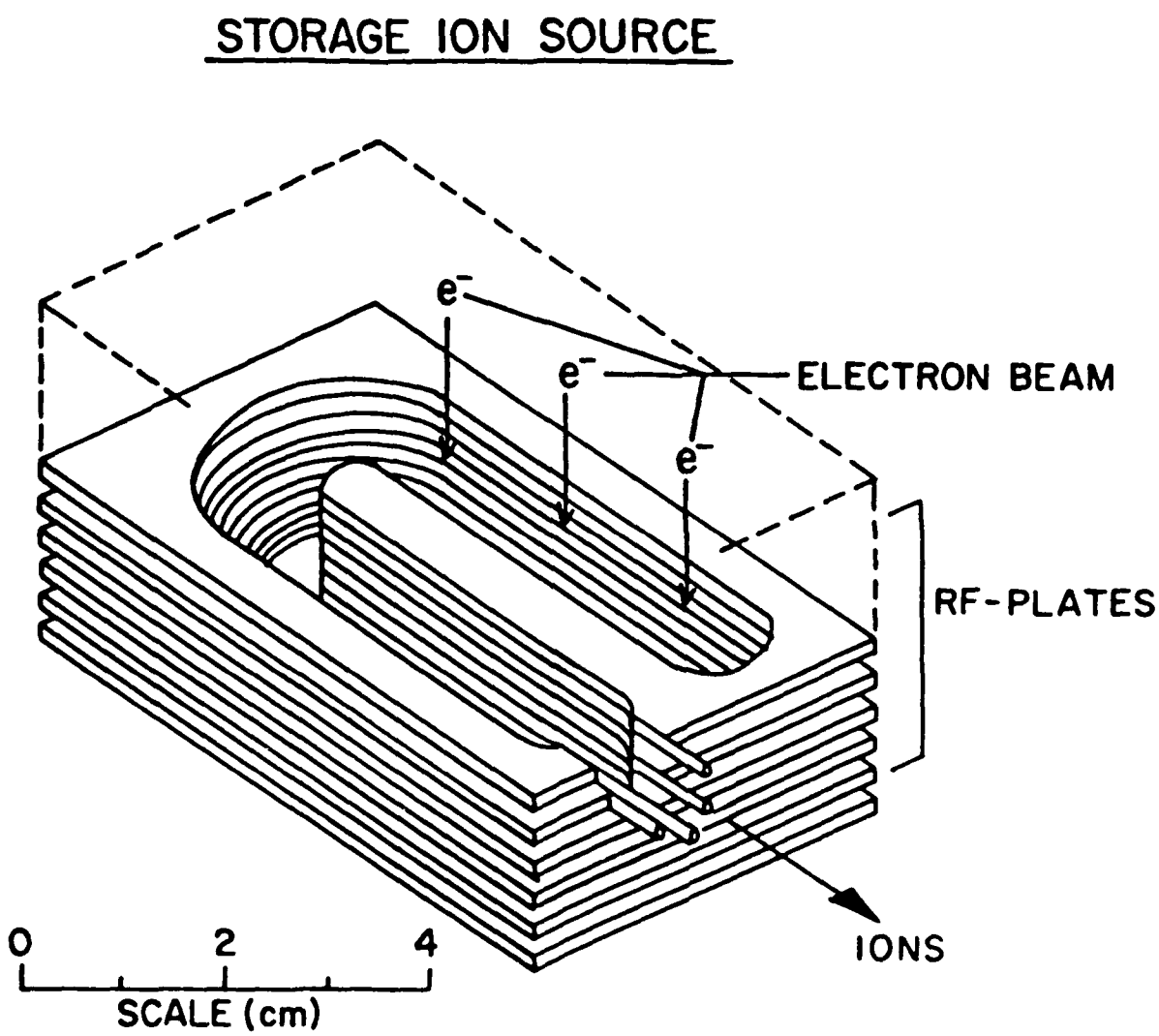

Fig.1. Schematic illustration of the radiofrequency trap ion source used in the present study.

At the present time total cross sections for reaction 1 are being measured. At a later date partial cross sections for reactions 1a and 1b will be examined using a technique already successfully exploited in this laboratory. See Appendix C.

Reaction 2 is important since it proceeds via an electronic transition from the ground electronic state of the ion to a repulsive upper state. See Fig. 2. For H_3^+ ions in the ground state $^1A_1'$, v=0, the energy required to reach the lowest repulsive state, namely the $^3E'$ state is calculated to be 14.76eV. This process therefore exhibits an energy threshold. Vibrationally excited H_3^+ ions will exhibit thresholds at lower energies. Thus a measurement of the threshold for reaction 2 will give an indication of the internal energy of the ions. (It should be noted that reactions 2a and 2b occur via different dissociation pathways for the same excited states and so they have the same energy thresholds. This is discussed in more detail in Appendix D)

Reactions 2a and 2b and 1 can be distinguished since they give rise to neutral products carrying, 1/3, 2/3 and the total primary beam energy respectively. The products are detected using a surface barrier detector which is energy sensitive. The pulse height distribution for the neutral products of H_3^+ collisions is shown in Fig. 3. (The peaks also contain contributions due to collisions with the residual gas in the interaction region. This background noise is removed however by electron beam modulation techniques, see Appendix A). The use of single

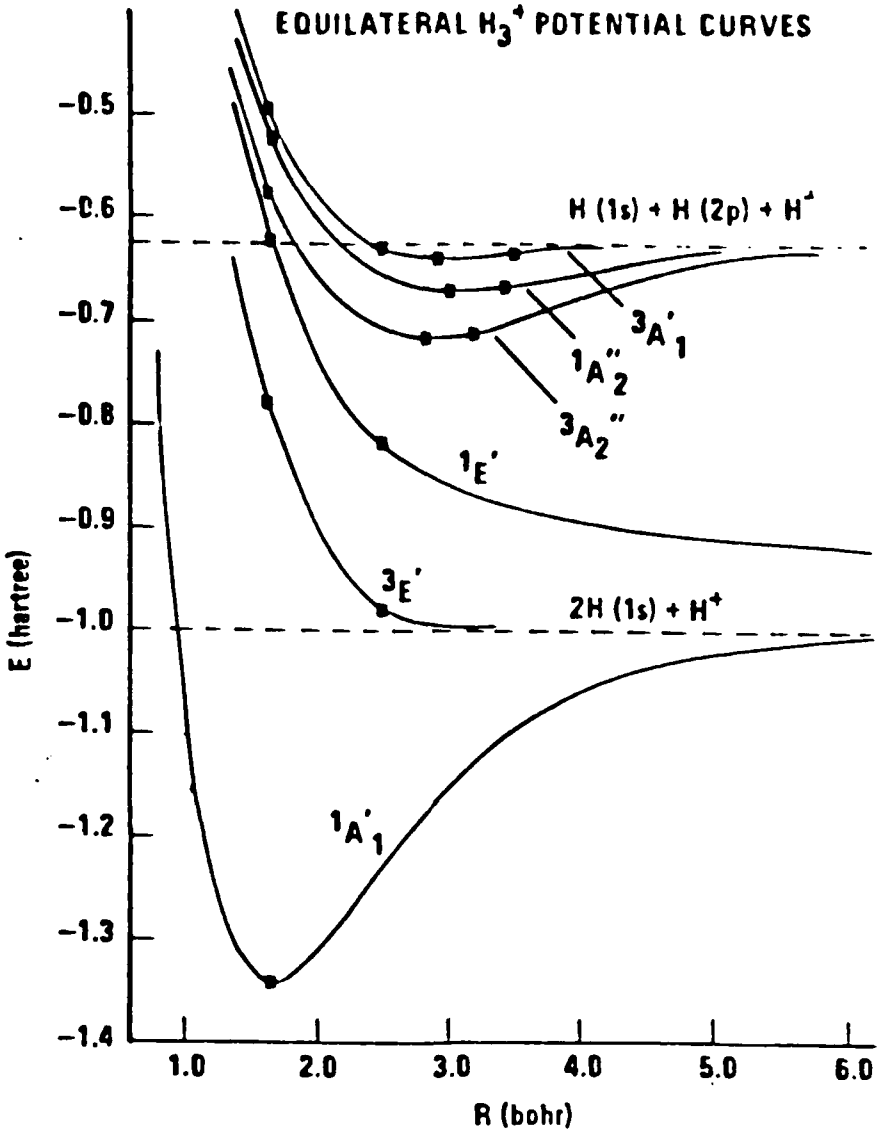

Fig.2. Potential energy curves for the ground and excited states of H_3^+ in D_{3h} symmetry. (Kawaoka,K. and Borkman,R.F. JCP 54,4234, 1971).

channel analysers allows pulses falling within a specified voltage range to be selected independantly so that reactions 2a, 2b and 1 can be measured separately.

RESULTS and DISCUSSIONS

Dissociative recombination and excitation measurements have been performed for H_3^+ ions formed under a variety of source pressures and gas mixtures. This series of measurements is not yet complete and so it is too early to make a definitive statement regarding the measured dissociative recombination cross section for completely relaxed ions. A discussion of measurements currently in progress and planned for the future will be given later.

Fig. 4 shows dissociative recombination cross sections for H_3^+ ions prepared in the trap source using pure hydrogen at low and moderate pressures.[1].

Also included are results taken previously using a conventional radiofrequency ion source.[10] (Mitchell et al, 1983).[2].

---

1. Operating pressures cannot be measured directly during the measurement since the ion source is electrically isolated in the terminal of the Van de Graaff accelerator. Instead the beamline pressure at the ground potential side of the accelerating column is used for monitoring relative source pressures.
2. These results are a factor of two lower than previously reported. This is due to an error in the form factor calculation which was subsequently detected.

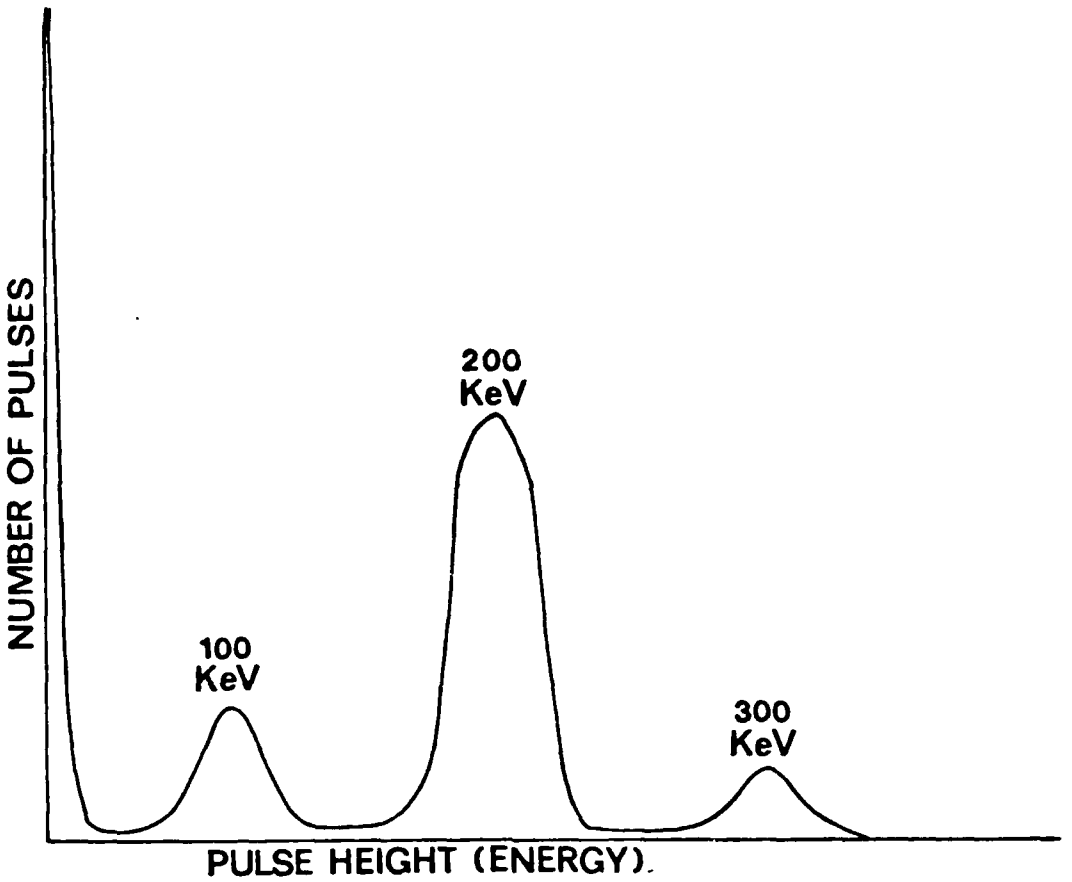

Fig.3. Pulse height spectrum for the products of 300kev H_3^+ collisions incident on a surface barrier detector.

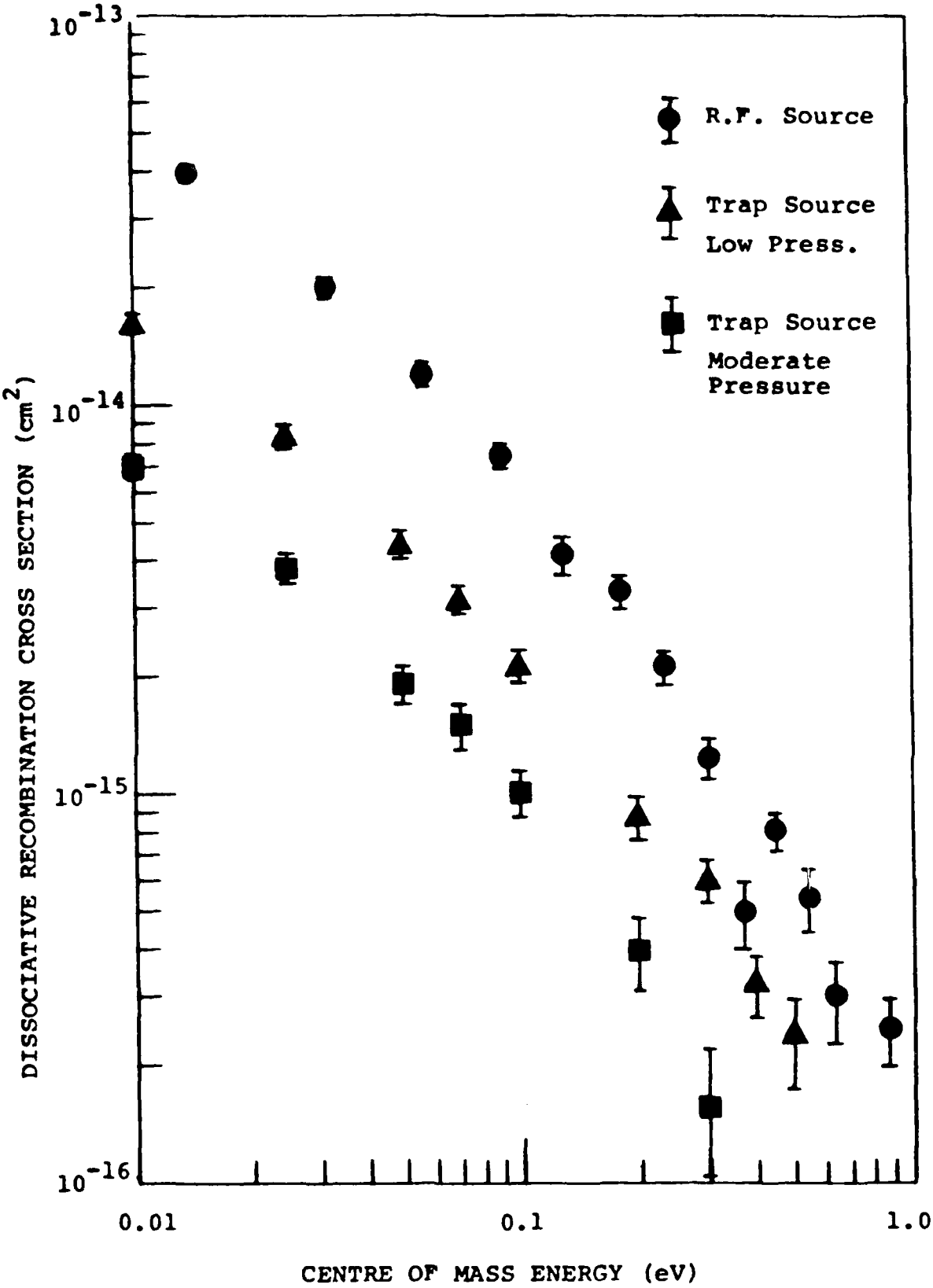

Fig. 4. Dissociative Recombination Cross Sections for H_3^+ ions formed in a conventional R.F. ion source and in the Trap source under different pressure conditions. Pure Hydrogen was used as the source gas.

It can be seen that even at low pressures, the r.f. trap ion source results are lower than previous measurements by a factor of eight. . The shape of the cross section curves is similar although it appears that at higher energies the curves converge.

In Fig. 5 similar measurements are presented for H_3^+ ions formed in the r.f. trap ion source using a helium hydrogen mixture at different pressures. As discussed in Appendix B, helium and neon buffer gases have been used in the ion source to quench higher vibrational states of H_2^+ ions. Since these ions are involved in the formation of H_3^+ ions it is possible that a lower mean vibrational state of H_2^+ may lead to H_3^+ ions being formed with less internal energy.

Collision induced dissociation studies, (Appendix B) which showed that the r.f. trap source could produce H_3^+ ions with internal energy, less than 0.5 eV, used a 5:1 Neon Hydrogen mixture as the source gas.

It is clear from a comparison of Figs. 4 and 5 that the presence of helium in the source does not alter the measured cross sections, at least at the concentrations used. More will be said on this subject later.

The internal energy of the H_3^+ used in this study can be examined directly by measuring the dissociative excitation reactions already discussed. (see Appendix D).

Because of increased background noise in the H and 2H channels (Fig. 3), these measurements take much more time to perform than the recombination measurements. Preliminary cross

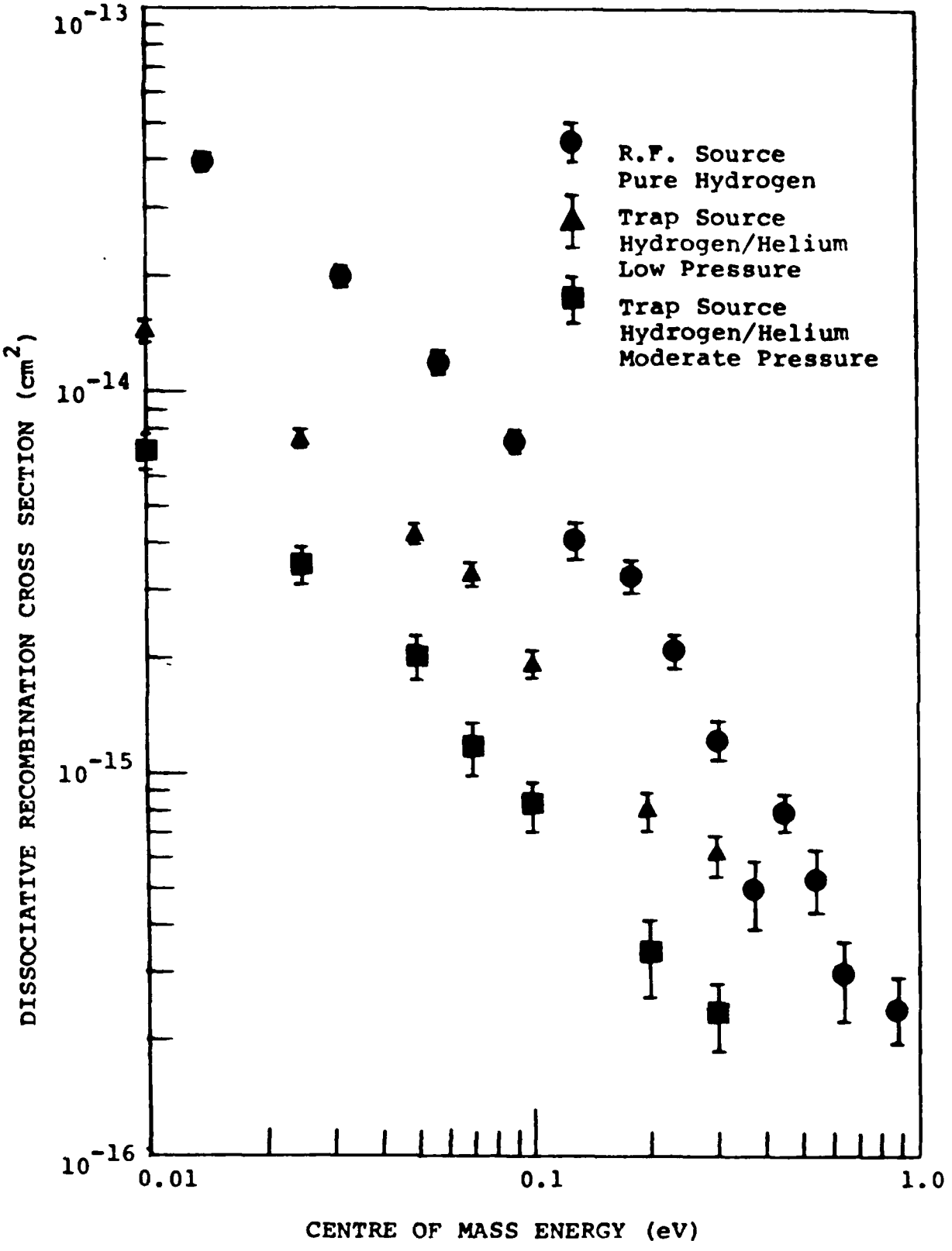

Fig.5. Dissociative Recombination Cross Sections for H_3^+ ions formed in a conventional R.F. source using pure Hydrogen and in a trap source using a 3:1 Hydrogen/Helium mixture.

section results for reaction 2a are shown in Fig. 6. A 3:1 Hydrogen Helium mixture was used with the source operating at the same moderate pressure as in Fig. 5.

It can be seen that the threshold for this reaction appears at an energy of ~ 13.5 eV. The predicted energy of this threshold is 14.76 eV for ground state H_3^+ ions. This would indicate that some of the ions used in this particular measurement have an internal energy of the order of 1 eV. The peak that appears at 15 eV is due to the excitation transition ($^1A_1' \rightarrow {}^3E'$). See Fig. 2. Because of the spin change this transition is optically forbidden but can occur via electron exchange. This process is only important close to threshold and so the peak is quite narrow. At 19.00 eV the ($^1A_1' \dashrightarrow {}^1E'$) transition can occur and this is allowed optically. This transition will exhibit a broad maximum as seen by Peart and Dolder (1974, 1975).

FUTURE STUDIES

The results presented here indicate that the enhanced collisional relaxation obtained with the trap ion source leads to H_3^+ recombination cross sections smaller than obtained previously in our aparatus using a conventional r.f. source. We have not however yet reached a point where all the H_3^+ ions can be said to be relaxed. Efforts are continuing to lower the internal energy of the H_3^+ ions even further. As mentioned earlier, a 5:1 Neon/ Hydrogen mixture used in the ion source will produce ions with

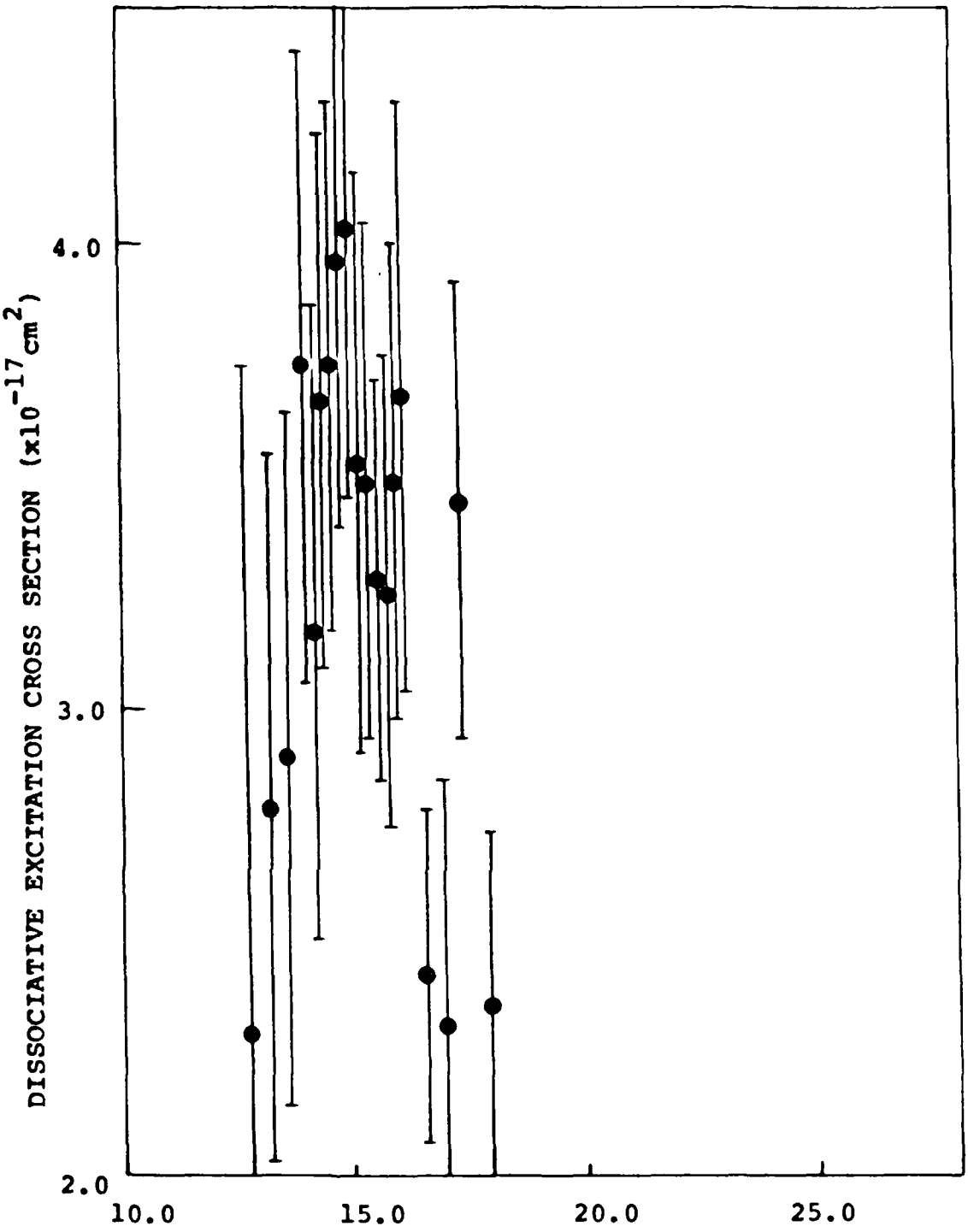

Fig.6.Dissociative Excitation Cross Sections for H_3^+ ions formed in the trap ion source using a 3:1 Hydrogen/Helium mixture at moderate pressure.

less than 0.5 eV internal energy. Such a mixture will be used in future measurements. Currently gas is fed into the ion source mounted in the terminal of the Van de Graaff accelerator via a glass gas line which runs from the high voltage terminal down to ground. It has been found that when neon is admitted to this line, high voltage breakdown occurs through the gas leading to unsatisfactory accelerator operation.

For the Neon/Hydrogen operations, an isolated gas bottle will have to be placed in the terminal of the Van de Graaff accelerator. This is a routine change but requires the opening of the accelerator tank and therefore has been delayed until the current measurements are complete.

Higher pressure operation will also be studied in order to lower the internal energy of the ions.

Measurement of the total cross section is not a particularly sensitive test of recombination mechanisms. Much more information can be gained by examining the branching ratio for the competing dissociation pathways. Furthermore this information is of great importance to H^- production as mentioned in the introduction.

Preliminary measurements have already been performed in this laboratory in which the individual cross sections for reactions 1a and 1b were determined. See Appendix C. These measurements will be repeated using relaxed ions. Kulander and Guest [4] have predicted that for low internal energies, reaction 1b cannot proceed. An experimental test of this will be most illuminating.

It will also be very interesting to see how the branching ratio varies for the isotopics variants H_2D^+, HD_2^+ and D_3^+.

These measurements are scheduled to begin in the Fall of this year.

REFERENCES

1. Hiskes, J.R. and A.M. Karo, Proceedings of 3rd Int'l Symposium on the Production and Neutralization of Negative Ions and Beams. (Ed. K. Prelec), AIP Conf. Proc. No. 111, p. 3, (1984).

2. Crandall, D.H. and F.W. Meyer, Proceedings of 2nd Int'l Symposium on the Production and Neutralization of Negative Ions and Beams, BNL Report 51304, p. 1, (1980).

3. Mitchell, J.B.A., J.L. Forand, C.T. Ng, D.P. Levac, R.E. Mitchell, P.M. Mul, W. Claeys, A. Sen and J. Wm. McGowan Phys. Rev. Lett. 51, 885, (1983).

4. Kulander, C. and M.F. Gues, J. Phys. B. 12, L501, (1979).

5. Michels, H.H. and R.H. Hobbs, App. J. 286, L27, (1984).

6. Adams, N.G., D. Smith, and E. Alge, J. Chem. Phys. 81, 1778, (1984).

7. Smith, D. and N.G. Adams, App. J. 284, L13, (1984).

8. Sen, A., Ph.D. Thesis, The University of Western Ontario, (1985).

9. Teloy, E. and D. Gerlich, Chem. Phys. 4,417, (1974).

10. Mitchell, J.B.A., Ng, C.T., Forand, L., Janssen, R. and McGowan, J.Wm., J.Phys. B 17, L909, 1984

11. Peart, B. and Dolder, K.T., J.Phys. B. 7, 1567, 1974

12. Peart, B. and Dolder, K.T., J.Phys. B. 8, L143, 1975.

APPENDIX A.

J Phys B Atom Molec Phys, Vol 10, No 18, 1977 Printed in Great Britain © 1977

Merged electron–ion beam experiments I. Method and measurements of ($e–H_2^+$) and ($e–H_3^+$) dissociative-recombination cross sections†

D Auerbach‡, R Cacak§, R Caudano||, T D Gaily, C J Keyser, J Wm McGowan¶, J B A Mitchell and S F J Wilk•

Department of Physics • and Centre for Chemical Physics, The University of Western Ontario, London, Ontario, Canada N6A 3K7

Received 17 May 1977, in final form 20 July 1977

Abstract. A merged-beam experiment designed to study collisions between electrons and molecular ions at very low energies and with high energy resolution is described. The theory behind the technique is reviewed and a comparison is made with other intersecting-beam techniques. Cross sections for dissociative recombination of H_3^+ and H_2^+ with electrons have been measured through the energy range 0·01–4 eV with an estimated energy resolution of approximately 0·04 eV. The structure found in both curves reflects the formation of Rydberg states of the molecules which in some cases choose to decay through the autoionisation and pair-production channels.

1. Introduction

Because of the importance of dissociative electron–ion recombination in atmospheric and fusion plasmas, gaseous lasers, and more generally in radiation and chemical processes, extensive experimental and theoretical attention has continuously been focused upon this problem. In our laboratory we have now developed a merged electron–ion beam experiment MEIBE, (pronounced Maybe and so christened because of the extensive problems we have encountered along the way). This experimental approach makes it possible for us to measure recombination cross sections with high accuracy, to determine the mechanisms of recombination and to examine the spectroscopy of the Rydberg states which apparently play an important role in the process.

Although we have already published two notes (Caudano *et al* 1975, McGowan *et al* 1976) which clearly demonstrate the potential of the method, it is in this series of papers that we will discuss in detail the method, and apply it to numerous studies. In this report, I of the series, we will focus upon the method and apply it to absolute measurements of cross sections for ($e–H_2^+$) and ($e–H_3^+$). In II, we analyse the recombination spectra and discuss the basic mechanisms of recombination in the light of what is now proposed theoretically.

In order to put the present study in perspective we briefly summarise what is now known of electron–ion recombination with particular attention to the hydrogen-ion systems. Since Bates and Massey (1947) and Bates (1950a, b) demonstrated that large two-body rates could be explained by the dissociative process,

$$AB^+ + e \rightarrow A + B$$

many laboratory measurements of rate constants $\alpha = \int \sigma(\varepsilon)\, d\varepsilon$ derived from the time history of the decay of a plasma have been reported. For most systems, which include atmospheric and all inert diatomics (except He_2^+), rates between 10^{-6} and 10^{-7} $cm^3 s^{-1}$ at 300 K have been found (Bardsley and Biondi 1971). ($e–He_2^+$) recombination remains the one exception where the diatomic recombination rate is known to be orders of magnitude less, (10^{-10} $cm^3 s^{-1}$ at room temperature) supposedly because no repulsive potential curves pass in the vicinity of the He_2^+ ground-state potential function. Although rates for ($e–H_3^+$) and ($e–H_2^+$) have been measured by the afterglow technique (Leu *et al* 1973) that for ($e–H_2^+$) has not, because of the difficulty one has in producing an H_2^+-dominated plasma. In experiments by Cunningham and Hobson (1969) not only was the temperature of the electron controlled in (e, Ar_2^+) and (e, Ne_2^+) studies but through the use of the gas-driven shock tube they were able to control the internal vibrational energy as well, thus making it possible to establish the importance of internal energy in the recombination process.

It is only within the last few years that cross section rather than reaction-rate measurements have been possible. Crossed-beam experiments on $e–D_3^+$ recombination leading to D(1s) + D(2p) and D(1s) + D(n = 4) dissociation products have been reported by Vogler and Dunn (1975) and Phaneuf *et al* (1975) respectively. Peart and Dolder (1973, 1974a, c) used an inclined-beam configuration (θ = 10°) to measure the total recombination cross sections for D_2^+ (all v), H_2^+ (all v) and H_3^+ (believed to be in the v = 0 state).

The use of the PF ion trap to store ions while an electron beam is superimposed upon the principal axis of the oscillating ions in the trap permitted Walls and Dunn (1974) to study the cross sections for recombination of electrons with O_2^+, H_3O^+, NH_4^+, N_2H^+, HCO^+ (Heppner *et al* 1976) and NO^+ (Walls and Dunn 1974). The resolution in this experiment was such that the effect of electronic excitation could be seen. When high-energy ions and electron beams with nearly equal velocity were carefully merged with θ near zero, Caudano *et al* (1975) and McGowan *et al* (1976), using the MEIBE apparatus described in this paper, were able to identify considerable structure in the $e–H_3^+$ and $e–H_2^+$ cross sections which could be correlated with Rydberg states of the H_3 and H_2 molecules. Furthermore, in the MEIBE experiments it was demonstrated that by the control of the relative populations of the ion vibrational levels in the ion source, a marked change in the structure within the cross section curve could be detected. With such control one eventually hopes to be able to unfold the cross section for each vibrational level of the H_3^+ ion and to identify the channel into which the recombining ion goes both as a function of centre-of-mass electron energy and ion internal energy.

† Supported by the National Research Council of Canada.
‡ Department of Chemistry, Johns Hopkins University, Baltimore, Md, USA.
§ Medical School, University of Colorado, Denver, Colorado, USA.
|| Centre for Chemical Physics Visiting Fellow on leave from Laboratoire de Spectroscopie Electronique, ESCA Facultes Universitaires, Namur, Belgium.
¶ Visiting Professor 1976–77, Laboratoire de Spectroscopie Electronique, Facultes Universitaires, Namur, Belgium.
• Department of Physics, University of Manitoba, Winnipeg, Manitoba, Canada.
• All correspondence to J Wm McGowan at this address.

Let us now look at some salient points associated with the theory. It is convenient to refer to recombination as either occurring through a direct or an indirect process. The community recognises the 'direct' process as one in which an electron and ion recombine to form a doubly excited state of the neutral molecule which may either autoionise or if the process is faster or of comparable speed dissociate giving either neutral products or a positive–negative ion pair. It is this channel which following Bates (1950a, b) has been thought to be responsible for the large measured rate constants.

The paper on (e–H_3^+) recombination by Bottcher (1976) represents the most recent application of scattering theory to describe direct recombination. He suggests that recombination proceeds primarily through the lowest doubly excited $^1\Sigma_g^+$ $1\sigma_u^2$ resonance state which is repulsive

$$H_2^+(v, J) + e \rightarrow H_2^{**}(^1\Sigma_g 1\sigma_u^2) \rightarrow H(1s) + H(nl)$$

rather than 'indirectly' through the sometimes autoionising Rydberg states H_2^R such that

$$H_2^+(v, J) + e \rightarrow H_2^R \rightarrow H_2^{**} \rightarrow H(1s) + H(nl).$$

As will become clear during the discussion of our results the 'indirect' process is in active competition with the 'direct' process, and in many ways dominates the detailed structure found. In the 'indirect' process the initial capture of the electron is caused by the transfer of energy either to electronic or nuclear motion (vibration or rotation) leading to an excited Rydberg state of the molecule. The resonance formalism describing this process is essentially that developed for excitation in electron–molecule systems leading to resonance excitation, dissociative attachment, associative detachment, associative ionization and so on (see Bardsley 1968, Nielsen and Berry 1971, Fano 1975). Electronic excitation of the molecular ion core is not usually considered as competitive although it is an open channel and is known to dominate in electron–atomic-ion recombination, often referred to as dielectronic recombination because the incoming electron excites the core while falling into an excited state of this new system. The excitation of nuclear motion of the recombining ion is most likely to be the dominant channel in the molecular analogue.

In this and the following paper, the detailed photoionisation studies carried out and reviewed by Dehmer and Chupka (1976) and the series of theoretical papers by Berry and Nielsen (1970a, b, Nielsen and Berry 1971) are extensively referred to. Although preliminary studies by Peatman (1976) of the energy spectrum of electrons emitted through photoionisation and those of electron impact ionisation (Weingartshofer *et al* 1975) where the importance of the triplet autoionising (and dissociating) states was stressed, will be of help to us as we identify the channels competing with the dissociative channel. Virtually nothing is available to help us with our (H_3^+–e) studies.

The importance of reducing the angle of intersection of recombining electron–ion beams to nearly zero was discussed at length by Peart and Dolder (1974a). At small angles, one can obtain, as we have, very high energy resolution in the centre-of-mass frame. Although the most successful, ours is not the first attempt to develop a merged electron–ion beam apparatus. Some success was attained by Hagen (1967) as he attempted to measure the (e–N_2^+) recombination cross section. Subsequently, Theard (1969) made preliminary measurements of (e–molecular-ion) cross sections and Mahadevan (1972) measured cross sections for the ionisation of positive ions.

In the sections which follow we discuss the kinematics of the merged-beam experiment, the details of our experimental technique, its limitations and its application to the cross section measurement for the recombination of (e–H_2^+) and (e–H_3^+).

2. Kinematics of the merged-beam experiment

Although described previously with reference to ion–ion merged beams by Neynaber (1969) and by Peart and Dolder (1974a) for the inclined electron–ion beam technique it is instructive to review the kinematics of the merged electron–ion beam experiment since it is illustrative of the extreme power of the method.

Let us consider the case of the interaction of a mono-energetic ion beam with velocity $\bar{v}_i$ with a mono-energetic electron beam with velocity $\bar{v}_e$ at an angle θ. The relative or centre-of-mass velocity of the two beams is given by

$$v_{cm} = |\bar{v}_i - \bar{v}_e| = (v_i^2 + v_e^2 - 2v_i v_e \cos\theta)^{1/2}. \tag{1}$$

In our experiments the ion velocity is kept fixed while the electron velocity is varied. Figure 1(*a*) shows a plot of v_{cm}/v_i as a function of v_e/v_i for the cases of $\theta = 0$ (merged beam), $\theta = \pi/2$ (crossed beam), for $\theta = \pi/18$ (the inclined beam of Peart and Dolder), $\pi/4$ and π (the opposed beam). It can be seen that in the merged beam case v_{cm} is symmetrical about $v_e/v_i = 1$ and for perfectly mono-energetic beams, zero relative velocity can be achieved. Thus for the inclined-beam case the minimum relative velocity occurs at $v_e/v_i < 1$ and is determined by the intersection angle. In the crossed-beam case, however, for $v_e \gg v_i$, v_{cm} tends towards v_e while for $v_e < v_i$, the relative velocity tends towards that of the ion which represents its lower limit.

Let us now consider the interaction energy in the centre-of-mass frame of reference. This is given by:

$$E_{cm} = \tfrac{1}{2}\mu(\bar{v}_i - \bar{v}_e)^2 = \mu[E_e/m_i + E_e/m_e - 2(E_i E_e/m_i m_e)^{1/2}\cos\theta] \tag{2}$$

where m_e, m_i and μ are the electron, ion and reduced masses respectively. Note that for the case of electron–ion collisions

$$\mu = m_e m_i/(m_e + m_i) \simeq m_e.$$

Equation (2) can be rewritten in terms of the energy of the ion reduced to that of the electron, i.e.

$$E_* = (m_e/m_i)E_i \tag{3}$$

such that

$$E_{cm} = E_* + E_e - 2(E_* E_e)^{1/2}\cos\theta. \tag{4}$$

In order to facilitate easy comparison with other studies and because in all of our experiments the ion energy E_i (i.e. E_*) is kept constant, it is therefore sensible for us to plot E_{cm} and E_e as dimensionless quantities normalised with respect to E_*. Such a plot is shown in figure 2 for $\theta = 0$ (MEIBE) and 10° (inclined-beams experiment).

For $\theta = 0$ we see immediately that when $E_e/E_* = 1$ the energy in the centre-of-mass frame goes to zero. Also for $E_{cm} < E_*$, there are two values of E_e corresponding to a given value of E_{cm}. However, the energy relation, unlike that for the velocity, is not symmetrical about $E_e/E_* = 1$.

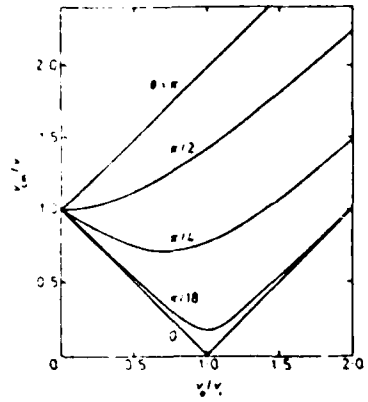

Figure 1. Variation of the normalised collision velocity v_{cm}/v_e with normalised electron velocity v_e/v_i for various values of the beam intersection angle.

Looking ahead to the actual merged-beam experiment, it is clear that as we scan the electron energy on either side of $E_e = E_+$, any real structure in the cross section curve on one side must appear asymmetrically on the other. (The slight asymmetry results from the fact that we have recorded our data as a function of E_e rather than as a function of v_e.) This is demonstrated in figure 3 where we plot the total number of signal counts against E_e for e–H_3^+ recombination. This data will be discussed in greater detail later. In figure 2 we also plot the case of $\theta = \pi/18 = 10°$, i.e. corresponding to the inclined-beam approach of Peart and Dolder. The curve here is similar in shape to that for $\theta = 0$ but does not reach zero centre-of-mass energy.

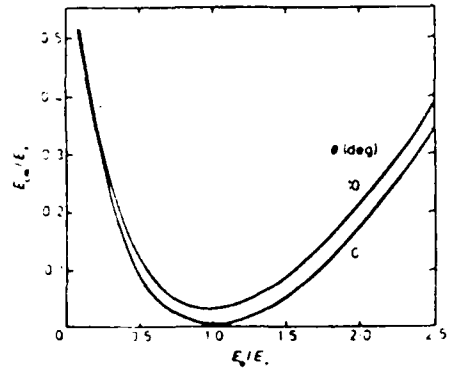

Figure 2. Variation of the centre-of-mass collision energy normalised to the electron-equivalent ion energy E_+ with the electron energy normalised to E_+ for $\theta = 0$ and 10°. Only for the merged-beam case is zero centre-of-mass energy accessible.

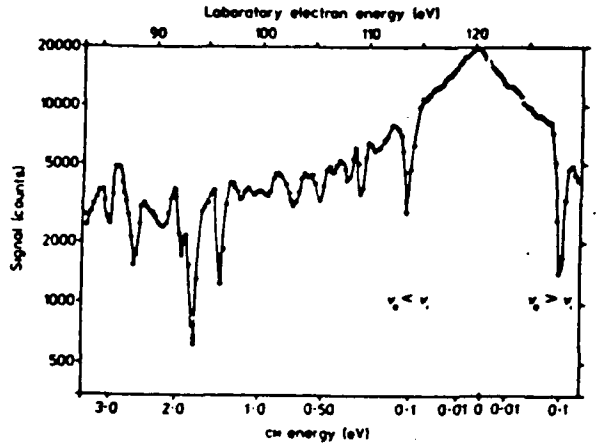

Figure 3. Plot of count rate against electron energy for the measurement of dissociative recombination in e–H_3^+ ($v = 0, 1, 2$) collisions. Also shown is the respective centre-of-mass energy scale.

In electron–ion beam experiments, it is important to examine the energy resolution in the centre-of-mass frame, ΔE_{cm} as a function of the energy spread of the electrons ΔE_e, the ions ΔE_i (in laboratory coordinates) and the uncertainty in the interaction angle $\Delta\theta$. Taking the partial derivative of equation (2), with respect to E_e, E_i and θ, one can obtain a first-order expression for ΔE_{cm}

$$\Delta E_{cm}/E_+ = |1 - (E_+/E_e)^{1/2}|\Delta E_e/E_+ + |(1 - (E_e/E_+)^{1/2}|\Delta E_i/E_i + 2(E_e/E_+)^{1/2}\theta\Delta\theta \quad (5)$$

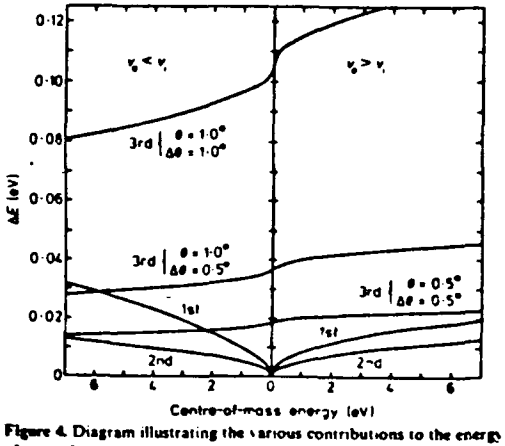

Figure 4. Diagram illustrating the various contributions to the energy spread in the centre-of-mass frame due to the spreads in the electron energy ΔE_e (first term), the ion energy ΔE_i (second term) and the angle of intersection ($\theta\Delta\theta$ (third term). In the above example, for the case of e–H_3^+ collisions, $E_+ = 443$ keV, $\Delta E_e = \pm 200$ eV, $\Delta E_i = \pm 0.1$ eV and θ and $\Delta\theta$ are as shown.

where θ was assumed small. For most of our discussion $\theta\Delta\theta$ is taken as $\Delta\theta^2$. A more extensive study of this term appears in §5.

One sees from equation (5) that when $E_e \simeq E_i$ the resolution of the electrons and the ions in the laboratory frame are substantially deamplified when transferred to the centre-of-mass frame. The main limit to the resolution comes from the uncertainty $\Delta\theta$ at a non-zero intersection angle θ.

In order to illustrate this figure 4 shows an estimate of the relative contributions to the energy spread in the centre-of-mass, ΔE_{cm}, as a function of centre-of-mass energy E_{cm} for ΔE_e, ΔE_i and $\theta\Delta\theta$. This is, for the case of e-H_2^+ recombination, the raw data which is shown in figure 3. In our experiments $\Delta E_e \simeq 0{\cdot}1$ eV, $\Delta E_i \simeq \pm 200$ eV and because $\theta\Delta\theta$ is the dominant term a variety of values are included. It can be seen that although the contributions due to the energy spreads of the ion and electron beams do increase with energy, they are greatly overshadowed by even quite small values of $\theta\Delta\theta$. This dramatically indicates the need for careful collimation and alignment of the two beams. In our experiment, slight inhomogeneities in the magnetic field in the interaction region cause some defocusing of the electron beam and thus ultimately lead to the lower limit of E_{cm} and ΔE_{cm} which we can attain.

3. Derivation of the cross section from experimental measurements

Considering again the case where two mono-energetic beams are completely superimposed, we shall assume that the ion beam with fixed velocity v_i acts as a target bombarded by an electron beam whose velocity v_e is variable. For the present we shall also assume that $v_e > v_i$. If we consider a small rectangular element of the ion beam (taken in the plane perpendicular to the direction of motion) width dx and height dy, then the target density of the ions is given by

$$\rho(x, y) = i_i(x, y)\,dx dy/(ev_i\,dx dy) \tag{6}$$

where $i_i(x, y)\,dx dy/e$ is the flux of ions passing through the element. The flux of electrons, ϕ_e, passing through the element is

$$\phi_e = i_e(x, y)\,dx dy/e. \tag{7}$$

Since in a merging-beam experiment, one beam is continuously overtaking the other, the distance over which the electrons and the ions interact is not simply the length of the collision region L. Instead an effective collision length must be defined which is a function of the relative velocities of the two beams. If the time taken by the electron to transverse the collision region is $t = L/v_e$ seconds, then in that time the ion beam will only have travelled a distance $L - L_{eff}$. It follows that

$$t = (L - L_{eff})/v_i = L/v_e \tag{8}$$

and so L_{eff} is given by

$$L_{eff} = L(1 - v_i/v_e). \tag{9}$$

Since the number of electron–ion collisions occurring per second is proportional to the flux of projectiles, the target density and the effective interaction length, it follows immediately that

$$c_n\,dx dy = \sigma_n \rho(x, y)\phi_e(x, y)\,L_{eff} \tag{10}$$

where $c_n\,dx dy$ is the number of recombination events occurring per second in the element $dx dy$ over the effective length L_{eff} leading to the formation of the nth recombination product. σ_n is the cross section for the formation of the nth recombination product.

The total product formation rate (in these experiments the measured neutral formation rate), may be found by integrating over the cross sectional areas occupied by the beams, i.e.

$$C_n = \iint c_n\,dx dy = (\sigma_n/ev_i)L(1 - v_i/v_e)\iint i_i(x, y)i_e(x, y)\,dx dy. \tag{11}$$

For our experiments this can conveniently be expressed in the form

$$C_n = (\sigma_n L/e^2)|(v_e - v_i)/v_e v_i|(I_e I_i/F) \tag{12}$$

where I_e and I_i are the total electron and ion currents and F is the quantity often referred to in crossed- or superimposed-beam experiments as the 'form factor'. This has the dimensions of area and can be written:

$$F = \left(\iint_{A_e} i_e(x, y)\,dx dy \iint_{A_i} i_i(x, y)\,dx dy\right)\left(\iint_A i_i(x, y)i_e(x, y)\,dx dy\right)^{-1}. \tag{13}$$

Thorough treatments of form factors have been given in the reviews of Harrison (1966) and Dolder (1969). The determination of F in our experiments is discussed in a note to be published by the same authors.

It should be noted that in equation (12) or in terms of cross section

$$\sigma_n = \frac{C_n e^2 F}{I_e I_i L}\left|\frac{v_e v_i}{v_e - v_i}\right| \tag{14}$$

only the magnitude of the relative velocity function is taken because the same interaction energy in the centre of mass can be obtained whether the electron velocity is greater or less than the ion velocity. It was noted earlier that the relative velocity is symmetrical about the point where $v_e = v_i$ and so equation (12) holds for either case.

Even though the velocity term in equation (12) tends to zero when $v_i \simeq v_e$, the fact that the cross section for dissociative recombination for a one-step process giving neutral atoms varies approximately as E_{cm}^{-1} leads to a slow variation in the count rate $C_n \propto (v_i - v_e)$ as we scan over many orders of magnitude of energy. A sample of our data has already been shown in figure 3 where the count rate for (H, H) pair production in e-H_2^+ recombination varies by approximately a factor of five whilst the general trend of σ_n varies by many orders of magnitude. The structure superimposed on the curve does not vary as E_{cm}^{-1} but rather reflects the formation of Rydberg states H_3^* during the collision. The details of this structure and how it was measured will be discussed more completely in II. Let it suffice to say now that the small change in C_n has been of tremendous advantage to us in gathering equal statistics at all energies in the centre of mass even though we have ranged our electron energy over many orders of magnitude.

4. Our apparatus and its use

Over the years of development of this experiment, the merged electron–ion beam apparatus has gone through a number of forms. Originally we had designed the

experiment such that the ion beam was brought along the axis of a magnetic field produced with a solenoid. A high-current unipotential ring cathode was mounted in the fringing field of the solenoid so that the electrons emitted from it were brought down along the field lines and merged with the ions over a path length of nearly a meter. At the end of the solenoid the electrons were then separated from the ions again with the aid of the fringing field and collected in a ring-shaped Faraday cup. The shape of the fringing fields could be altered with the aid of auxiliary magnetic coils mounted at the ends of the solenoid. The velocity of the electrons relative to the ions was varied by applying suitable voltages to a grid structure which extended the length of the solenoid. This form of the apparatus (Cacak *et al* 1971) is similar to that originally envisaged by Hagen (1967), Theard (1969) and Mahadevan (1972).

Although as pointed out, the guidance of the electron beam along the magnetic axis was easily achieved, it was often found to be hollow and the current density fluctuated along the length of the overlapping region as a function of the energy of the electrons. It was clear that the angle of attack of the electrons onto the ions was changing as a function of all parameters and hence the energy resolution and overlap would also rapidly vary as a function of v_e. Any structure observed in this apparatus would always have been suspect. Furthermore it had been our intention to use getter pumping distributed along the inside of the solenoid, however with the introduction of the grid and electron scanner systems this became difficult. Hence it became virtually impossible to obtain the low vacuum required to minimise the background noise caused by the interaction of the ions with the residual gas.

In 1973 an entirely new approach was adopted which proved successful. The coil producing the solenoid guide field was eliminated and replaced by a pair of trochoidal analysers (Stamatovic and Schulz 1970) and a weak 25 G magnetic field supplied by coils external to the vacuum tank housing the interaction region. The immediate advantage of this system was that it opened up the interaction region, thus allowing for efficient pumping. Figure 5 shows a schematic outline of the arrangement of the apparatus.

To see how the merging and demerging of the beams is actually affected it is useful to examine the trajectory of an electron entering a region of mutually perpendicular electric and magnetic fields. This is illustrated in figure 6. If the magnetic field lines are parallel to the axis of the electron beam and the electric field is perpendicular to the axis then the electrons perform a series of jumps as shown. After leaving the region where the electric field is applied the electrons move in a direction parallel but offset from their original direction.

It can be shown that if the electric field E and magnetic field B are arranged so that

$$E = 12.56(V_0)^{\frac{1}{2}}/ln \tag{15}$$

$$B = 21.16(V_0)^{\frac{1}{2}}/n \tag{16}$$

where V_0 is the acceleration voltage of the electrons and n is the number of jumps that the electrons make, then after travelling an axial distance l cm, they are offset from their original axis by a distance d cm. Furthermore, the vectorial velocity distribution of the electrons entering and leaving the trochoidal analyser is preserved.

The merging and demerging analysers used in this apparatus were 12.4 cm and 6.2 cm long respectively and the electrons were shifted by 2.5 cm so that their trajectories coincided with those of the ions. A fixed axial magnetic field of 25 G was

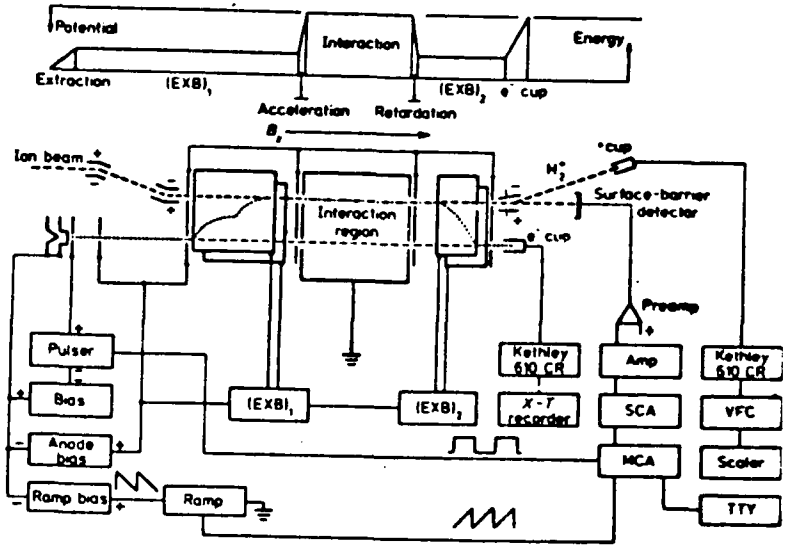

Figure 5. Schematic outline of the experimental arrangement showing the associated electronics. Also shown is the arrangement of the potentials experienced by the electrons during their passage through the apparatus.

used and the potentials experienced by the electrons along their path were arranged so that their energy with respect to the analysers was constant. This was achieved by using floating power supplies to generate the transverse electric fields in the analysers. These power supplies were held at the same potential as the anode of the electron gun and this in turn was kept at a fixed potential with respect to the cathode. The potential on the cathode was varied with respect to ground using a ramp generator and the final acceleration of the electrons was performed between the exit aperture of the first trochoidal analyser and the entrance aperture to the collision region. The latter was held at ground potential to facilitate the monitoring of the beam with the scanners. The distance between the acceleration electrodes in front of the intersection region was kept small (<1 mm) to minimise end effects. After traversing

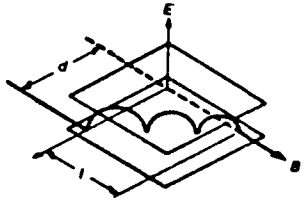

Figure 6. Illustration of the motion of an electron in the $E \times B$ field of a trochoidal analyser.

the 7.62 cm long intersection region the electrons were decelerated to the anode potential before entering the second trochoidal analyser where they were unfolded from the ions. Finally they were collected in a Faraday cup held at ground potential and protected with properly biased guard rings. The arrangements of the electrodes and of the electron potentials are illustrated schematically in figure 5.

The major difficulty which was found to arise with this arrangement was due to inhomogeneities in the axial magnetic field caused by interaction with the earth's magnetic field and by the fact that the 304 stainless-steel chamber had sufficient permeability that when large pumping ports were cut in it, distortion of the axial magnetic field occurred. Efforts were made to minimise these effects by installing horizontal and vertical Helmholtz coils around the apparatus so that fine tuning of the direction of the axial magnetic field could be accomplished. Also in order to minimise the problem, the length of the interaction region was shortened from 1 m to 7.62 cm. With the inclusion of these modifications the complete merging of the two beams was accomplished, allowing valid results to be obtained from the apparatus over a wide energy range.

It should be pointed out that although the ions travel on collinear paths with the electrons, they are affected to a negligible extent by the potentials described above, because their energies are so much greater than the electron energies.

In §2 it was shown that high energy resolutions are obtained at low centre-of-mass energies even with beams having relatively large laboratory energy spreads. For this reason it was not necessary for the energy of the electrons to be highly resolved.

The electron beam was produced from an indirectly heated TV gun cathode and after initial acceleration and collimation it was passed directly into the first trochoidal analyser where it was merged with the ion beam. No attempt was made to obtain a highly monochromatic beam and in fact the energy spread was estimated to be about 0·1 eV once the electron beam had passed the low-resolution analyser. It should be noted, however, that the use of the analysers to merge the electron and ion beams, makes possible the production of high-resolution electron beams if and when necessary. A discussion of resolution follows in §5. Typical electron beam currents used in our measurements were between 15 and 30 μA but no variation in the measured cross section was found as I_e was varied from 5 to 35 μA. For these currents and electron energies in excess of 40 eV, no measurable space-charge effects were expected or encountered.

Turning now to the production of the ion beam the design considerations for this had to take into account signal and background count rates, desired energy ranges and the excitation state of the target ions. It has been pointed out earlier that the kinematics of the merged-beam technique allow very low centre-of-mass energies to be achieved by matching the velocities of the two beams. This offers a great advantage in that no restrictions are placed on the actual laboratory energies of the individual beams in order to reach low centre-of-mass energies. Conventional crossed-beam experiments are limited in their lower limit of energy by the difficulty of producing and handling electrons of very low energy. Particularly serious are the effects of contact potentials and stray magnetic fields.

In order to exploit the kinematic advantage of the merged-beam technique the ion beam was produced in a 450 keV Van de Graaff accelerator (High Voltage Engineering Corporation Model AN400). Thus for example a 440 keV beam of H_2^+ ions corresponds to an equivalent electron energy E_e of approximately 120 eV for zero centre-of-mass energy. Van de Graaff accelerators tend to be inherently unstable

in their energy and so an auxiliary stabilisation system is required to produce a stable ion energy. The conventional means of stabilising the beam is to monitor the ion beam on a pair of slits connected through a differential amplifier feedback system to the corona points located near the terminal of the accelerator. Adjustment of the voltage of these points allows the terminal voltage to be adjusted by drawing more or less charge from the dome. Such a system allows the energy of the ion beam to be stabilised to within about ±1 keV.

In order to improve our centre-of-mass energy resolution it was desirable for us to improve on the energy spread of the ion beam. This was done by changing from slit stabilisation to column current stabilisation. The terminal of the accelerator is connected to ground through a chain of resistors with a total resistance value of approximately $10^{10}\,\Omega$. The current flowing through this resistor chain is a direct function of the terminal voltage. The difference between this current and an auxiliary stable current source was used to drive the corona stabiliser. Extra feedback from the capacitive pick-up assembly on the accelerator pressure tank was used for ripple suppression. This system had the advantage of providing approximately 0·05% stability which is independent of the ion beam current.

After mass analysis the ion beam passes through a differentially pumped region before entering the collision chamber. With the means of a turbo-molecular pump this region was maintained at approximately 1×10^{-8} Torr.

Prior to entering the interaction region the trajectory of the ion beam was kinked using two sets of electrostatic deflectors. This was done to remove from the beam any fast neutrals formed in the beam during its long passage through the background gas in the beam transport system. After collision with the electron beam, the ion beam was analysed electrostatically into its component charge states. The primary positive ions were collected in a Faraday cup (with guard ring) while the neutrals formed by the dissociative recombination reaction

$$e + H_2^+ \rightarrow H + H$$

were detected using a lithium-drifted solid-state detector which had a surface area of 300 mm² and an energy resolution of 29 keV for alpha particles. The efficiency with which H atoms and H_2 molecules are detected is known from manufacturers' specifications and from C F Barnett (1974 private communication) to be 100%. It was important for the detector to have a large surface area in order to accommodate the spatial spread of the dissociative products.

Originally the main sources of background noise in this experiment came from the interaction of the primary ions with the slit edges at the ends of the collision region and with the background gas leading to fast H and H_2 neutrals. The contributions from these processes were limited by careful collimination and alignment of the ion beam and by reduction of the pressure in the interaction region. The latter was achieved by isolating the interaction region from the rest of the main vacuum chamber and by pumping it with a Granville-Phillips UHV pump which reduced the pressure to approximately 2×10^{-9} Torr. The ion and electron beams entered and left the interaction region via small apertures which presented low-conduction paths to the molecules in the rest of the tank.

Also processes such as charge transfer and dissociative charge transfer leading to H_2 and H + H products respectively were separated from processes leading to single H atoms by means of the energy selectivity of the solid-state detector. Thus, for example, for a 440 keV H_2^+ beam the former two processes were registered as

pulses corresponding to a 440 keV particle (or two 220 keV particles arriving simultaneously) at the detector while the latter was registered as a single 220 keV particle since in the dissociation of H_2^+ the kinetic energy of the molecule is distributed approximately evenly between the dissociation products. The same arguments apply in the case of H_3^+.

By using a single-channel analyser on the output of the detector with a window set to transmit only those pulses corresponding to a 440 keV particle (or two 220 keV particles) those signals arising from the collisional dissociation of H_2^+ on the background gas could be rejected. It may be noted in passing that the energy resolution of solid-state detectors increases with incident particle energy and so the merged-beam technique which allows high-energy beams to be used has a special advantage in this respect. Peart and Dolder (1974a, c) used a similar technique but because they used a 40–60 keV ion beam, they could not completely resolve the neutral products.

In order to separate the signal due to recombination collisions from the remaining background the electron beam was modulated before the trochoidal analyser and gating techniques were used to register separately the count rate in the detector when the electron beam was on (corresponding to signal + background) and when it was off (corresponding to background only). It was found that the electron beam did not give rise to any detectable background so single-beam modulation was sufficient for signal recovery†. In order that background count rates did not become too high for the detector to handle (that is leading to pile up), the current in the ion beam had to be decreased to less than 5×10^{-9} A. Below this ion current, no non-linear effects associated with the background count rate were observed.

We obtained cross sections as follows. The ion and electron beams were made to merge and the overlap of the beams was measured using the scanning system described by Keyser *et al* (1978). Because the electron beam was more stable and uniform and because electrons in the fringe of the beam produced no background, it was arranged that the ion beam (with a diameter of 2.5 mm) be contained within the electron beam (diameter 3.5 mm). The window of a single-channel analyser was set to accept only those pulses from the detector corresponding to the neutral dissociative-recombination products desired. The output of the SCA was then fed into a multichannel analyser, MCA. The time base for this instrument was supplied externally by a voltage ramp from the ramp generator. This was in phase with the ramp used to vary the electron energy so that each of the selected channels of the MCA collected signals corresponding to a particular energy. The electron modulation signal (also developed by the ramp generator) was fanned out to the beam pulser and to the MCA. This too was in phase with the electron energy ramp so that during one ramp the signal plus background was measured while in the next only the background was registered. The MCA was arranged so that counting pulses were added to their respective channels during the signal ± background mode and subtracted from them during the background (B) mode so that only the true signals due to dissociative recombination were finally stored.

As explained earlier, equal centre-of-mass energies could be obtained for electron energies both greater than or less than the ion energy. For each experiment the range of the electron energies was selected to include contributions from both sides

† In an earlier design the electrons had been modulated by applying a chopping voltage across the trochoidal analysers. However, this was found to move the ion beam sufficiently to cause spurious signals due to the collision of the beam fringe with surfaces. To eliminate this effect the modulation was then performed by biasing the cathode plate of the electron gun with a square-wave-form voltage.

of the $E_{cm} = 0$ peak. The near mirror symmetry in the experiment served to check the calibration of the electron and ion energies. A typical spectrum obtained in this way has already been shown for $(e\text{–}H_2^+)$ in figure 3.

As outlined above, it was necessary to demonstrate that the measured cross section was invariant with changes of I_e and I_i. We had also to establish that the measured value which should depend only upon E_{cm} did not change as the ion beam energy changed. This we did for several electron–ion recombination pairs, several values of E_{cm} and over ion energies between 300 and 450 keV. In no case was a variation in the cross section observed.

Other parameters required for the calculations of the cross section were the ion and electron currents and the form factor F, measured at 5 eV intervals for the electron laboratory energy in order to verify the constancy of overlap. The electron beam into a voltage-to-frequency converter whose output was accumulated in a trometer whose output was fed directly onto the Y axis of an x–y recorder.

The ion beam on the other hand was less stable and for this reason its current was converted to digital form and registered on a scaler. This was accomplished by feeding the output of the Keithley 610BR electrometer used to monitor the ion beam into a voltage-to-frequency converter whose output was accumulated in a scaler.

In practice it has been found that runs of up to seventy hours duration have been required to produce results which are statistically better than 10%. During this time small changes in the form factor do occur which although not affecting the relative structure in the cross sections, make it difficult to obtain absolute magnitudes. In order to overcome this it has been found convenient to measure the cross sections accurately for several fixed centre-of-mass energies and to normalise to these the continuous results (Caudano *et al* 1975, McGowan *et al* 1976), taken with a ramped electron energy. This has allowed the relative calibration of results for different target ions to be obtained easily.

5. Energy resolution and experimental accuracy

In §2, the magnitude and asymmetries of the electron energy resolution in the centre-of-mass frame were discussed and the relation of the electron energy resolution to the spread in energies of the ion and electron beams and to the angular spread was formulated. In practice it is possible to obtain approximate estimates of ΔE_e and ΔE_i but $\theta\Delta\theta$ could not be directly measured. In order to determine the actual energy resolution, ΔE_{cm}, a study of the profiles of the cross section and count rate against energy plots was made. Also, from the FWHM of the spectral structure found, one can estimate the upper limit to the resolution. It is essential that these estimates be consistent with the values derived from the angular spectra seen with the beam scanner.

During an experimental run the ion energy is kept fixed and the energy of the electrons is varied so that for part of the time they are travelling faster than the ions while at other times they are slower. While the electron energy varies the dissociated neutral product signals are collected in up to 200 channels of a multichannel analyser so that each channel corresponds to a particular electron energy. Figure 3 shows a typical spectrum obtained in this way. One consequence of this type of measurement is that some of the channels could possibly correspond to extremely

small centre-of-mass energies ($\sim 10^{-3}$–10^{-6} eV). However energies of this order are much less than the actual spread of the collision energy in the centre-of-mass energy frame limited primarily because of the angular spread. This manifests itself in the fact that the channel does not collect as many counts as it would if its width in the centre-of-mass frame was greater than the energy resolution. As a result an artificial change of slope of the cross section with energy occurs at low energies.

The theory of dissociative recombination referred to in §1 predicts an E^{-1} Coulombic energy dependence for the cross section below about 10^{-2} eV and an approximate $E^{-\frac{1}{2}}$ above. This is in keeping with Wigner's threshold law for an exothermic process with a Coulombic force (Wigner 1948). This implies that the cross section should be infinite at $E_{cm} = 0$, which cannot occur in reality. It can be seen from figure 3, however, that the count rate tends to a finite value as $E_{cm} \to 0$. Although the concept of an infinite cross section is non-physical and some modification of the theory is required to avoid this it was decided to examine the effects of folding various angle-dependent energy resolutions into a E_{cm}^{-1}-dependent cross section to see if our results could be reproduced. In this way it was hoped to obtain an estimate of our resolution due to our angular uncertainty. This approach is of course distorted by the spectral structure observed in our data, yet the approach does represent another consistency check.

Experimentally we know that the ion and electron beams both pass cleanly through the entrance and exit holes of the interaction region. For the electrons there are two limiting cases: (i) there is a very small angular spread but rather the electrons follow a trajectory through the region such that they are at an angle with the ion beam during most of the passage; (ii) the electrons on the average have $\theta = 0$ but *with an angular spread* $\Delta\theta$. *We consider these limiting cases in turn.* In the region $E_{cm} < 0{\cdot}01$ eV we assume with some good reason that $E_{cm} = f(\theta, \Delta\theta)$ only.

(i) *Small* $\Delta\theta$, θ *finite*

Assuming $\sigma = E_{cm}^{-1}$, the count rate can be expressed as

$$C_n = KE_e^{-1/2} E_{cm}^{-1/2} \tag{17}$$

K is a constant and E_{cm} is given by equation (2). In figure 7, equation (17) is plotted for various values of θ (in radians) together with the experimentally measured count rate for the case $e\text{-}H_2^+$ ($v = 0, 1, 2$) recombination. This data was chosen for comparison simply because there is likely to be less contribution due to spectroscopic effects. It is seen that $\theta = 0{\cdot}012$ rad $= 0{\cdot}69°$ provides a good fit to the experimental curve.

(ii) $\theta \simeq 0$, $\Delta\theta$ *finite*

The experimentally measured count rate is then given by

$$C_n = \int_0^{\Delta\theta} \mathrm{d}p_e (E_{cm}^{-1/2} f(p_e) K E_e^{-1/2}) \tag{18}$$

where $f(p_e)$ is the distribution of electron momenta. This distribution was assumed to be constant and also the effects of changing E_e were ignored, i.e.

$$f(p_e) = \begin{cases} \text{constant} \times \delta(E - E_e) & \theta < \Delta\theta \\ 0 & \theta > \Delta\theta. \end{cases}$$

Equation (18) then reduces to

$$C_n = K' E_e \int_0^{\Delta\theta} E_{cm}^{-1/2}\, \mathrm{d}(\cos\theta). \tag{19}$$

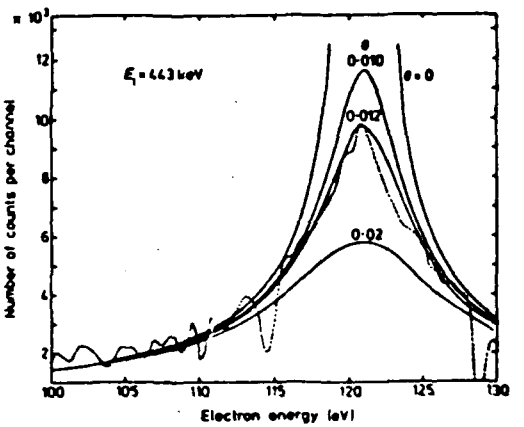

Figure 7. A plot of the count rate for the merged-beam experiment evaluated (equation (17)) taking σ = constant × E_{cm}^{-1} for various values of intersection angle. The full curves are the calculated count rates and the broken curve shows the experimentally measured count rate for $e\text{-}H_2^+$ ($v = 0, 1, 2$) collisions.

Equation (19) was evaluated for various values of $\Delta\theta$ and these were then compared with the experimental curve as shown in figure 8. It can be seen that a value of $\Delta\theta \sim 1{\cdot}5°$ agrees fairly well with our measurement. For the case of $\theta = 0$ and $\Delta\theta$ finite the spread of the energy in the centre-of-mass frame is given by

$$\Delta E \sim E_{cm}(\Delta\theta) - E_{cm}(0) \sim (E_e E_+)^{1/2} \Delta\theta^2. \tag{20}$$

Hence this implies a centre-of-mass energy spread of approximately 0·08 eV at $E_{cm} = 0$. The above comparison was made for values of $E_{cm} < 0{\cdot}2$ eV since in this region the E_{cm}^{-1} cross section dependence is expected to be fairly accurate.

Neither of these two approaches are expected to accurately model the real situation since the first assumes a finite intersection angle but zero angular spread whilst the second assumes perfect symmetry of the two beams about each other. However, they do provide limits to the energy resolution and the shift of the energy scale due to a non-zero intersection angle.

Inclusion of a finite $\Delta\theta$ in the first approach would tend to lower the theoretical curve even further due to contributions arising from opposite sides of the $E_{cm} = 0$ peak in the count rate. Similarly as θ is increased from zero the value of $\Delta\theta$ must decrease in order for the theoretical curve obtained in the second approach to match the experimental points. This would tend to decrease the energy resolution from that obtained in the $\theta = 0$ case.

If $\theta = 0{\cdot}69°$ this would mean that when the ion and electron beams had equal velocity then the minimum centre-of-mass energy resolvable would be approximately 17 meV. The energy scale in figures 9–11 would therefore have to be shifted by this amount. However, this represents an upper limit to this shift. Any shift would not make sense within the present accuracy of the experiment.

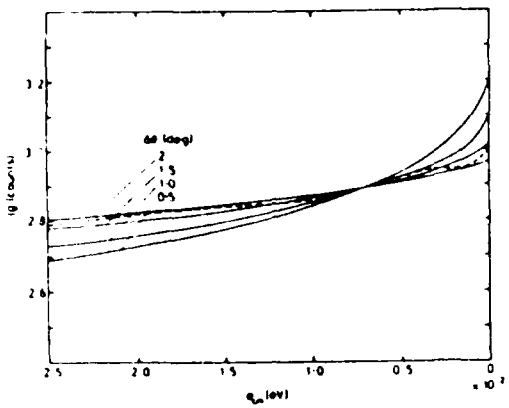

Figure 8. The logarithm of the number of neutral counts obtained during an experimental measurement of $e\text{-}H_2^+$ ($v = 0, 1, 2$) are plotted as a function of centre-of-mass energy (broken curve). This curve is compared with curves calculated (equation (19)) by convoluting the expression $C_v = kE_{cm}^{-1/2}E_v^{-1/2}$ over the momentum distribution of the electron beam about the ion beam assuming $\theta = 0$ for various values of $\Delta\theta$ the spread of the electron beam (see text for details).

An examination of the spectral structure which is most evident above $E_{cm} = 0{\cdot}1$ eV suggests that the contribution due to the uncertainty in θ and $\Delta\theta$ must be even smaller since those due to ΔE_v and ΔE_i are known as are the widths of the autoionising and predissociating levels taken from the photoionisation results reported by Dehmer and Chupka (1976).

In summary then, the contribution to the energy spread of the colliding electron in the centre of mass due to uncertainties in ΔE_v and ΔE_i appears to best be described by the lowest of the curves associated with the third term of equation (5) as plotted in figure 4. As a result we expect $\Delta E_{cm} \simeq 0{\cdot}02$ eV for E_{cm} near zero and $\Delta E_{cm} \leqslant 0{\cdot}04$ eV for $E_{cm} \simeq 1$ eV.

Another problem which does arise in the experimental arrangement which we have described is that of spiralling of the electrons around the axial magnetic field lines. This can occur if the electrons have any velocity component perpendicular to the field lines. This would lead to an uncertainty in the path length over which the beams interact making calculation of absolute cross sections difficult. Taylor *et al* (1974) have examined this problem in detail and in their analysis they showed that the diameter D and pitch P of the spiral path were given by

$$D = 67{\cdot}4\, V_\perp^{1/2}/B \tag{21}$$

$$P = 212\, V_\parallel^{1/2}/B \tag{22}$$

where D and P are in mm. B is in Gauss and where $V_\perp$ and $V_\parallel$ (in eV) are the kinetic energies perpendicular and parallel to the magnetic field lines. In our experiment the ion beam is very stiff (large momentum) and remains parallel to the magnetic field lines. However, for the electrons we have shown in the above discussion that

the average angle between the beams is of the order of 0·69°, so knowing this and $V_\parallel$ we can calculate the transverse kinetic energy component $V_\perp$ from the expression

$$(\sin 0{\cdot}69)^2 = V_\perp/V_\parallel \tag{23}$$

and hence determine D and P. For 100 eV electrons moving in a 25 G magnetic field, equations (21) and (22) give values of 0·3 mm for the spiralling diameter and 8·5 cm for the pitch. Hence it can be seen that over the interaction length of 7·62 cm this has a negligible effect on the measured cross section.

Our measurement of integrated profiles of the electron and ion beams taken at three places between the entrance and exit holes are consistent with the above discussion.

Before discussing the results it is necessary to comment on the accuracy of the measurement. Since we have been concerned mainly with the structure in the cross sections, our primary emphasis has been on achieving good statistical accuracy and on the close determination of the centre-of-mass energy.

The neutral-atom signal from which the cross section is computed is determined from the subtraction of two measured quantities namely, the $(S + B)$ count rates and the (B) count rates alone. Since the collision processes are random and the numbers involved are very large, they are described by Poisson statistics. Thus the percentage error in the number of signal counts measured is given by:

$$\frac{\Delta S}{S} = \frac{(S + B_1)^{1/2} + B_2^{1/2}}{S} \times 100\,(\%) \tag{24}$$

where S is the number of signal counts and B_1 and B_2 are the total number of background noise counts measured with the electron beam on and off, respectively. Note that for a successful measurement, $B_1 = B_2$, i.e. care must be taken to ensure that the timing of the electron beam modulation frequency is accurately set and that effects such as pressure modulation which can lead to greater noise count rates when the electron beam is on than when it is off, are eliminated.

Typical signal-to-background ratios of 12% were encountered in our measurements reported here and the cross sections were measured for 200 different values of the electron energy, corresponding to 0·25 eV laboratory channel widths in each case. For the H_2^+ results, the accuracy ranges from ~5% for $E_{cm} < 0{\cdot}1$ eV to ~15% for $E_{cm} > 0{\cdot}1$ eV. For H_3^+ $\Delta S/S$ was 12% for $E_{cm} < 0{\cdot}1$ eV and ~25% for $E_{cm} > 0{\cdot}1$ eV. In each case binomial smoothing was applied twice to each set of results to compensate for these uncertainties. The application of smoothing techniques to the analysis of structure in cross sections has been discussed previously by McGowan *et al* (1968) and they show that the statistical errors can be reduced by a factor of 0·67 for single smoothing and by 0·57 overall by double smoothing. The disadvantage of using such techniques, however, is in the subsequent reduction of energy resolution which can effectively smear out fine-structure details.

Absolute calibration of collision energies is frequently a difficult problem but the de-amplification of the energy achieved in merged-beam experiments makes the problem less severe. In this experiment the energy of the ion beam was calibrated by measurement of the current flowing through the column resistors of the Van de Graaff, whose values were accurately known. Comparison with the results of a charge transfer into the continuum experiment reported by Meckbach *et al* (1977) served to confirm this calibration technique. In all our measurements the ion energy

was kept fixed at 4.39 ± 2 keV and the electron energy was then calibrated from this value by measuring the position of the centre of our count rate, shown in figure 3. This centre was determined by the symmetry of the structure on each side of the peak. The range of the ramp voltage used to vary the electron energy was accurately measured with a Hewlett-Packard DVM and hence the centre-of-mass energy scale was calibrated, knowing the zero energy point and the electron energy range. In the manner just described the laboratory electron energy could be calibrated to within plus or minus one point, that is, 0·25 eV. This is then de-amplified in the centre-of-mass frame so that, for example, at 0·1 eV centre-of-mass energy, this value is known to within 0·015 eV while at 1 eV the energy of the resonance structure is known to within 0·007 eV.

6. Results and discussion

Measurements of dissociative recombination between electrons and H_3^+ and H_5^+ ions giving only neutral products, have been made with this apparatus. The high-resolution inherent in the merged-beam technique has enabled fine structure to be observed in these cross sections. Crudely speaking our interpretation of this structure is that it arises from the formation of compound (Rydberg) states which compete with direct dissociative recombination by decaying into a number of competitive channels which include autoionisation and ion pair production. This will be discussed in more detail in II.

6.1. (e–H_3^+) *recombination*

Cross sections for dissociative recombination in e-H_3^+ (all v) collisions are illustrated in figure 9. The H_3^+ ions were formed using pure hydrogen gas in an RF discharge ion source and the vibrational state population was assumed to be either that predicted by Franck–Condon factors or more likely one measured by von Busch and Dunn (1972) from photodissociation studies of H_3^+. Also shown in figure 9 are the results of Peart and Dolder (1974a) for e-H_3^+ collisions. There is excellent agreement between their measurements and our results, indicating that the prime difference between the experiments is one of resolution.

As proposed by McGowan *et al* (1976) we continue to maintain that the dips in the cross section curve for e-H_3^+ (all v) recombination are of spectral line widths and are principally associated with the formation of H_3 Rydberg states which decay through autoionisation (primarily in the region below 1 eV) and pair production (above 1 eV).

In the (all v) case the many H_3^+ (v) levels each has associated with it fine structure at specific values of E_{cm}. As a result, for many values of v in the ion beam, structure tends to be washed out. Furthermore, a comparison has been made with the recent calculation of cross section by Bottcher (1976) for e-H_3^+ (all v). The gross structure appearing in the theoretical result which merely reflects the Franck–Condon overlap of the function for H_3^+ $^2\Sigma_g^+$ (v, J) and H_3^{**} ($^1\Sigma_g^+$ $1s_3^2$) does not appear in our high-resolution experiments at all, though the direct process no doubt represents part of the total measured cross section.

The relative population of vibrational states of H_3^+ ions in the interaction region can be altered by using mixtures of H_2 and insert gases in the ion source. Detailed

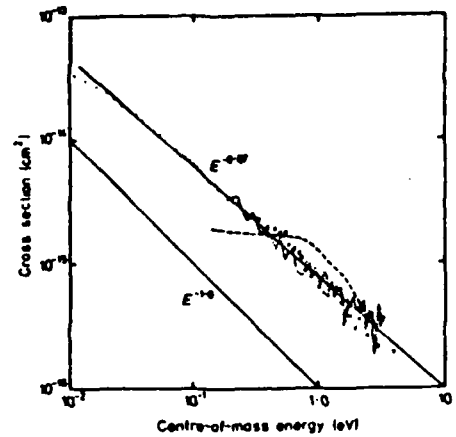

Figure 9. Dissociative recombination cross sections for H_3^+ (all v) measured with the merged-beam apparatus, plotted on a logarithmic scale against centre-of-mass energy. Also shown are the experimental results of Peart and Dolder (1974a) taken with an inclined-beam configuration (×) and recent theoretical calculations of Bottcher (1976) obtained by averaging over a von Busch and Dunn (1972) vibrational-state distribution (broken curve).

studies by Chupka and Russell (1968) of H_3^+–He and H_5^+–Ne reactions at low ion energies demonstrated that HeH^+ and NeH^+ are formed if the H_3^+ ions are vibrationally excited with $v > 2$ and $v > 1$, respectively. By using gas mixtures in our ion source it was established that these reactions could be used to change the population of vibrationally excited ions drawn from the source. In figure 10 we give the results obtained when between a 5 to 10% He in H_2 mixture was used. This has led to a H_3^+ ion beam which we suggest was dominantly in $v = 0$–2. The relative proportion of each of the vibrational states is as yet not established. The details of the experiments in which the vibrational population has been changed along with an analysis of the spectroscopic structure observed will be given in II.

Although the slope of this curve is similar to that for H_5^+ (all v) there is considerable difference in the distribution of what we have called spectroscopic structure associated with the temporary formation of Rydberg or e-H_5^+ resonance states. The structure is definitely more pronounced in the case where only a few vibrational levels are present. In figure 10 we compare our H_5^+ ($v = 0, 1, 2$) results with the value resulting from Bottcher's calculation when the relative vibrational distribution is taken as (1:2:2). Although there is a marked difference in the magnitude of the cross section and the shape at lower energies the dip in the experimental cross section between 1 and 2 eV no doubt reflects the 'direct' dissociative recombination mechanism whereas the fine structure must be associated with the 'indirect' mechanism, e.g. the temporary formation of Rydberg states. In an earlier publication, McGowan *et al* (1976) pointed out that the fine structure in this region could well be associated with the decay of the Rydberg states into H^*–H^- pairs. This has yet to be verified.

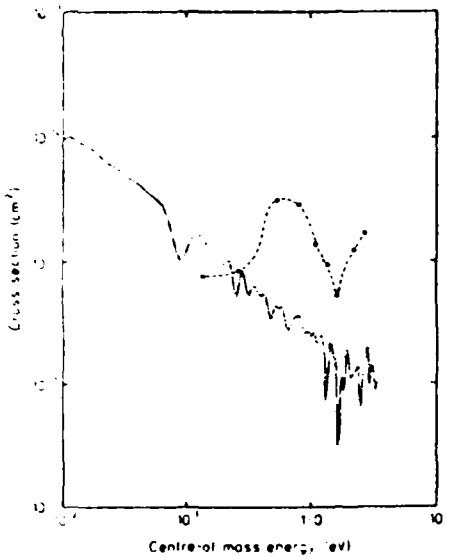

Figure 10. Dissociative-recombination cross sections for H_3^+ ($v = 0, 1, 2$) plotted against centre-of mass energy on a logarithmic scale. The method employed for the vibrational selection is described in the text. Also shown is a theoretical prediction obtained by averaging Bottcher's results (1976) for the first three vibrational states of H_3^+ in the ratio 1:2:2:0 Ca

Nielsen and Berry (1971) have looked carefully at the relationship between $(H + H^*)$ associative ionisation and $e\text{-}H_3^+$ dissociative recombination both proceeding through intermediate Rydberg states. Their analysis is far from complete for it does not allow for a general treatment of states correlating to the $n = 2$ level of the separated atom. Within the model, dissociative recombination has a $\sigma \propto E_{cm}^{-1}$ dependence for energies below 0.006 eV. In the vicinity of 300 K (0.027 eV) an approximate $E_{cm}^{-1.35}$ law would apply while at even higher interaction energies, higher inverse power laws are expected. We find that for energies greater than 0.01 eV the general slopes of the curves for both H_3^+ (all v) and H_3^+ ($v = 0, 1, 2$) are more consistent with an $E_{cm}^{-0.5}$ law. If indeed a power law can be applied.

At lower energies because of the effects of our energy resolution it is not possible to make an accurate comment on the energy dependence.

The fact that the absolute magnitudes of the cross sections for H_3^+ ($v = 0, 1, 2$) + e recombination are a factor of 2.65 lower than those for H_3^+ (all v) + e is in general agreement with the predictions of Nielsen and Berry (1971).

They suggested that dissociative recombination is favoured from vibrationally excited states of the molecular ion ($v = 5$–8) decaying primarily into the $n = 3$ states of the separated atoms.

6.2. ($e\text{-}H_3^+$) *recombination*

The cross section for dissociative recombination in $e\text{-}H_3^+$ collisions are shown in figure 11. These results are entirely new, representing longer counting times (better statistics) than we had in the preliminary report by Caudano *et al* 1975. However, there is good qualitative agreement with our previous findings. Whereas with $e\text{-}H_3^+$ (all v) we found excellent agreement in magnitude with Peart and Dolder in this instance for ($e\text{-}H_3^+$) our measured absolute values are lower though generally follow the same slope as their cross section. Where earlier we felt that the cross section against electron E_{cm} curve could well be represented by a single sloping curve exactly equal to that found by Peart and Dolder (1974c) and Leu *et al* (1973) we now feel that the simple slope approach is very much of an over-simplification which it must always be if there is strong interference between several direct dissociative channels, pair production, autoionisation, predissociation and so on.

The distribution of excited states of H_3^+ *has not been measured in our experiment* but because our discharge source runs at pressures in excess of 10^{-2} Torr and because the structure we observe in the total cross section curve is so pronounced we had originally concluded that we were dealing with H_3^+ (ground state) or at least a distribution similar to that used in the experiments of Peart and Dolder (1974b, c). However the difference in the absolute cross section as measured in our experiments and that obtained in theirs and those of Leu *et al* (1973) suggest that there may

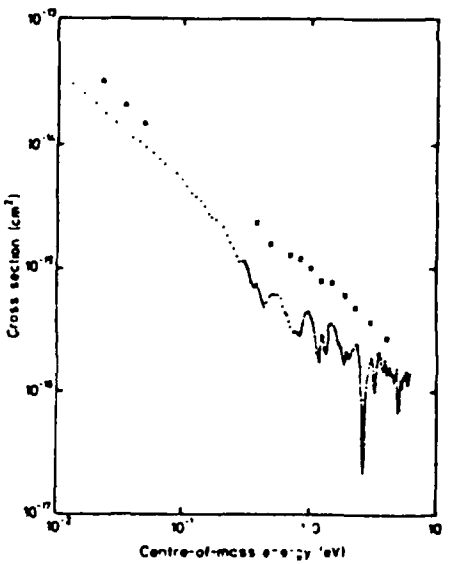

Figure 11. Dissociative-recombination cross sections for H_3^+ plotted against centre-of-mass energy. Also shown are the results of Peart and Dolder (1974c) using an intersected-beam technique (×) and of Leu *et al* (1973) taken with a plasma afterglow technique (Δ).

be a difference. Furthermore, Blakley *et al* (1977) have recently reported that the distribution of vibrationally excited H_3^+ depends critically upon source pressure. This may explain the difference between the measured values. As we have already demonstrated for H_3^+ a change in the distribution of vibrational levels in the ion beam has a dramatic effect upon the cross section obtained.

As with e-H_3^+ recombination we associate the structure in the e-H_3^+ with Rydberg excitation and decay into competitive ionisation channels. In fact the large variation from linearity may well reflect this. For small molecular ions like H_3^+ it is to be expected that there will be a well developed Rydberg system which the merged-beam experiments will permit us to study in detail.

7. Comment

With the merged electron-ion beam experiments we now have the potential to

(i) measure cross sections for recombination to very low centre-of-mass energies.

(ii) determine the dependence of cross section upon the internal energy of the ion,

(iii) examine the various channels into which the recombining system decays,

(iv) look at the details of Rydberg spectroscopy of known systems like (H_3^+–e) and unknown and normally inaccessible systems like (H_3^+–e).

It is already clear that recombination for H_3^+ and most likely all other small systems cannot simply be categorised as due to either the 'direct' or 'indirect' process, but rather due to active competition between both. As resolution improves and the various decay channels are investigated under high resolution, it is expected that we will be able to understand the process sufficiently well that detailed theoretical modelling can be done for these and other systems.

Acknowledgments

It is our pleasure to thank Irold Schmidt of the Centre for Chemical Physics, instrument maker, for his excellent craftsmanship and C F Barnett and J A Ray for their help with detectors.

References

Bardsley J N 1967 *Proc. 5th Int. Conf. on Physics of Electronic and Atomic Collisions, Leningrad* I P Flaks and E S Solovyov (Leningrad: Nauka) Abstracts p 338
——1968 *J. Phys. B: Atom. Molec. Phys.* **1** 349, 365
Bardsley J N and Biondi M A 1970 *Adv. Atom. Molec. Phys.* vol 6, ed D R Bates and I Estermann (New York: Academic Press) p 1
Bates D R 1950a *Phys. Rev.* **77** 718
——1950b **78** 492
Bates D R and Massey H S W 1947 *Proc. R. Soc. A* **192**
Berry R S and Nielson S E 1970a *Phys. Rev. A* **1** 383
——1970b *Phys. Rev. A* **1** 395
Blakley C R, Vestal M L, Futrell J H 1977 *J. Chem. Phys.* **66** 2392
Bottcher C 1976 *J. Phys. B: Atom. Molec. Phys.* **9** 2899
von Busch F and Dunn G H 1972 *Phys. Rev. A* **5** 1726

Cacak R K, Caudano R, Gaily T D and McGowan J Wm 1971 *Proc. 7th Int. Conf. on Physics of Electronic and Atomic Collisions, Amsterdam* ed J Kistemaker (Amsterdam: North-Holland) Abstracts p 992
Caudano R, Wilk S F J and McGowan J Wm 1975 *Proc. 9th Int. Conf. on Physics of Electronic and Atomic Collisions, Seattle* ed J S Risley and R Geballe (Seattle: University of Washington Press) p 389
Chupka W A and Russell M E 1968 *J. Chem. Phys.* **49** 5426
Cunningham A J and Hobson R M 1969 *Phys. Rev.* **185** 98
Dehmer P M and Chupka W A 1976 *J. Chem. Phys.* **65** 2243
Dolder K T 1969 *Case Studies in Atomic Collision Physics* vol 1, ed E W McDaniel and M R C McDowell (Amsterdam: North-Holland) p 249
Fano U 1975 *J. Opt. Soc. Am.* **65** 979
Hagen G 1967 *Proc. 5th Int. Conf. on Physics of Electronic and Atomic Collisions, Leningrad* ed I P Flaks and E S Solovyov (Leningrad: Nauka) Abstracts p 165
Harrison M F A 1966 *Brit. J. Appl. Phys.* **17** 371
Heppner R A, Walls F L, Armstrong W T and Dunn G H 1976 *Phys. Rev. A* **13** 1000
Keyser C J, Auerbach D, Caudano R, McGowan J Wm, Mitchell J B A and Wilk S F J 1978 submitted for publication
Leu M T, Biondi M A and Johnsen R 1973 *Phys. Rev. A* **8** 413
McGowan J Wm, Caudano R and Keyser J 1976 *Phys. Rev. Lett.* **36** 1447
McGowan J Wm, Fineman M A, Clarke E M and Hanson H P 1968 *Phys. Rev.* **167** 52
Mahadevan P 1972 *Proc. R. Soc. A* **327** 317
Meckbach W, Chiu K C R, Brongersma H and McGowan J Wm 1977 *J. Phys. B: Atom. Molec. Phys.* **10** 3255
Neynaber R H 1969 *Adv. Atom. Molec. Phys.* vol 5, ed D R Bates and I Estermann (New York: Academic Press) p 57
Nielsen S E and Berry R S 1971 *Phys. Rev. A* **4** 865
Peart B and Dolder K T 1973 *J. Phys. B: Atom. Molec. Phys.* **6** L359
——1974a *J. Phys. B: Atom. Molec. Phys.* **7** 236
——1974b *J. Phys. B: Atom. Molec. Phys.* **7** 1567
——1974c *J. Phys. B: Atom. Molec. Phys.* **7** 1948
Pearman W B 1976 *J. Chem. Phys.* **64** 4093, 4368
Phaneuf R A, Crandall D H and Dunn G H 1975 *Phys. Rev. A* **11** 528
Stamatovic A and Schulz G J 1970 *Rev. Sci. Instrum.* **41** 423
Taylor P O, Dolder K T, Kaupilla W E and Dunn G H 1974 *Rev. Sci. Instrum.* **45** 538
Theard L P 1969 *Proc. 6th Int. Conf. on Physics of Electronic and Atomic Collisions, Cambridge, Mass.* ed I Amdur (Cambridge: MIT Press) Abstracts p 1042
Vogler M K and Dunn G H 1975 *Phys. Rev. A* **11** 1983
Walls F L and Dunn G H 1974 *J. Geophys. Res.* **79** 1911
Weingartshofer A, Clarke E M, Holmes J K and McGowan J Wm 1975 *J. Phys. B: Atom. Molec. Phys.* **8** 1552
Wigner E P 1948 *Phys. Rev.* **73** 1002

J. Phys. E: Sci. Instrum., Vol. 12, 1979. Printed in Great Britain

Beam-scanning system for determination of beam profiles and form factors in merged-beam experiments

C J Keyser, H R Froelich, J B A Mitchell† and J W McGowan
Department of Physics and Centre for Chemical Physics, The University of Western Ontario, London, Ontario, Canada N6A 3K7

Received 13 July 1978

Abstract A beam-scanning system for a merged electron–ion beam experiment is described. This system is used to determine the horizontal and vertical beam profiles and the form factors at three different locations along the axis of the beams. Design details of the wedge-shaped scanners and the electronic circuit for obtaining beam profiles and form factors are described. The form factor derivation for merged beams is given and an expression in terms of measured quantities is derived.

1 Introduction

The use of colliding beams of particles has become a well established technique for the study of atomic and molecular processes. To determine an absolute cross-section in any colliding-beam experiment, it is necessary to investigate the spatial distributions of particle fluxes in the interacting beams over the interaction region and to evaluate an overlap integral which depends on these particle fluxes. For merged beams, the overlap integral is three-dimensional and is given by

$$\Omega = \iiint_V J_1(x, y, z) J_2(x, y, z)\, dx\, dy\, dz \qquad (1)$$

where $J_1(x, y, z)$ and $J_2(x, y, z)$ are the particle fluxes of the two beams and the integration must be performed over the entire volume V of the interaction region. For the relatively large interaction lengths which occur in merged-beam experiments, the problem of determining the overlap integral at sufficiently frequent intervals during an experiment can be very formidable, both in terms of measuring the fluxes at a sufficient number of positions in the interaction region and in terms of computing the integral from the measured fluxes.

Recently two beam-scanning systems for determining the overlap integral in merged-beam experiments have been described. Nitz *et al* (1976) have developed a system which consists of a mechanical beam scanner with pinhole apertures to sample the beams at selected positions in the interaction region and an analogue calculator to compute two-dimensional overlap integrals from the sampled currents. The two-dimensional integrals measured by the system at four positions along the length of the interaction region are then numerically integrated to find the three-dimensional overlap integral. This system is relatively fast and simple, but the choice of points at which the beam can be sampled is limited by geometric constraints. A much more elaborate beam-scanning system for completely automated determination of the three-dimensional overlap integral has been described by Sethuraman *et al* (1977). Their system uses a small square aperture, formed by a pair of crossed slits, to sample the beams. A small on-line computer adjusts the aperture position in three dimensions over the entire interaction region, stores the measured beam fluxes for each point sampled, and calculates the overlap integral. This system can provide comprehensive information about beam structures in the interaction region. In this case the computed overlap integral is sensitive to rapid spatial variations in particle fluxes.

Although these two previously described beam-scanning systems differ greatly in complexity and in the number of points at which the beams are sampled, they are both based on direct sampling of the beams by measuring the particle fluxes passing through a small aperture of known area placed at different positions in the interaction region. In the system which we have developed for our merged electron–ion beam experiment (MEIBE) (Auerbach *et al* 1977) we have used a different approach based on differential scanning of the interacting beams. The principle of differential scanning has long been applied in the monitoring of charged-particle beams with various types of rotating-wire current probe (Hortig 1964, Bond and Gordon 1972, Prudnikov *et al* 1974, Jagger *et al* 1967); however, a rotating-wire scanner is not suitable for our application, in which two beams of charged particles overlap, because it cannot respond selectively to each beam. When the measurement is done by transmission the current variations become very small compared with the total currents on the Faraday cups. Instead of a thin wire, a narrow slit would be a logical alternative as a scanning device for merged beams, but a very narrow slit with well defined and precisely parallel straight edges is difficult to construct. To avoid this difficulty, we have devised a differential scanning system in which the basic scanning element is a very straight knife edge. The merged beams are mechanically scanned, in two perpendicular directions across the beams and at three positions along the length of the interaction region, by a set of three knife-edged shutters. The transmitted electron and ion beam currents are subsequently differentiated electronically to obtain the beam profiles. This method of knife-edge scanning with electronic differentiation is equivalent to scanning with an infinitely narrow slit. Now the accuracy is not limited by the size of the beams. This system is relatively simple, both mechanically and electronically. It does not provide such detailed information about beam structures as the system of Sethuraman *et al* (1977), but it is sensitive to beam irregularities as the knife edges scan two-dimensionally across the entire beam area. We have used the system with the MEIBE for the past three years and have found it to be a fast and convenient system for determining beam positions, checking the alignment of the beams and for measuring beam profiles and finding overlap integrals. This system can also be used with a modified scanner in inclined-beam experiments.

2 Form factor derivation

The form factor takes account of the variation of the particle densities across the beams. Detailed discussions of this quantity have been given by Dolder (1969) and Harrison

† Present address: The Brookhaven National Laboratory, Associated Universities Inc., Upton, Long Island, New York 11973, USA.

(1966) for crossed and inclined beams. The following describes the case where the two beams are merged. If we consider the case where two monoenergetic beams are completely superimposed, we shall assume that the first beam with fixed velocity v_1 acts as a target bombarded by a second beam whose velocity v_2 is variable. The target density in a small element of the first beam, taken in the plane perpendicular to the direction of motion, with width dx and height dy, is given by

$$\rho(x,y)=\frac{j_1(x,y)\,dx\,dy}{ev_1\,dx\,dy} \tag{2}$$

where $j_1(x,y)\,dx\,dy/e$ is the flux of particles passing through the element. The flux of particles from the second beam which pass through the element is given by

$$\phi_2=j_2(x,y)\,dx\,dy/e. \tag{3}$$

If the second beam takes a time $t=L/v_2$ to traverse the collision region of length L, then in that time the slower target beam will only have travelled a distance $L-\Delta L$. The difference in the distances travelled by each beam is the effective collision length; now since

$$t=(L-\Delta L)/v_1=L/v_2, \tag{4}$$

then

$$\Delta L=L(1-v_1/v_2). \tag{5}$$

The number of collisions $c\,dx\,dy$ occurring per second in the element is proportional to the flux of projectiles, the target density and the effective collision length. Hence

$$c\,dx\,dy=\sigma\rho(x,y)\phi_2(x,y)\Delta L \tag{6}$$

where σ is the reaction cross-section. To calculate the total collision rate C, we must integrate over the entire cross-sectional areas occupied by the beams, so

$$C=\iint c\,dx\,dy=(\sigma/e^2v_1)L(1-v_1/v_2)\iint j_1(x,y)j_2(x,y)\,dx\,dy. \tag{7}$$

The integral in equation (7) is only finite when the beams overlap and is therefore called the overlap integral. The three-dimensional overlap integral of equation (1) is given by this integral multiplied by L/e^2. Equation (7) is often expressed in terms of the total beam currents I_1 and I_2:

$$C=(\sigma/e^2v_1)L(1-v_1/v_2)I_1I_2/F \tag{8}$$

where

$$F=\frac{\iint j_1(x,y)\,dx\,dy\iint j_2(x,y)\,dx\,dy}{\iint j_1(x,y)j_2(x,y)\,dx\,dy} \tag{9}$$

and is called the form factor.

If we assume that beam 1 has uniform density and that beam 2 is completely immersed in it then F reduces to the area of the larger target beam and is independent of the shape of the smaller beam. Hence the form factor takes account of the area of overlap and the spatial density of both target and projectile beams.

3 Description of the beam-scanning system

Important considerations in the design of the beam scanner were the small beam sizes, the compact size of the scanning system and suitability for operation in a high-vacuum chamber. The pressure in the interaction region was 1.3×10^{-7} Pa (1×10^{-9} Torr) and the total beam currents ranged from 10^{-10} to 10^{-8} A for the ion beam and from 10^{-7} to 10^{-5} A for the electron beam. Other design objectives were good sensitivity to small differences in beam intensities, fast recording of the beam profiles and convenient determination of the form factor.

In the MEIBE an axial magnetic field is used to confine a low-energy electron beam and, in combination with a crossed electric field in a trochoidal analyser, to merge this beam with an ion beam just before the interaction region. After leaving this region the beams are separated by a second trochoidal analyser and a pair of deflection plates.

The mechanical details of the scanning system are shown in figures 1 and 2. Three identical stainless steel scanning sectors are spaced along a motor-driven shaft which is mounted alongside the merged-beam path in the vacuum chamber. The angular displacement between the first and second sectors and between the second and third sectors is 10°. Each sector has a circular-slotted opening through which the beams can pass. The mean radius r of the slot is 71·8 mm (2·828 in). The slot in each sector is interrupted near the midpoint of its arc by a small opaque sector with two straight edges h_1–h_2 and v_1–v_2. When the sector is rotated the beams are scanned first in the horizontal direction by the leading edge h_1–h_2 as the beams are covered and then by the trailing edge v_1–v_2 in the vertical direction as the beams are uncovered again. With the 10° offset between the successive sectors, the beams are scanned consecutively at three different locations. When one of the

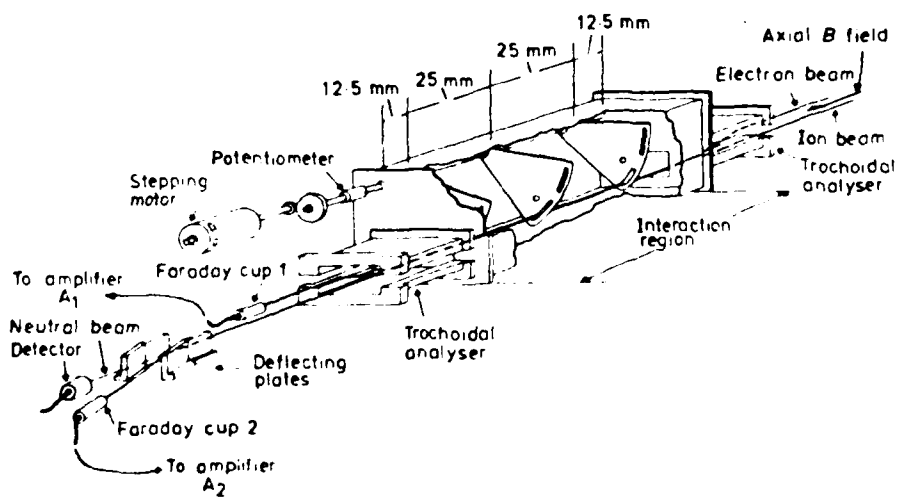

Figure 1 Diagram of the scanning system in the merged-beams experiment. The scanning sectors are shown located in the interaction region.

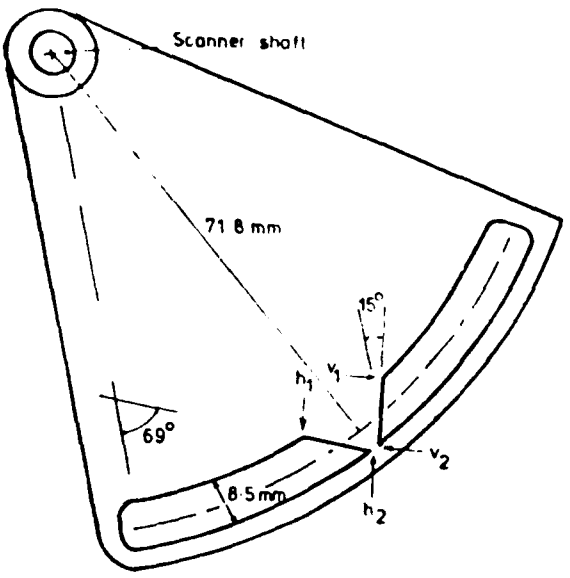

Figure 2 Diagram of a scanning sector.

knife edges interrupts the beams, the currents on the Faraday cups vary according to the beam areas that remain unobstructed. The change in Faraday cup output current as the knife edge moves a small distance δ across a beam is therefore a measure of the beam current in the strip of the beam with width δ that is traversed by the knife edge. By differentiation of the Faraday cup output currents as the knife edge moves with constant speed across the beams the profile of each beam is produced, in the form of current per infinitesimal strip of beam at the instantaneous position of the knife edge.

The electronics are shown in figure 3. In our system, the Faraday cup output currents are fed to amplifiers A_1 and A_2. The outputs of A_1 and A_2 are differentiated by the identical differentiators D_1 and D_2 which provide the horizontal and vertical profiles of both beams. The outputs of D_1 and D_2 are multiplied in the analogue multiplier M which feeds integrator I. The output of I can be used to determine the overlap integral. The high-frequency response of D_1 and D_2 is limited by R_2 and C_2; the high-frequency cut-off is $1/2\pi R_2C_1 = 1/2\pi R_3C_2$. D_1, D_2 and I have the same time constant, $\tau = R_3C_1 = R_4C_3$. The scanners are driven by a stepping motor with a step angle of 1·8° and a gear reduction ratio of 220. The nonlinear motion of the knife edge for one step is so small that the influence on the differentiators is negligible. The angular velocity ω of the scanners ranges from 0·014 to 0·028 rad s^{-1}. The stepping motor was used in order to record a small section of the scan, for convenient speed control and for future computer interfacing. The angular position of the scanners is a function of the output voltage of a potentiometer, which is driven by the scanner shaft. This voltage is applied to the X input of the X–Y recorder.

4 Determination of beam profiles and of the overlap integral of two merged beams from measured quantities

During each scan parts of the beams are intercepted by the shutter and hence the currents measured at the Faraday cups can be expressed in terms of the current densities at the shutter positions:

$$i_H(\epsilon) = \int_{\epsilon}^{a}\int_{-b}^{b} j(x,y)\,dx\,dy \tag{10}$$

$$i_V(\eta) = \int_{-a}^{a}\int_{\eta}^{b} j(x,y)\,dx\,dy \tag{11}$$

where $x = \epsilon$ is the position of the scanner edge during the horizontal scan and $y = \eta$ is its position during the vertical scan, a and b are limiting apertures, and $j(x,y)$ is the current density of either the ion or electron beam.

Electronic differentiation of i_H or i_V during a scan gives

$$\frac{di_H(\epsilon)}{dt} = \frac{di_H(\epsilon)}{d\epsilon}\frac{d\epsilon}{dt} = \frac{d\epsilon}{dt}\int_{-b}^{b} j(\epsilon,y)\,dy \tag{12}$$

$$\frac{di_V(\eta)}{dt} = \frac{di_V(\eta)}{d\eta}\frac{d\eta}{dt} = \frac{d\eta}{dt}\int_{-a}^{a} j(x,\eta)\,dx. \tag{13}$$

These are the current densities integrated over the length of the scanner edge and multiplied by the speed of the edge.

Current measurements made during the scans can be used to calculate the two-dimensional overlap integrals if certain assumptions are made concerning the profiles of the beams. Beam profile measurements show that both beams have profiles that are very nearly Gaussian. We shall therefore assume that the current densities in the beams can be described

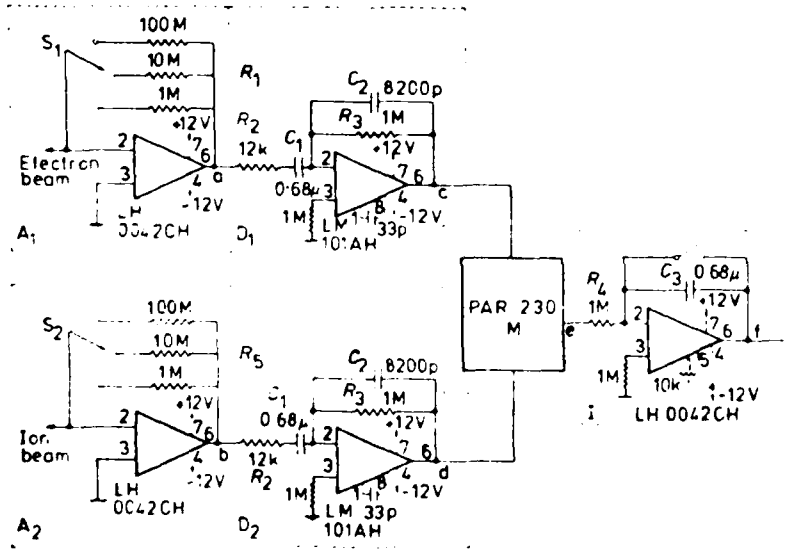

Figure 3 Circuit diagram.

by the expressions

$$j^+(x,y) = J^+ \exp\left(-\frac{x^2}{k_1^2} - \frac{y^2}{k_2^2}\right) \tag{14}$$

$$j^-(x,y) = J^- \exp\left(-\frac{(x-x_0)^2}{k_3^2} - \frac{(y-y_0)^2}{k_4^2}\right) \tag{15}$$

where j^+, j^- are the ion and electron current densities, J^+, J^- are their peak values, k_1, k_2, k_3, k_4 are the halfwidths of the profiles at J/e, and x_0, y_0 are the distances between the centres of the beams measured along the horizontal and vertical axes.

When the scanner edge has moved to a position $x = \epsilon$ during the horizontal scan, so that only that part of the beams for which $x > \epsilon$ passes the shutter, then the currents measured at the Faraday cups can be written (if aperture sizes are much greater than the widths of the beams):

$$I_H^+(\epsilon) = J^+ \int_\epsilon^\infty \exp\left(-\frac{x^2}{k_1^2}\right) dx \int_{-\infty}^{\infty} \exp\left(-\frac{y^2}{k_2^2}\right) dy$$

$$= J^+ \frac{\pi k_1 k_2}{2}\left(1 - \operatorname{erf}\frac{\epsilon}{k_1}\right) \tag{16}$$

and

$$I_H^-(\epsilon) = J^- \frac{\pi k_3 k_4}{2}\left(1 - \operatorname{erf}\frac{\epsilon - x_0}{k_3}\right). \tag{17}$$

Similar expressions are obtained for currents $i_V^+(\eta)$, $i_V^-(\eta)$ measured during the vertical scan when the scanner edge is at $y = \eta$. The total currents in the beams are given by $I^+ = J^+ \pi k_1 k_2$ and $I^- = J^- \pi k_3 k_4$. Electronic differentiation during the horizontal scan produces

$$\frac{di_H^+(\epsilon)}{dt} = \frac{di_H^+(\epsilon)}{d\epsilon}\frac{d\epsilon}{dt} = -J^+ \pi^{1/2} k_2 \exp\left(\frac{-\epsilon^2}{k_1^2}\right)\frac{d\epsilon}{dt} \tag{18}$$

$$\frac{di_H^-(\epsilon)}{dt} = -J^- \pi^{1/2} k_4 \exp\left(-\frac{(\epsilon - x_0)^2}{k_3^2}\right)\frac{d\epsilon}{dt}, \tag{19}$$

and similarly during the vertical scan

$$\frac{di_V^+(\eta)}{dt} = -J^+ \pi^{1/2} k_1 \exp\left(-\frac{\eta^2}{k_2^2}\right)\frac{d\eta}{dt} \tag{20}$$

$$\frac{di_V^-(\eta)}{dt} = -J^- \pi^{1/2} k_3 \exp\left(-\frac{(\eta - y_0)^2}{k_4^2}\right)\frac{d\eta}{dt}. \tag{21}$$

Electronic multiplication of corresponding derivatives of ion and electron currents and integration during the scans result in horizontal and vertical overlap integrals:

$$O^H = \int \frac{di_H^+(\epsilon)}{dt}\frac{di_H^-(\epsilon)}{dt}dt = \frac{d\epsilon}{dt}\int_{-\infty}^{\infty} \frac{di_H^+(\epsilon)}{d\epsilon}\frac{di_H^-(\epsilon)}{d\epsilon}d\epsilon$$

$$= \frac{d\epsilon}{dt} J^+ J^- \pi k_2 k_4 \exp\left(-\frac{x_0^2}{k_1^2 + k_3^2}\right)\frac{k_1 k_3}{(k_1^2 + k_3^2)^{1/2}}\pi^{1/2} \tag{22}$$

$$O^V = \frac{d\eta}{dt} J^+ J^- \pi k_1 k_3 \exp\left(-\frac{y_0^2}{k_2^2 + k_4^2}\right)\frac{k_2 k_4}{(k_2^2 + k_4^2)^{1/2}}\pi^{1/2}. \tag{23}$$

The quantity actually required is the two-dimensional overlap integral:

$$O = \int_{-\infty}^{\infty}\int_{\infty}^{\infty} j^+(x,y) j^-(x,y)\,dx\,dy$$

$$= \int_{-\infty}^{\infty}\int_{\infty}^{\infty} J^+ \exp\left(-\frac{x^2}{k_1^2} - \frac{y^2}{k_2^2}\right) J^- \times \exp\left[-\left(\frac{x - x_0}{k_3^2}\right)^2 - \left(\frac{y - y_0}{k_4^2}\right)^2\right] dx\,dy$$

$$= \frac{J^+ J^- \pi k_1 k_2 k_3 k_4}{(k_1^2 + k_3^2)^{1/2}(k_2^2 + k_4^2)^{1/2}} \exp\left(-\frac{x_0^2}{k_1^2 + k_3^2} - \frac{y_0^2}{k_2^2 + k_4^2}\right). \tag{24}$$

Comparison with equations (22) and (23) shows that the overlap integral can be expressed as

$$O = \frac{O^H O^V}{I^+ I^-}\frac{1}{(d\epsilon/dt)(d\eta/dt)} = \frac{O^H O^V}{I^+ I^-}\frac{1}{\omega^2 r^2} \tag{25}$$

where ω is the angular velocity of the scanners and r is the distance from the axis of rotation of the scanner to the position of the beams. The form factor from equation (9) becomes

$$F = \frac{(I^+)^2 (I^-)^2}{O^H O^V}\omega^2 r^2. \tag{26}$$

5 Beam scanner operation

As the scanners rotate and start intercepting the beams the varying Faraday cup output currents i^- and i^+ are converted by A_1 and A_2 to voltages

$$V_a = -i^- R_1 \tag{27}$$

and

$$V_b = -i^+ R_b \tag{28}$$

where R_1 and R_b are the feedback resistors of A_1 and A_2. The outputs of D_1 and D_2 are

$$V_c = \tau\, dV_a/dt \tag{29}$$

and

$$V_d = \tau\, dV_b/dt. \tag{30}$$

After multiplying V_c by V_d, the output of I is

$$V_I = -(\tau R_1 R_b / V_{ref}) \int_0^t (di^+/dt)(di^-/dt)\,dt \tag{31}$$

where τ is the time constant of D_1 and D_2, and V_{ref} is the

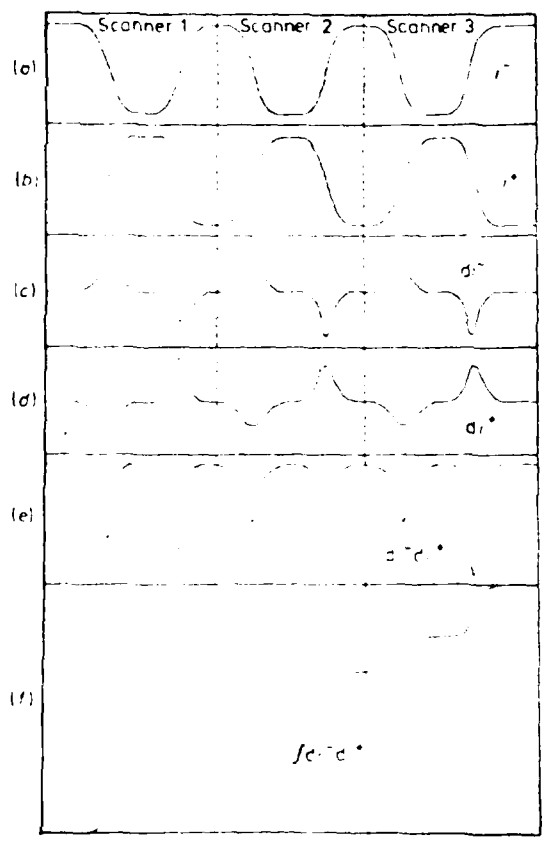

Figure 4 Outputs of the individual elements of the measurement system reproduced on an X-Y recorder.

proportionality constant of multiplier M. ($V_{a,b,c,d,f}$ are measured at points a, b, c, d, f of figure 3.) The horizontal and vertical overlap integrals from equations (22) and (23) can be expressed as

$$O^{H(V)} = V_f^{H(V)} V_{rel} / \omega r \tau R_1 R_b. \tag{32}$$

Then the form factor from equation (26) becomes

$$F = \nu_a^2 \nu_b^2 \omega^2 r^2 \tau^2 / V_f^H V_f^V V_{rel}^2 \tag{33}$$

where ν_a and ν_b are the output voltages of A_1 and A_2 when the beams are not obstructed.

In inclined-beam experiments we only have to scan the beams in the vertical direction, thus the form factor is

$$F = I^- I^+ / O^V = \nu_a \nu_b \omega r \tau / V_f V_{rel}. \tag{34}$$

Figure 4 shows the results, associated with actual scans, reproduced on an X–Y recorder. The intercepted beam currents are shown in (*a*) and (*b*), the horizontal and vertical beam profiles in (*c*) and (*d*), the products of these profiles in (*e*) and the horizontal and vertical overlap integrals in (*f*).

Under normal operating conditions the positions of the beams are adjusted until the ion beam contains the electron beam and the merged beams are aligned along the axis of the interaction region.

The average values of the three horizontal and three vertical overlap integrals are used to calculate the form factor F from equation (33). The system has been used with the MEIBE and has been found to be a fast and accurate way of checking beam positions and determining the form factor.

Acknowledgment

This work was supported by the National Research Council of Canada (Natural Sciences and Engineering Research Council) and the US Department of Energy.

References

Auerbach D, Cacak R, Caudano R, Gaily T D, Keyser C J, McGowan J W, Mitchell J B A and Wilk S F J 1977 Merged electron–ion experiments I. Methods and measurements of (e–H_2^+) and (e–H_3^+) dissociative-recombination cross-sections
J. Phys. B. Atom. Molec. Phys. **10** 3797–819

Bond C D and Gordon S E 1972 A wide-aperture high-gain beam profile scanner
Nucl. Instrum. Meth. **98** 513–23

Dolder K T 1969 *Case Studies in Atomic Collision Physics* vol 1 ed E W McDaniel and M R C McDowell (Amsterdam: North-Holland) pp 249–334

Harrison M F A 1966 The determination of atomic collision cross-sections using crossed electron and ion beams (and some sources of error in such experiments)
Br. J. Appl. Phys. **17** 371–82

Hortig G 1964 A beam scanner for two-dimensional scanning with one rotating wire
Nucl. Instrum. Meth. **30** 355–6

Jagger J W, Page J G and Riley P J 1967 A simple ion beam scanner
Nucl. Instrum. Meth. **49** 121–4

Nitz D E, Geis M W, Smith K A and Rundel R D 1976 Rapid determination of the overlap integral in a merging-beam system
Rev. Sci. Instrum. **47** 306–10

Prudnikov I A, Toropov A S, Chichikalov Yu F and Khokhryakov I V 1974 Device for determination of charged-particle beam profile and position
Nucl. Instrum. Meth. **114** 101–4

Sethuraman S K, Gibson J R and Moruzzi J L 1977 An automatic beam-scanning system in merged-beams experiments
J. Phys. E: Sci. Instrum. **10** 14–6

APPENDIX B.

PRODUCTION OF LOW VIBRATIONAL STATE H_2^+ IONS FOR DISSOCIATIVE RECOMBINATION STUDIES

Amarjit Sen*, J. Wm. McGowan† and J.B.A. Mitchell
Department of Physics and
Centre for Chemical Physics
The University of Western Ontario
London, Ontario, Canada. N6A 3K7

ABSTRACT

A storage ion source (Teloy & Gehrlich, 1974) based on the principle of confinement of charged particles by inhomogeneous oscillatory electric fields, has been built for the production of H_2^+ ions in low vibrational states. Using a gas mixture of H_2 and rare gases (Ne and He) in the ion source at high pressure, higher vibrational states of H_2^+ ions have been effectively quenched by ion-molecule reactions and collisional deactivation. A low-energy crossed ion-atom beam apparatus has been built for determining the internal energy of the H_2^+ ions by the threshold measurement of collisional dissociation with a He jet. With a H_2+Ne mixture (1:5 ratio) in the source at 80 mtorr, the H_2^+ ions are found to be in v=0 and 1 states only.

*Argonne National Laboratory, Argonne, Illinois 60439, USA.
†Director, National Museum of Science and Technology,
1867 St. Laurent Blvd, Ottawa, Ontario. Canada. K1A 0M8

INSPEC NO: 34.50, 35.20, 41.80 G

INTRODUCTION

Reaction rates for atomic collision processes are often very sensitive to the initial state of excitation of the reactants. This is particularly true for endothermic reactions in which an energy threshold must be reached before the reaction can proceed. Experimental studies of such processes frequently involve the use of reactants whose excitation state populations are not well defined and so it is difficult to make comparisons with theoretical analyses which assume initial energy states to be known. Studies of collisions involving molecular ions offer particularly serious problems in this regard since the ions are usually formed with a range of vibrational and rotational energy states populated. In some cases electronic excitation may also be present. A comprehensive review of the effects of internal excitation on reaction rates and of methods of controlling and measuring excited state populations has been given by Tiernan and Lifschitz, (1981).

The purpose of the present paper is to describe the production of H_2^+ ions with low internal energies by ion-molecule reactions in a storage ion source. This paper deals with experimental determination of the internal energies of H_2^+ ions by collision-induced dissociation measurements. Studies involving H_3^+ ions with low internal energies are described separately (Sen & Mitchell, 1986). Preliminary reports of these experiments have been presented elsewhere. Sen et al, 1985a,b,c.

The impetus for this study comes from the need for low vibrational state ion beams for use in studies of electron-molecular ion recombination. Over the last few years, a number of measure-

ments of the dissociative recombination, (DR) of molecular ions with electrons have been made in this laboratory using the merged beam technique. Mitchell and McGowan (1983), McGowan and Mitchell (1985). DR is believed to proceed via the capture of electrons into a doubly excited autoionizing state of the neutral molecule which subsequently dissociates carrying away the excess recombination energy in the form of kinetic energy of the dissociation products. In this way, the recombination is stabilized. Fig. 1 shows the potential energy curves for H_2 and H_2^+. The electron is

believed to be captured into the $^1\Sigma_u^+$ state thus: -

$$e + H_2^+(^2\Sigma_g^+, v) \rightarrow H_2^{**}(^1\Sigma_u^+) \rightarrow H(1S) + H(nl)$$

The intermediate autoionizing state is diabatic in form and its energy has been calculated by Guberman, (1983) and by Hazi et al, (1983). It can be seen that this state intersects the ground electronic state of the H_2^+ in the vicinity of the v=2 level. This means that the probability for low energy electrons recombining with H_2^+ ions in the v=0 or 1 states should be small (Guisti-Suzor et al, 1983). A fuller discussion of this topic is given by Mitchell, (1986).

H_2^+ is a homonuclear molecule so that vibrational states cannot decay via dipole transitions. Lifetimes for decay through electric-quadrupole transitions have been calculated by Bates and Poots, (1953), giving typical values of 10^6 secs.

In Fig. 1 it can be seen that the ground state of H_2^+ is offset from that of H_2 so that H_2^+ ions formed from the impact of energetic electrons on H_2 will have all 19 available vibrational states populated according to a Franck-Condon distribution. Von Busch and Dunn, (1972) measured the photodissociation of H_2^+ ions and by comparing their results with cross sections for individual vibrational state transitions, calculated by Dunn (1968), they were able to determine the vibrational population of the H_2^+ ions. They found that their measured distribution resembled the Franck-Condon distribution quite closely although some redistribution of energy towards lower vibrational states was noted.

The Von Busch and Dunn distribution is compared with the calculated Franck-Condon distribution in Table I. It can be seen that 90% of all the ions have $v \leq 6$ with the distribution peaked around $v=2$.

Brenton et al (1984) have used a measurement of the translational energy spectra of the H^++H products arising from 6KeV H_2^+ + He collisions to determine the vibrational state distributions of H_2^+ ions formed from electron impact with 19 different precursor molecules. Essentially they found very little difference from the Von Busch and Dunn distribution.

Chupka and Russell, (1968) have used photoionization techniques to study ion molecule reactions involving state selected H_2^+ ions and the inert gases Helium and Neon, namely: -

T A B L E I

H_2^+

VIBRATIONAL POPULATIONS

v	Von-Busch & Dunn	Franck-Condon	Energy below (ev) Dissociation Limit
0	0.119	0.092	2.645
1	0.190	0.162	2.374
2	0.188	0.176	2.118
3	0.152	0.155	1.877
4	0.125	0.121	1.651
5	0.075	0.089	1.44
6	0.052	0.063	1.243
7	0.037	0.044	1.059
8	0.024	0.030	0.890
9	0.016	0.021	0.734
10	0.0117	0.0147	0.593
11	0.0082	0.0103	0.465
12	0.0057	0.0072	0.351
13	0.00374	0.0051	0.252
14	0.00258	0.0036	0.168
15	0.00175	0.0024	0.100
16	0.00109	0.0016	0.0491
17	0.00056	0.0008	0.027
18	0.00012	0.0002	0.002

Taken from Cohen et al, 1960.

$$H_2^+(v \geq 3) + He \rightarrow HeH^+ + H$$

$$H_2^+(v \geq 2) + Ne \rightarrow NeH^+ + H$$

These reactions are both endothermic for lower v. They are found however to have large rate coefficients for H_2^+ ions with vibrational levels greater than 3 or 2 respectively. Hence in an ion source, such states will react away so that the emerging beam of H_2^+ ions will have only the 0, 1 and 2-levels, or the 0 and 1 levels populated. Theard and Huntress (1974) have shown that H_2^+ ions can also be vibrationally de-excited in non-reactive encounters with Helium and Hydrogen gases. Such events will help to lower the average population of vibrational states even further. This presupposes however that the H_2^+ ions have sufficient time inside the source to complete their reactions.

Herman and Pacak, (1977) have used reactive quenching to prepare vibrationally selected beams of H_2^+. The H_2^+ ions were formed in an electron impact source which operated with a 5:1 Neon, Hydrogen mixture at a pressure of $5 \times 10^{-2} - 10^{-1}$ Torr. Collision induced dissociation of the H_2^+ ions with Helium atoms was studied and it was found that for the H_2/Ne mixture, this reaction exhibited an energy threshold at 2.1 - 2.2 eV. This indicated that indeed higher vibrational states were removed although comparison with Table I indicated that perhaps v=2 states were present in the beam.

A number of experimental measurements of the dissociative recombination of H_2^+ have been performed using a variety of intersecting beam techniques*. Peart and Dolder, (1973/74), McGowan and Mitchell, (1977), Phaneuf et al, (1975), Vogler & Dunn (1975). In all these experiments the ions were in a range of vibrational states. An attempt to quench the higher states was made by Auerbach et al, (1977) by using a H_2/He mixture in the R.F. ion source used to prepare the ions. It was found that this caused a factor of 2 decrease in the cross section. McGowan and Mitchell, (1977) repeated this measurement and also tried a H_2/Ne mixture which led to a further decrease of a factor of 1.6

Sen (1985) has modelled the ion chemistry in the R.F. ion source in order to calculate the vibrational population of the emerging ions. Blakley et al, (1977) have shown that the residence time for ions in a source is given by: -

$$\tau_{RES} \sim (1/D_a) \cdot (r/2.4)^2$$

where Da is the ambipolar diffusion coefficient and r is the radius of the cylindrical ion source. Using diffusion coefficient data of Brown (1966) the residence time for the source used by Auerbach et al was calculated to be 30μs. The modelling procedure used by Sen (1985) is described by Theard and Huntress.

*(H_2^+ recombination cannot be studied using plasma techniques since the reaction $H_2^+ + H_2 \rightarrow H_3^+ + H$ rapidly dominates the loss of the H_2^+ ions.)

It was found that for typical source operating pressures, states up to v = 6 were still populated. This indicates that the r.f. source is not suitable for state selection since the residence time of the ions in the source is too short.

The ion source described in this paper is based on the design of Teloy and Gerlich, (1974). It uses an oscillatory inhomogeneous electric field to trap and guide slow ions in a specially designed cavity. In this way ions are stored for several milliseconds enabling them to make many de-exciting collisions.

THE TELOY SOURCE

Teloy and Gerlich, (1974) have described an ion source which they designed and constructed to produce ion beams with very low internal energies. In their source, electron bombardment is used to create ions from the source gas. These ions are then trapped for several milliseconds using an inhomogeneous oscillating electric field. This gives them time to make many de-exciting collisions. The principle of ion trapping using an inhomogeneous radiofrequency field is described in their paper. Within the field region an effective potential is set up which is given by:

$$V_{eff} = \frac{e^2 E_{ac}^2 (r)}{4 m w^2} + e V_s(r_0)$$

Here E_{ac} is the amplitude and w the angular frequency of the applied r.f. field. m is the ion mass and V_s is a static potential set up by a superimposed d.c. electric field. Fields can be arranged so that this potential describes a well within which the ion can be trapped.

The ion source consists of a stack of ten parallel and equi-spaced stainless steel plates, (6.35 cm x 2.54 cm x .157 cm) which are separated by 2 mm diameter sapphire balls. See Fig. 2. Each plate has a U - shaped channel cut in it, except for the top and bottom plates which have a rectangular slot, (4.4 cm x .13cm) located adjacent to one limb of the U-channel. All plates were electropolished. Alternate plates are connected together electrically to form two sets of electrodes which are in turn connected to a radiofrequency power source.

The top and bottom plates have a small (~2V) positive dc bias voltage applied with respect to the mean potential of the r.f. plates, to repell positive ions. The whole set of plates is also maintained at a dc voltage of (214 V) to assist with the eventual extraction of the ions.

A thoriated tungsten (1% Th) filament wire (0.25 mm diameter) is mounted above the slit which when heated provides the ionizing electron beam. The stack of plates is mounted horizontally on a vertical stainless steel flange. A gas feed line is connected to the latter.

Electrons from the filament are accelerated by a potential of 100V between the filament and the top plate into one limb of the U-channel where ions are formed by electron impact ionization of the source gas. The ions diffuse around the U-channel, trapped by the applied r.f. and d.c. fields before being extracted through an exit hole in the other limb. This exit hole is specially shaped so that it has an octopolar geometry by fitting short stainless rods to the five middle plates. (Fig. 2). This multipole configuration assists in the focussing of the emerging stream of ions allowing for efficient transport to the following optical elements.

Typical operating parameters of the ion source are listed in Table II.

T A B L E I I

Filament voltage	7 V
Filament current	5 A
Electron energy	100 eV
Electron current	0.1 mA
R.F. frequency	17.5 MHz
R.F. Amplitude	100 - 160 V_{pp}
Gas pressure	10 - 100 m Torr
Ion current extracted	5×10^{-8} A

EXPERIMENTAL APPARATUS

An ion-atom crossed beam apparatus has been constructed for the study of collision induced dissociation, (CID), and ion-molecule reactions at low energies. Fig. 3 shows a schematic of the experimental arrangement.

Ions from the Teloy source are extracted at 214 eV and are focussed by an einzel lens onto a collimating aperture through which the beam enters the main interaction region. The ions are mass selected by the Wien filter and enter a multi-element electrostatic lens system which produces a monoenergetic low-energy ion beam. Sen, (1985). This system is based upon an original design of Gustafsson and Lindholm, (1962), modified by Herman et al, (1969). The ions enter the collision region which is maintained at the potential of the last element of the deceleration lens. This therefore determines the energy of the beam in the collision region.

The neutral target beam is produced using a collimated hole structure, (Typical hole diameter 5 microns), to form a gas jet. The jet is directed vertically downwards into the throat of a trapped diffusion pump.

The ion beam and the neutral jet intersect at right angles. Following the collision the primary and product ions are accelerated by the post collision acceleration system and are focussed by an electrostatic quadrupole lens onto the entrance slit of the magnetic sector mass spectrometer. The ions are finally collected using a channel electron multiplier. The (CID) reaction

is studied by monitoring the number of H^+ ions arising from the collision of H_2^+ with He atoms.

Since there was always some residual gas in the chambers, collisional dissociation of H_2^+ with the residual gas molecules, X, gave rise to unwanted H^+ ions which formed the background i.e., $H_2^+ + X \rightarrow H^+ + H + X$. Also some H^+ were formed as a result collisions of primary H_2^+ with aperture edges. These extraneous background H^+ ions were separated from the signal H^+ by modulation of the neutral He beam. This modulation was performed manually with the help of two identical molecular beams.

As mentioned earlier, the primary molecular jet intersected the ion beam at right angles at the interaction region. A secondary jet was located outside the interaction region. Both the jets were connected to the same gas supply with a valve system that allowed one or the other to be operated at a given time. With the primary jet 'OFF' and secondary jet 'ON', the product H^+ ions detected on the channeltron represented the background, B. Then, with the secondary jet 'OFF' and the primary jet 'ON', the product H^+ ions detected on the channeltron were the signal plus background, S+B.

The purpose of the secondary jet was to keep the pressure in the chamber constant at all times thereby making the background contribution the same in each modulation interval. It was assumed that other experimental conditions remained fairly stable during each modulation interval (of the order of a few minutes).

Data were normalized with respect to the same number of primary H_2^+ ion counts in each interval. Therefore, the two backgrounds were presumed to remain the same and the true signal was obtained as the difference of the two, i.e., (S+B) - B = S.

It is important to recognize that there are two distinct backgrounds formed in the collisional dissociation process depending on their origin. The first, background 1, is due to the product H^+ ions formed in the interaction region which are subsequently accelerated by the acceleration voltage, V_{AC}. These H^+ ions have an energy approximately half the energy, V_I, of the primary H_2^+ ions in that region plus V_{AC}. i.e. ($\frac{1}{2}V_I + V_{AC}$). The second, Background 2, is formed due to dissociation of primary H_2^+ ions after the post acceleration system. Thus, these product H^+ ions have an energy equal to half the total energy of the primary H_2^+ ions, i.e. 1/2 ($V_{AC} + V_I$). Obviously, these two sets of background products will have different energies and so will require different magnetic field strength to deflect them into the detector, thus allowing for their discrimination.

The absolute density of the Helium atom jet was not determined so absolute cross sections for CID could not be measured in this experiment. Care was taken, however, to ensure that jet parameters were held constant throughout the measurements so that relative cross sections could be obtained.

STUDIES OF COLLISION INDUCED DISSOCIATION

The collision induced dissociation, (CID), of H_2^+ ions colliding with helium atoms has been studied down to 0.6 eV centre of mass energy using the crossed beam apparatus. From these measurements, the thresholds for dissociation and hence the internal energy of the ions was determined.

The CID of H_2^+ by Helium is represented thus: -

$$H_2^+ (v) + He \rightarrow H^+ + H + He$$

The process is endothermic by 2.65 eV for ground state, v=0, H_2^+ ions. If H_2^+ ions are present in the beam with higher vibrational states, the endothermicity will be less, See Table I, and so the threshold for the appearance of H^+ will decrease, indicating the presence of excited states.

Collision induced dissociation of diatomic molecular ions has been explained by a two-step model, Los and Govers, (1978). In the first step, the molecular ion is excited to an electronic (repulsive) state or to the vibrational-rotational continuum of the ion. In the second step, the ion dissociates into a neutral and a charged fragment. When the collision occurs in a time smaller than the vibrational period, it is likely that the two aspects of the process can be treated separately.

At high collision energies, (keV range), the CID of H_2^+ by He is assumed to proceed through vertical Franck-Condon type transitions from the $1s\sigma_g$ ground state to the first excited $2p\sigma_u$ state. Caudano et al, (1962), Gibson and Los, (1967), Los and Govers,

(1978), Meierjohann and Vogler, (1976/77), Jaecks et al (1983) and Durup et al, (1969). This excited state then dissociates. At low collision energies, (few eV), the process of CID departs substantially from the Franck-Condon transitions and non-vertical or diagonal transitions, to the vibrational-rotational continuum predominate as a result of slow collisions, McGowan and Kerwin, (1964) and Vance and Bailey, (1966). These studies indicate that a large amount of energy transfer is involved which implies that the collisions must be quite intimate.

Since the amount of vibrational quenching in the ion source depends on the type and number of ion-molecule reactions occurring, the source was operated at different pressures and with different gas mixtures.

Figure 4 shows relative cross sections for H^+ fragment production from H_2^+ + He collisions, plotted as a function of energy. Both the laboratory and the centre of mass energies are shown together with the positions of the thresholds corresponding to each initial vibrational state. For the H_2^+ + He system the centre of mass collision energy is 2/3 of the laboratory kinetic energy of the H_2^+ ions. (The thermal velocities of the helium atoms being much less than the ion velocity).

The uncertainty in the primary ion energy at the lowest value of energy is 0.1 eV. Vertical error bars in Fig. 4 show statistical fluctuations in the measured signals. Near threshold, the number of product H^+ ion signals is very small and so statistical errors are quite large.

With H_2 gas in the source, operated at low pressures, (10 m Torr) the threshold for H^+ production is close to 0.6 eV indicating that vibrational levels as high as v = 9 are present in the beam. By increasing the pressure, the threshold could be raised indicating that higher states were being quenched. This effect was not very strong however and at 50 m torr pressure, states with v = 6 were still present in the beam.

When a H_2/Ne mixture (1:5) was used however the quenching of the higher states was much more effective as can be seen from the figure. In this case the threshold shifted to 2.3 eV indicating that most of the H_2^+ ions were in the v = 0 or 1 levels. This shows that the ions are stored for a sufficient time to allow the quenching reactions to remove all the higher levels. Similar results were found when a H_2/He mixture was used except as expected, the H_2^+ beam was found to contain v = 0, 1 and 2 levels.

These experiments were repeated with a colutron ion source in place of the Teloy source. This is a commercially available arc discharge type of source (Colutron Research Corporation, USA) which operates at a fairly high pressure, (100 m torr). Fig. 5 shows the results obtained with this source using a similar H_2/Ne mixture. Here the threshold is in the vicinity of 1.0 eV implying that higher vibrational states are present. This result shows the importance of source residence time on the resulting internal energy distribution of the ions.

ACKNOWLEDGEMENT

The authors would like to acknowledge E. Teloy and D. Gerlich for helpful discussions concerning the design of the ion source.

Work supported by the Canadian National Science and Engineering Research Council, the U.S. Department of Energy and the U.S. Air Force Office of Scientific Research.

FIGURE CAPTIONS

1. Energy levels for H_2^+ and H_2 relevant to the dissociative recombination process.

2. The storage ion source showing the arrangement of the plates with u-channels and Octupolar exit hole.

3. Schematic diagram of the crossed beam apparatus. The potentials in the different regions are shown ion the lower part.

4. Relative cross sections for the CID of H_2^+ formed in the storage ion source with pure H_2 and a mixture of H_2 and Ne (1:5). Threshold energies for the different vibrational levels of H_2^+ are shown.

5. Relative cross sections for the CID of H_2^+ ions formed in a colution source with a mixture of H_2 and Ne (1:5). Threshold energies for the different vibrational levels of H_2^+ are shown along the energy axis.

REFERENCES

1. Auerbach, D., R. Cacak, R. Caudano, T.D. Gaily, C.J. Keyser, J.Wm. McGowan, J.B.A. Mitchell and S.F.J. Wilk, (1977), J. Phys. B10, 3797.
2. Blakley, C.R., M.L. Vestal and J.H. Futrell, (1977) J. Chem. Phys. 66, 2392,.
3. Brenton, A.G., P.G. Fournier, B.L. Govers, E.G. Richard, and J.H. Beynon (1984), Proc. R. Soc. A. 395, 111.
4. Brown, S.C., (1966), Basic Data of Plasma Physics. (The MIT Press, Cambridge, MA).
5. Caudano, R., J.M. Delfosse, J. Steyaert, (1962) J. Ann. Soc. Sci. Bruxelles Ser. 176, 127 (1962).
6. Chupka, W.A. and M.E. Russell (1968) J. Chem. Phys. 48 1518.
7. Cohen, S., J.R. Hiskes and R.J. Riddell, (1960), UCRL-8871.
8. Dunn, G.H., (1968), Phys. Rev. 172, 1.
9. Durup, J., P. Fournier and P. Dong, (1969), Int. J. Mass. Spect. and Ion Phys. 2, 311.
10. Gibson, D.K. and J. Los, (1967), J. Physica 35, 258.
11. Guberman, S.L., (1983), J. Chem. Phys. 78, 1404.
12. Guisti-Suzor, A., J.N. Bardsley and C. Derkits, (1983) Phys. Rev. 28A, 682.
13. Gustafsson, E. and E. Lindholm, (1960), Arkiv Fysik 18, 219.
14. Hazi, A.U., C. Derkits and J.N. Bardsley, (1983), Phys. Rev. A. 27, 1751.

15. Herman, Z., J. D. Kerstetter, T. L. Rose and R. Wolfgang (1969) Rev. Sci. Instrum. 40, 538.

16. Herman, Z. and V. Pac'ak, (1977), Int. J. Mass Spectrom. and Ion Phys. 24, 355.

17. Jaecks, D.H., O. Yenen, M. Natarajan and M. Mueller, (1983), Phys. Rev. Lett. 50, 825.

18. Los, J. and T.R. Govers, (1978), In Collision Spectroscopy, ed. R.G. Cooks, (Plenum Press, New York).

19. McGowan, J. Wm. and L. Kerwin, (1964) Can. J. Phys. 42, 972.

20. McGowan, J. Wm. and J. B. A. Mitchell, (1977), Abstracts of Papers, ICPEAC, Paris.

21. McGowan, J. Wm. and J.B.A. Mitchell (1984) in Electron Molecule Interactions and Their Applications, Vol. 2, ed. L.G. Christophorou, Academic Press, Inc., N.Y.

22. Meierjohann, B. and M. Vogler, (1976), J. Phys. B. 9, 1801.

23. Meierjohann, B. and M. Vogler, (1977), J. Phys. A 282, 7.

24. Mitchell, J.B.A. and J.Wm. McGowan (1983) in Physics of Ion-Ion and Electron-Ion Collisions, Nato ASI, Baddeck, Nova Scotia, eds. F. Brouillard and J.Wm. McGowan, Plenum Press N.Y. p. 279.

25. Mitchell, J.B.A., (1986) in Physics of Electron-Ion and Ion-Ion Collisions, NATO ASI Han-sur-Lesse, Belgium Collisions ed. F. Brouillard, Plenum Press, N.Y. (to be published).

26. Peart, B. and K.T. Dolder, (1974), J. Phys. B7, 236.

27. Peart, B. and K.T. Dolder, (1973), J. Phys. B6, L. 359.

28. Sen, A., Ph.D. Thesis (1985), The University of Western Ontario.

29. Sen, A. and J.B.A. Mitchell, (1985b), Abstracts of Papers XIVth ICPEAC, Stanford, p. 600.

30. Sen, A., J.Wm. McGowan and J.B.A. Mitchell (1985a) Abstracts of Papers, XIVth ICPEAC Stanford, p. 667.

31. Sen, A. and J. B. A. Mitchell, (1985c) Abstract of papers, SNEAP-85, Argonne National Laboratory, Argonne.

32. Sen, A. and J.B.A. Mitchell, (1986), (In preparation).

33. Teloy, E. and D. Gerlich, (1974), Chem. Phys. 4, 417.

34. Theard, L.P. and W.T. Huntress Jr., (1974), Chem. Phys. 60, 2840.

35. Tiernan, T.O. and C. Lifschitz, (1981) in the Excited State in Chemical Physics Part 2. ed. J. Wm. McGowan, Adv. Chem. XLV, 82.

36. Vance, D.W. and T.L. Bailey, (1966) J. Chem. Phys. 49, 3411.

37. VonBusch, F. and G.H. Dunn, (1972), Phys. Rev. A5, 1726.

38. Vogler, M. and G. H. Dunn, (1983), Phys. Rev. A11, 1975.

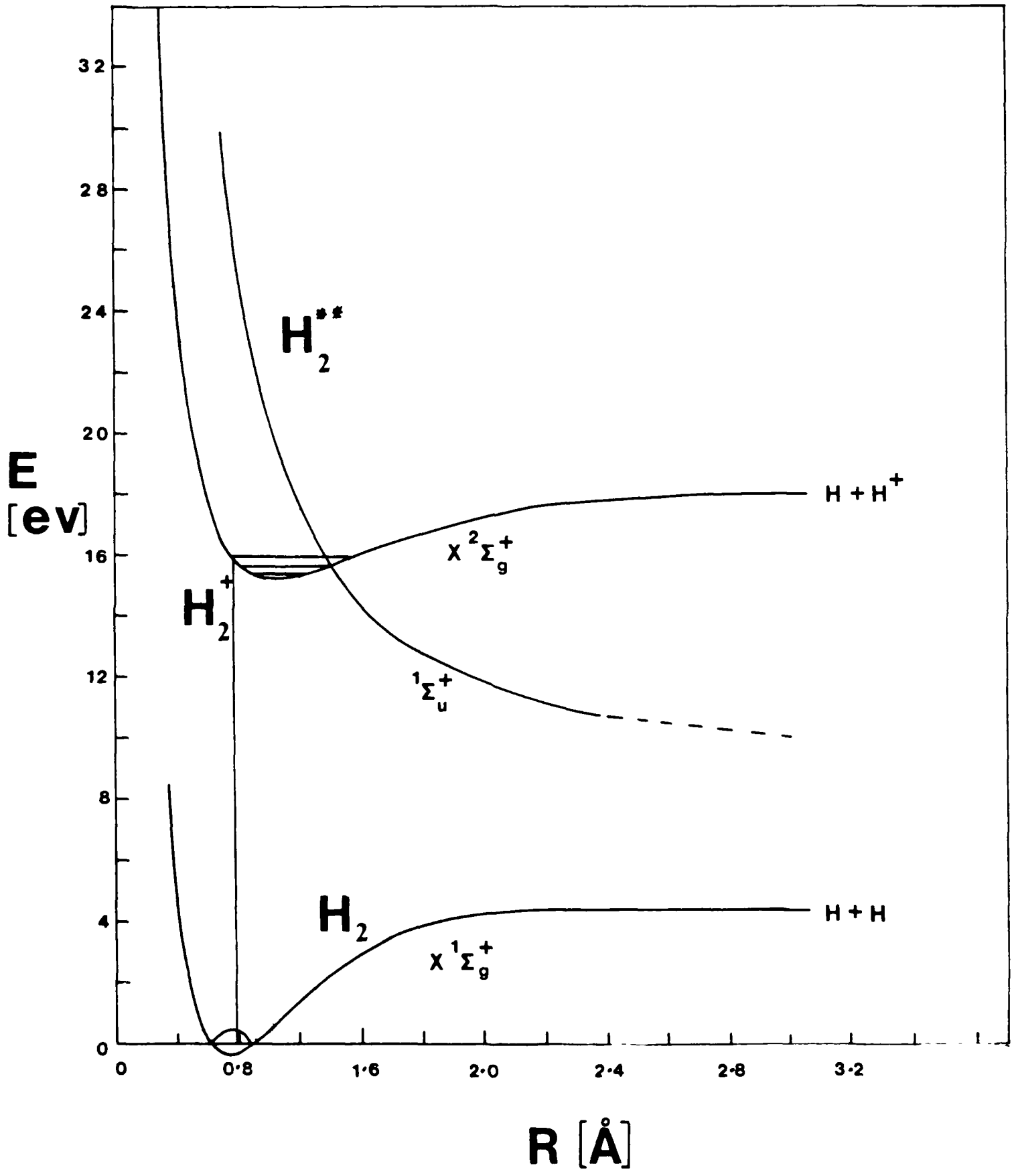
E
[ev]
32
28
24
20
16
12
8
4
0
0
0·8
1·6
2·0
2·4
2·8
3·2
R [Å]
H₂**
H₂⁺
H₂
X ²Σg⁺
¹Σu⁺
X ¹Σg⁺
H + H⁺
H + H

STORAGE ION SOURCE

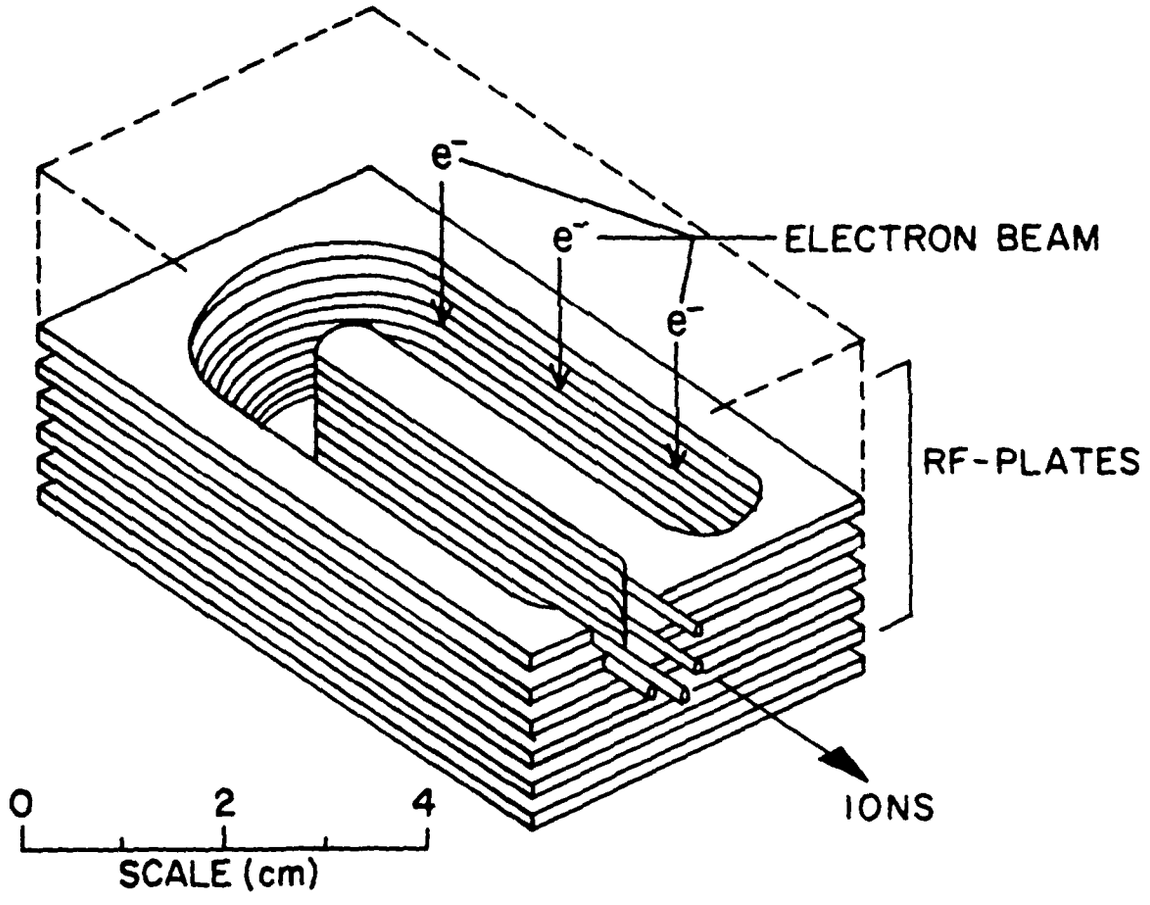

ANL-P-18,033

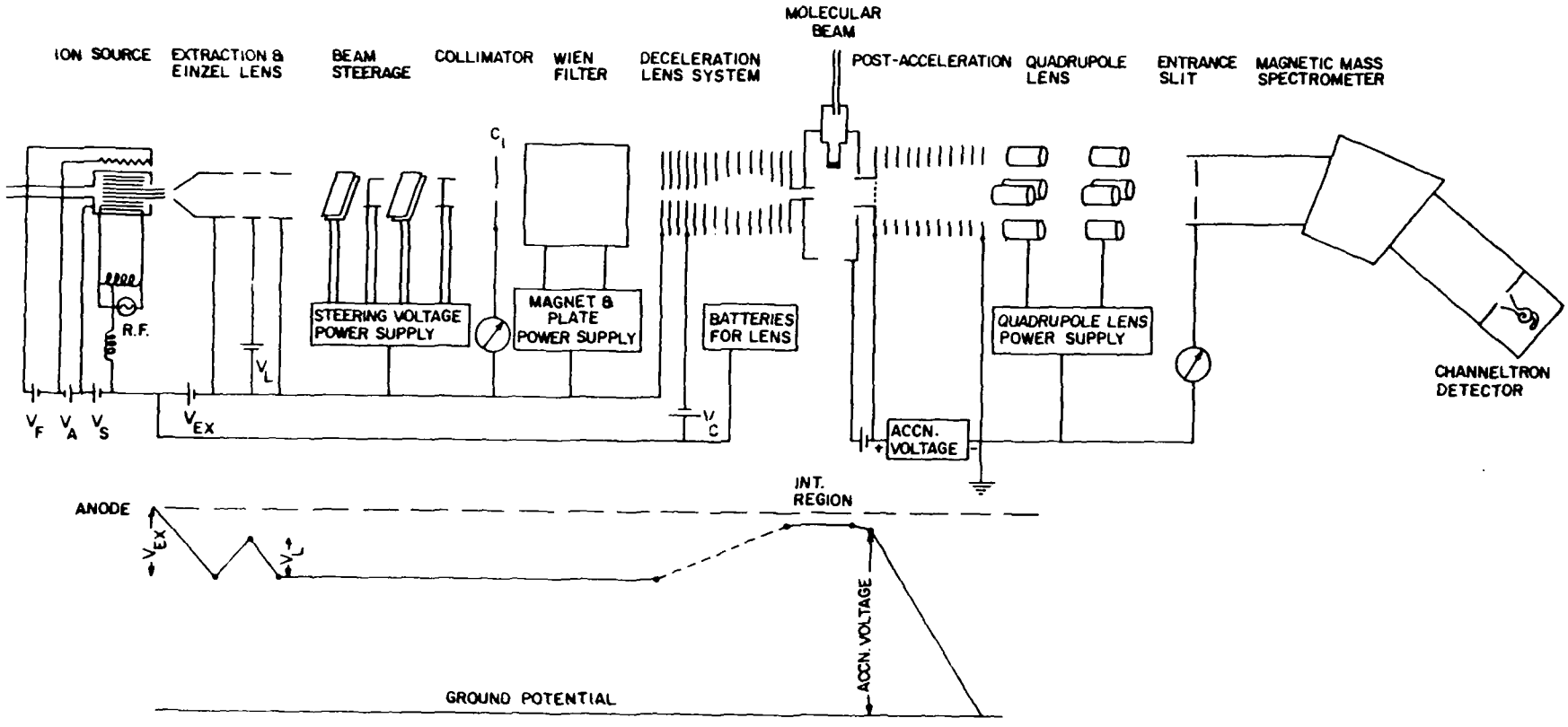
ION SOURCE
EXTRACTION & EINZEL LENS
BEAM STEERAGE
COLLIMATOR
WIEN FILTER
DECELERATION LENS SYSTEM
MOLECULAR BEAM
POST-ACCELERATION
QUADRUPOLE LENS
ENTRANCE SLIT
MAGNETIC MASS SPECTROMETER
R.F.
STEERING VOLTAGE POWER SUPPLY
MAGNET & PLATE POWER SUPPLY
BATTERIES FOR LENS
QUADRUPOLE LENS POWER SUPPLY
CHANNELTRON DETECTOR
ACCN. VOLTAGE
V_F V_A V_S
V_{EX}
V_L
V_C
C_1
ANODE
INT. REGION
V_{EX}
V_L
ACCN. VOLTAGE
GROUND POTENTIAL

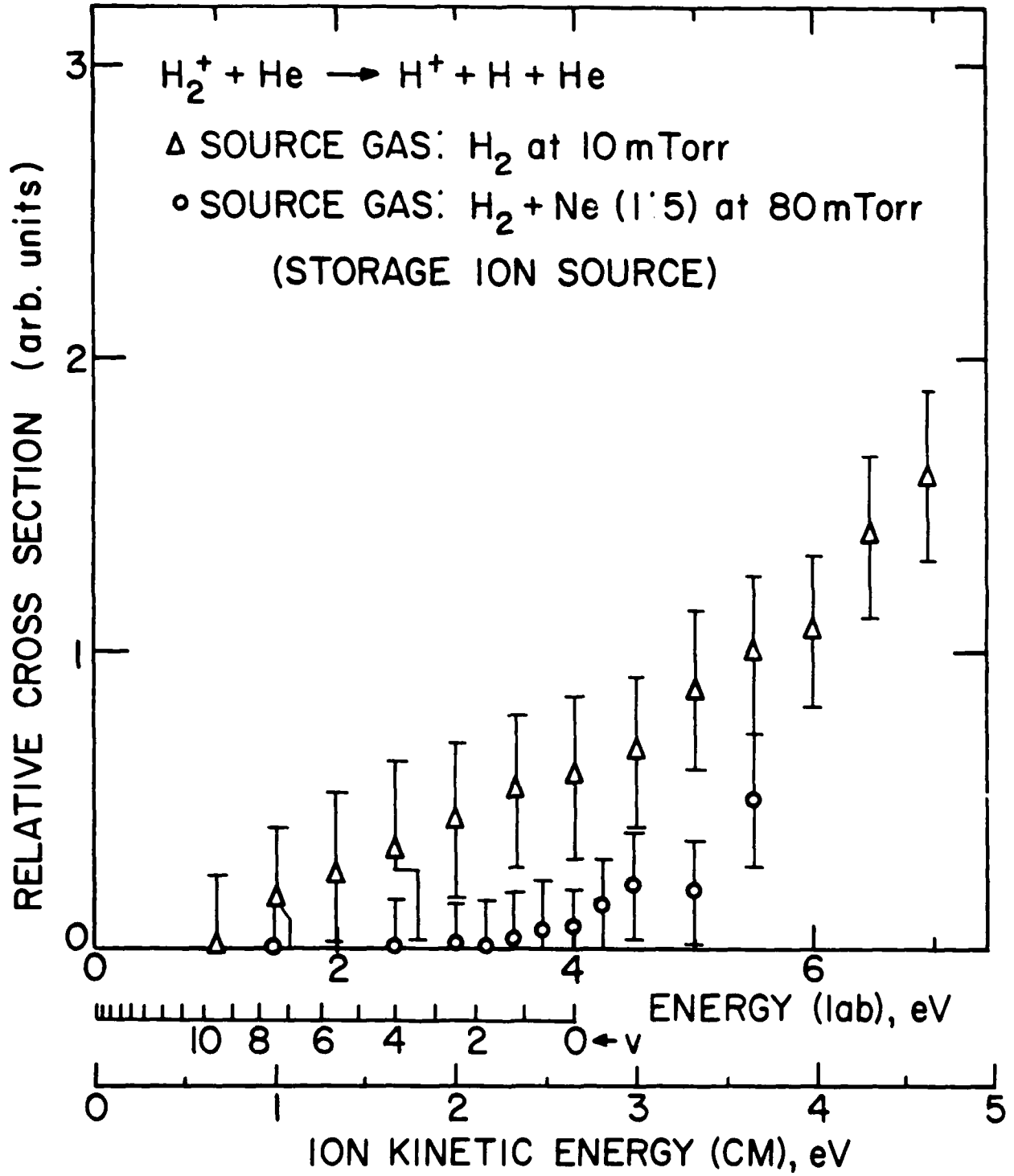
$H_2^+ + He \rightarrow H^+ + H + He$
△ SOURCE GAS: H_2 at 10 mTorr
○ SOURCE GAS: H_2 + Ne (1:5) at 80 mTorr
(STORAGE ION SOURCE)
RELATIVE CROSS SECTION (arb. units)
0
1
2
3
0
2
4
6
ENERGY (lab), eV
10 8 6 4 2 0 ← v
0
1
2
3
4
5
ION KINETIC ENERGY (CM), eV

ANL-P-18,031

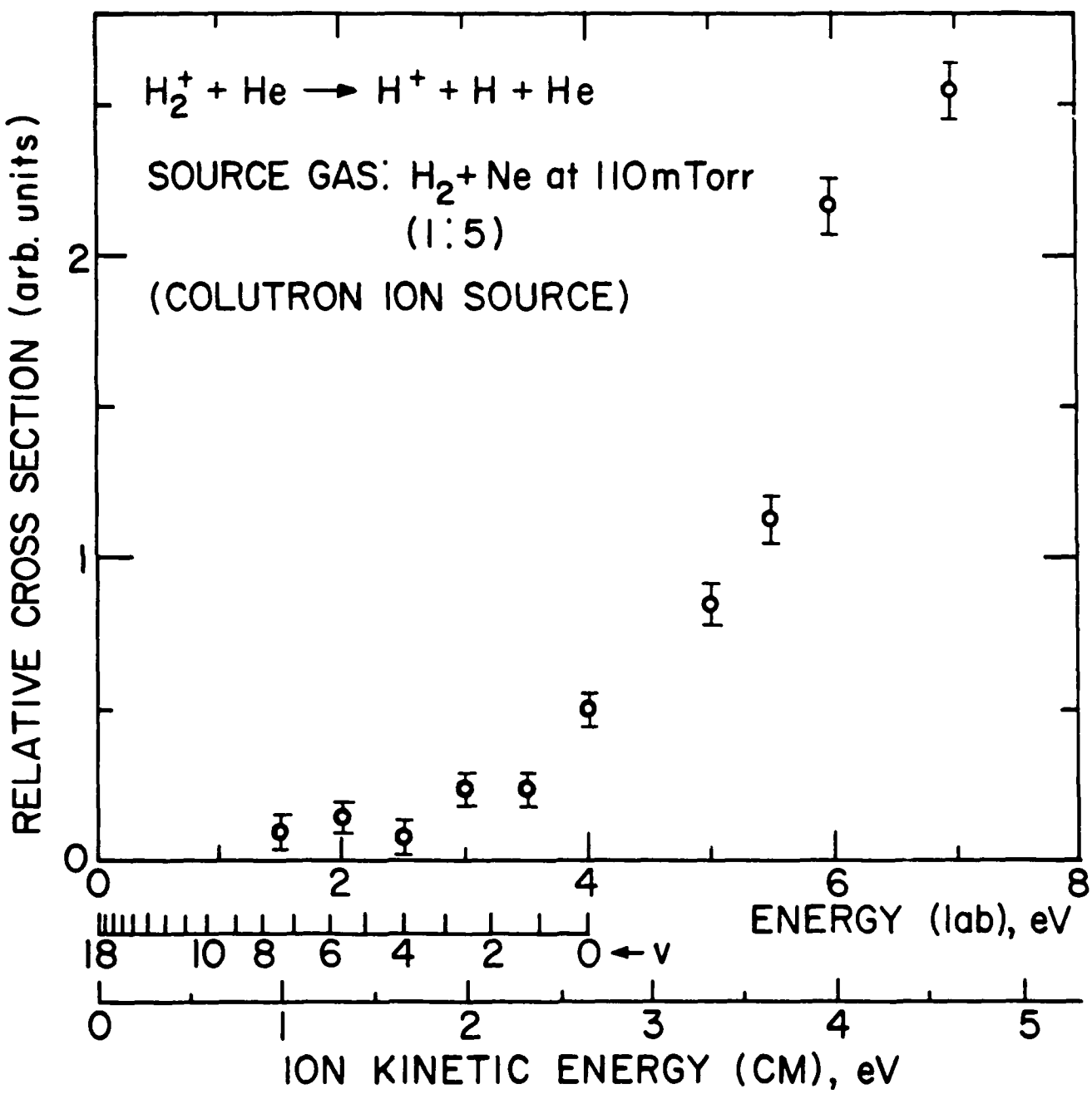
$H_2^+ + He \rightarrow H^+ + H + He$
SOURCE GAS: H_2 + Ne at 110 mTorr
(1:5)
(COLUTRON ION SOURCE)
RELATIVE CROSS SECTION (arb. units)
0
1
2
0
2
4
6
8
ENERGY (lab), eV
18
10
8
6
4
2
0 ← v
0
1
2
3
4
5
ION KINETIC ENERGY (CM), eV

Submitted to J.Phys.B (Letters).

PRODUCTION OF H_3^+ IONS WITH LOW INTERNAL ENERGY FOR STUDIES OF DISSOCIATIVE RECOMBINATION

Amarjit Sen* and J.B.A. Mitchell

Department of Physics

The University of Western Ontario

London, Ontario, Canada. N6A 3K7

ABSTRACT

An rf trap ion source has been used to produce H_3^+ with low vibrational energy. Internal energy of the ions has been measured by Collision Induced Dissociation to be less than 0.5eV. The implication of this to studies of dissociative recombination is discussed.

*Current Address: Physics Division, Argonne National Laboratory

Argonne, Illinois. 60439, U.S.A.

INSPEC NO: 34.50, 35.20, 41.80G

In a recent paper, Sen et al (1986) have described Collision Induced Dissociation, (CID), measurements which were performed to demonstrate that a radiofrequency trap ion source, (Teloy and Gerlich, 1974) using a Hydrogen-Neon (1:5) mixture could produce H_2^+ ions with only the first two vibrational levels populated. This paper describes a similar experiment which shows that the same ion source can produce H_3^+ ions with low internal energies. A preliminary report on this work has already appeared. (Sen et al, 1985).

H_3^+ is an ion which plays an important role in astrophysics, planetary atmospheric chemistry and negative ion source technology. It is formed in a hydrogen plasma via the reaction: -

$$H_2^+ + H_2 \rightarrow H_3^+ + H \qquad \text{--- (1).}$$

Laboratory studies of this reaction indicate that the H_3^+ ions are produced with an initial internal energy of about 2eV, (Leventhal and Friedman, 1968). If however they are formed in a sufficiently dense environment, they can make de-exciting collisions such as:-

$$H_3^+(v) + H_2 \rightarrow H_3^+ + H_2^* \qquad \text{--- (2).}$$

Kim et al, (1974).

The dissociative recombination of H_3^+, namely: -

$$e + H_3^+ \rightarrow H + H + H \qquad \text{--- (3a).}$$

$$\rightarrow H_2(v) + H \qquad \text{--- (3b).}$$

is an important electron loss process in hydrogen plasmas and has received considerable attention experimentally. Total cross section or rate coefficient measurements for reaction 3 have been made by Leu et al (1973), Peart and Dolder (1974), Auerbach et al (1977), Mathur et al (1978), MacDonald et al (1984) and Mitchell et al (1984). Mitchell et al (1983) have also measured the branching ratio for reactions 3a and 3b. Results from all these measurements agree with each other to within a factor of two. In all cases it was found that the reaction probability was large at low energies, (~1.0eV) decreasing as the energy increased.

More recently Adams et al (1984) have examined H_3^+ recombination using the Flowing Afterglow Langmuir Probe, (FALP) technique and have found a very small rate coefficient for reaction 3, (~1.0 x $10^{-11}cms^3s^{-1}$, Smith, private communication, 1986), at temperatures of 95 and 300K.

Of particular significance is the fact that this result seems to agree with theoretical predictions of Kulander and Guest (1979) and Michels and Hobbs (1984). Calculations have shown that the curve crossing between the ground state of the H_3^+ ion and the neutral repulsive diabatic state through which the recombination proceeds, lies 0.9eV above the ground vibrational state. This implies that the recombination should have a small probability at low energies.

Adams et al have argued that the H_3^+ ions in their apparatus are vibrationally cold due to the many de-exciting collisions which they make in the high pressure, (~1Torr) environment of the FALP experiment.

Based upon an analysis of Blakely et al (1977) it has been estimated that approximately 60% of the H_3^+ ions used in the experiments of Auerbach et al (1977) and Mitchell et al (1983, 1984) were vibrationally excited. This was because the residence time of the ions in the r.f. ion source used to produce the H_3^+, estimated to be 30 microseconds, was too short to allow for complete de-excitation of the ions, at the operating pressure of the source, (100 m Torr). It is perhaps not surprising then that the merged beam results disagree with those of Adams et al.

For the case of the afterglow studies of Leu et al (1973) and MacDonald et al (1984), it is more difficult to understand the discrepancy. The plasma in the afterglow apparatus is not too dissimilar to that in the FALP apparatus.

Adams et al nave suggested that perhaps the afterglow results were affected by contamination of the plasma with H_5^+ ions which are known to have a very large recombination rate coefficient. Biondi (private communication 1985) has argued that this is not so.

Clearly there is a need for further investigation on this subject in order to resolve the controversy. Of prime importance for such a study is a careful measurement of the internal energy of the ions which are recombining. Peart and Dolder (1974b, 1975)

tested a number of electron impact ion source configurations in an effort to produce de-excited H_3^+ ions. They used electron impact dissociative excitation studies to probe the internal energies of the ions. This process, namely: -

$$e + H_3^+ \rightarrow H^+ + H + H + e \qquad \text{--- (4).}$$

occurs through an electronic transition to an excited repulsive state and thus exhibits an energy threshold. This threshold will be lowered for vibrationally excited H_3^+ ions. (For futher information on this topic see Mitchell, 1986). From their measurements Peart and Dolder concluded that indeed their ions were de-excited Other measurements of H_3^+ internal energy have been performed by Leventhal and Friedman (1969), Smith et al (1975), Kim et al (1974), Blakely et al (1977) and Vogler (1979). The latter author has suggested that under any source conditions emerging H_3^+ ions will have both the ground A vibrational state and the first excited E state populated.

EXPERIMENTAL METHOD

As mentioned earlier, the conventional r.f. ion source used for merged beam studies of dissociative recombination by Auerbach et al (1977) and by Mitchell et al (1983, 1984) has too short a residence time to allow the H_3^+ ions to relax completely. An alternative source, designed by Teloy and Gerlich (1974), uses an

inhomogeneous radiofrequency electric field to confine ions, produced by electron impact, for several milliseconds prior to extraction. Such a source, illustrated in Figure, 1 has been under test in this labortory. Collision Induced Dissociation, (CID), of H_3^+ on He atoms has been used as a probe to measure the internal energy of the ions.

The ions formed in the trap source are accelerated to 200eV, mass analyzed using a Wien filter and the dec-celerated using a multi-element lens system. (Sen, 1985). The slow ions are then made to collide with a Helium atom beam which intersects the ion beam at right angles. Following the collisions, the primary and product ions are re-accelerated to 2 keV, focussed onto the entrance slit of a magnetic sector mass spectrometer, and detected using a channel electron multiplier. Collision of the primary ion beam with the residual gas in the interaction region also gives rise to dissociation fragments. These are distinguished from true signals by performing measurements with and without the atom beam present, keeping the conditions in the interaction chamber constant with the aid of a second nonintersecting atom beam. Since the density of the target atom beam is not measured directly, only relative cross sections can be determined using this apparatus. This is sufficient for the present purpose however since the important quantity to be measured is the threshold for the Collision Induced Dissociation of the H_3^+ ions.

Further information concerning this apparatus is given in Sen et al 1986 and Sen, 1985.

RESULTS AND DISCUSSION

Collision Induced Dissociation, (CID), of H_3^+ can proceed via the following reactions: -

$$H_3^+ + He \rightarrow H^+ + H_2 + He \quad -4.35eV \qquad \text{--- (5a)}$$

$$\rightarrow H_2^+ + H + He \quad -6.19eV \qquad \text{--- (5b)}$$

$$\rightarrow H^+ + H + H + He \quad -8.84eV \qquad \text{--- (5c)}$$

These reactions were studied by measuring the appearance of the H^+ and H_2^+ fragments as a function of centre of mass energy. The results of these measurements are shown in Figure 2. Also shown on the figure are the calculated energy thresholds for these reactions for ground state H_3^+ ions. The uncertainty in the primary ion energy at the lowest value of energy is 0.1eV. Vertical error bars in Figure 2 show statistical fluctuations in the measured signals.

These data were taken with the ion source operating with a Hydrogen-Neon mixture in the ratio of 1:5 at a pressure of 35 mTorr. It is apparent from the positions of the thresholds for reactions 5a and 5b that the H_3^+ ions emanating from the source have less than 0.5eV of internal energy.

The energies of the vibrational states of H_3^+ are tabulated in Table I together with relative initial populations as derived by Smith and Futrell (1975), for H_3^+ ions formed from reaction 1, prior to any collisional or radiative de-excitation. The table

does not distinguish between different vibrational modes. It can be seen that the CID results suggest that the H_3^+ ions formed in the ion source have relaxed so that only the first and possibly the second vibrational levels remain populated.*

The H_3^+ ions have sufficiently low internal energies that they should have very small recombination coefficients according to the predictions of Michels and Hobbs (1984).

The ion source has been mounted in the terminal of a 400 keV Van de Graaff accelerator which is used as the injector for the Merged Electron Ion Beam Experiment in this laboratory. Ion currents of ~1 x 10^{-9}A have been obtained in the apparatus. These are comparable with currents used in previous recombination studies. Measurements of H_3^+ recombination are currently in progress and will be reported elsewhere.

ACKNOWLEDGEMENTS

The authors would like to thank E. Teloy and D. Gerlich for their assistance in the construction of the ion source. Support from Natural Sciences and Engineering Research Council of Canada and from the U.S. Air Force Office of Scientific Research is much appreciated.

* It should be noted that radiative relaxation of vibrationally excited H_3^+ ions will occur in a time of ~10^{-2}s. (OKA, 1981). since the ions are trapped in the source for several milli-seconds, (Teloy & Gerlich, 1974), this should also have a significant effect on the excited state population of the ions.

TABLE I

DISTRIBUTION OF VIBRATIONAL EXCITATION IN H_3^+ FORMED FROM REACTION (1) PRIOR TO DE-EXCITATION.

(Smith & Futrell, 1975).

H_3^+ Vibrational Quantum Number	Population Fraction	E^* (H_3^+) (eV)
0	0.031	.0
1	0.085	0.37
2	0.147	0.74
3	0.204	1.12
4	0.203	1.49
5	0.147	1.86
6	0.082	2.23
7	0.039	2.60
8	0.013	2.98
9	0.001	3.35

FIGURE CAPTIONS

1. Schematic view of the radiofrequency trap ion source.

2. Relative cross sections for the collision induced dissociation of H_3^+ on He. The thresholds for reactions 5a and 5b are indicated by arrows on the energy axis.

REFERENCES

1. Adams, N.G., S. Smith and E. Alge, J. Chem. Phys. 81, 1778, (1984).

2. Auerbach, D., R. Cacak, R. Caudano, T.D. Gaily, C.J. Keyser, J. Wm. McGowan, J.B.A. Mitchell and S.F.J. Wilk, J. Phys. B., 10, 3797, (1977).

3. Blakely, C.R., M.L. Vestal and J. H. Futrell, J. Chem. Phys. 66, 2392, (1977).

4. Kim. J.K., L.P. Theard and W.T. Huntress, In. J. Mass Spectrom Ion Phys. 15, 223, (1974).

5. Kulander, C. and M.F. Guest, J. Phys. B., 12, L501 (1979).

6. Leu, M.T., M.A. Biondi and R. Johnsen, Phys. Rev. A7, 292, (1973).

7. Leventhal, J.J. and L. Friedman, J. Chem. Phys. 49, 5543, (1968).

8. Leventhal, J.J. and L. Friedman, J. Chem. Phys. 50, 2928, (1969).

9. MacDonald, J.A., M.A. Biondi and R. Johnsen, Planet Space Sci. 32, 651, (1984).

10. Mathur, D., J.B. Hasted and S.U. Khan, J. Phys. B. 12, 2043 (1979).

11. Michels, H.H. and R.H. Hobbs, App. J. 286, L27, (1984).

12. Mitchell, J.B.A., J.L. Forand, C.T. Ng, D.P. Levac, R.E. Mitchell, P.M. Mul, W. Claeys, A. Sen and J.Wm. McGowan Phys. Rev. Lett. 51, 885, (1983).

13. Mitchell, J.B.A., C.T. Ng, L. Forand, R. Janssen and J. Wm. McGowan, J. Phys. B. 17, L909, (1984).

14. Mitchell, J.B.A. in Physics of Electron-Ion and Ion-Ion Collisions. NATO ASI, Han-Sur-Lesse, Belgium. (Ed. F. Brouillard and P. DeFrance), Plenum, New York, (1986).

15. Oka, T., Phil. Trans. Roy. Soc. Lond. A303,543, (1981).

16. Peart, B. and K.T. Dolder, J. Phys. B. 7, 1948, (1974a).

17. Peart, B. and K.T. Dolder, J. Phys. B. 7, 1567, (1974b).

18. Peart, B. and K.T. Dolder, J. Phys. B. 8, L143, (1975).

19. Sen, A., Ph.D. Thesis, The University of Western Ontario, (1985).

20. Sen, A. and J.B.A. Mitchell, Abstracts of papers, XIVth ICPEAC, Palo Alto, CA (1985), p. 600.

21. Sen, A., J.Wm. McGowan and J.B.A. Mitchell, (Submitted to J. Phys. B.), (1986).

22. Smith, D.L. and J. H. Futrell, J. Phys. B. 8, 803, (1975).

23. Teloy, E. and D. Gerlich, Chem. Phys. 4, 417, (1974).

24. Vogler, J., Phys. Rev. 19, 1, (1979).

ANL-P-18,028

STORAGE ION SOURCE

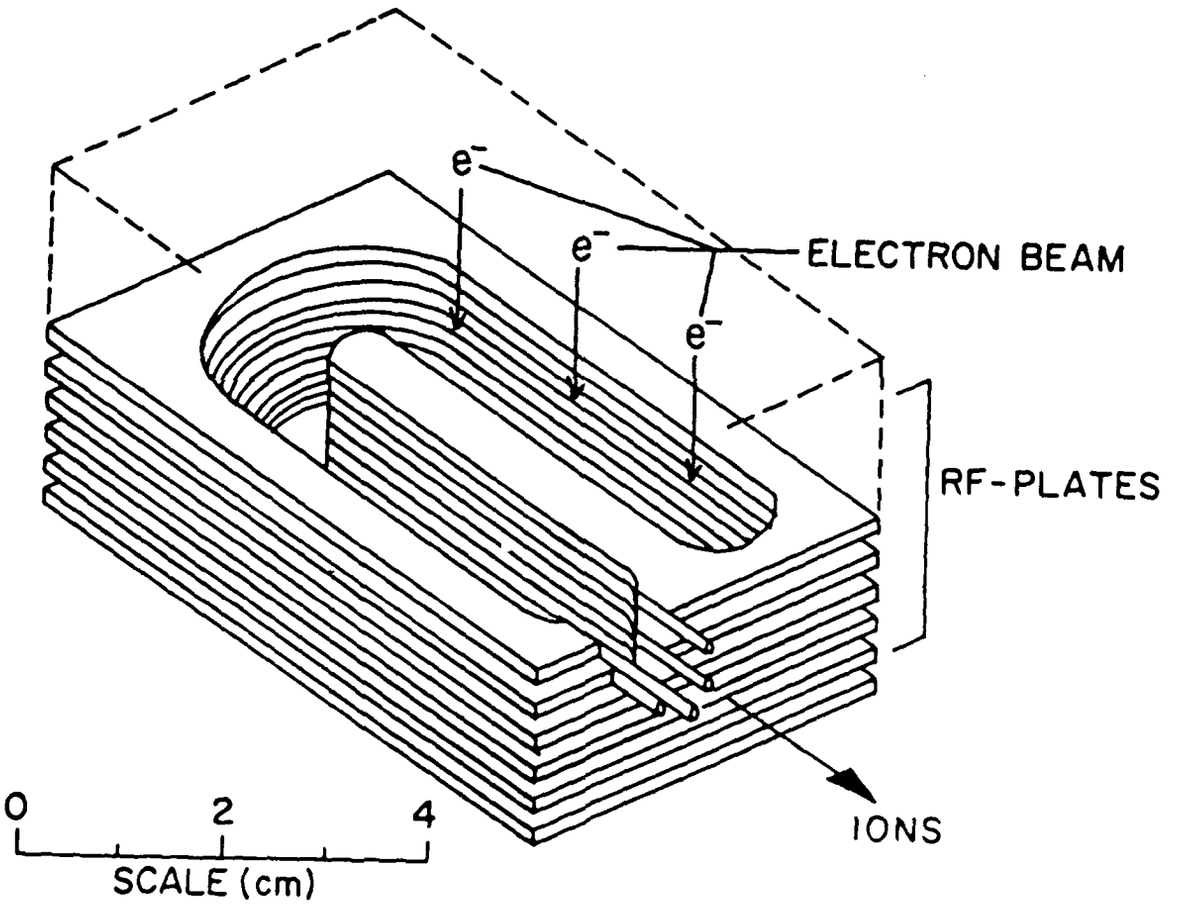

Fig.1.

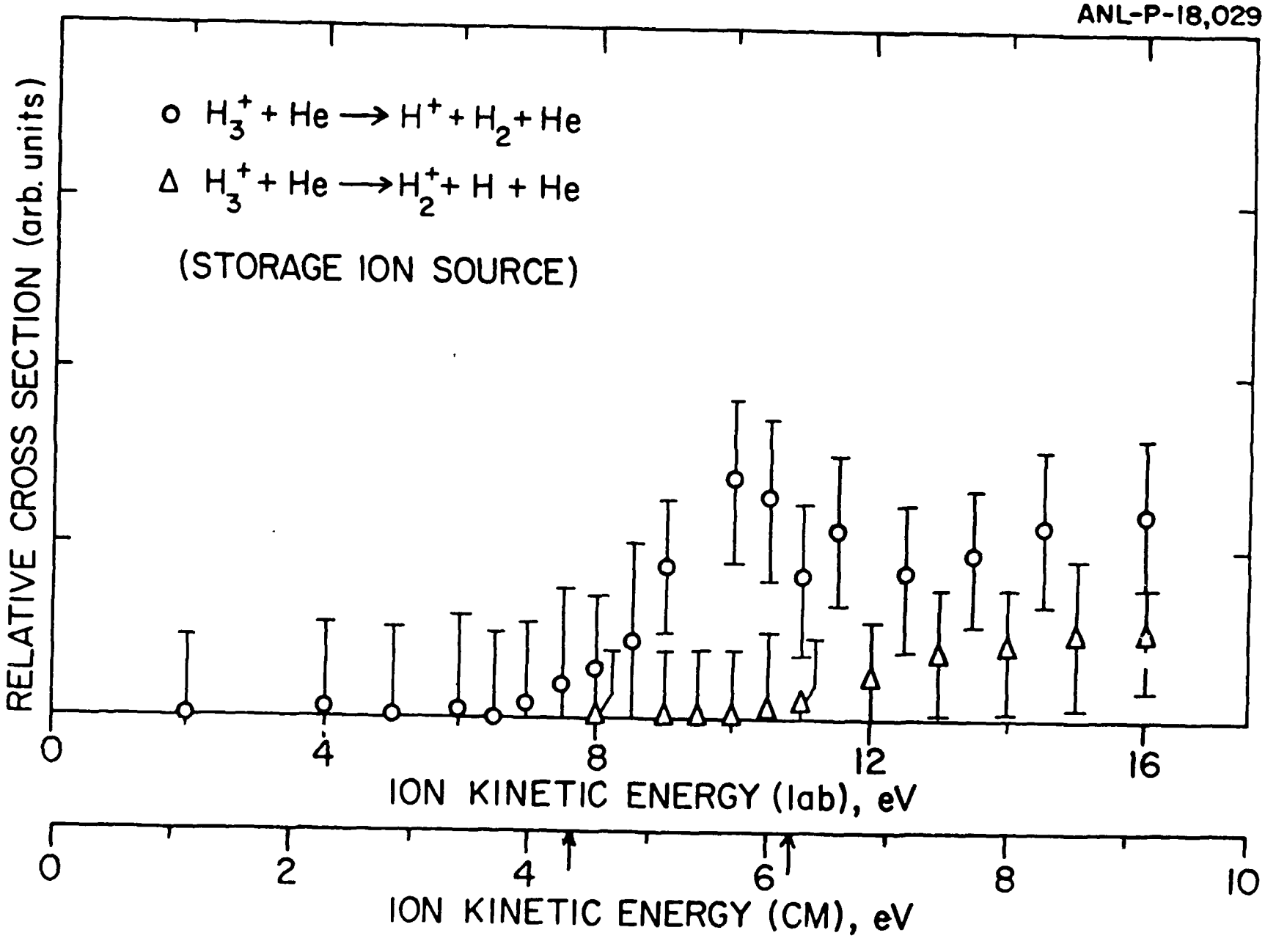
ANL-P-18,029
o $H_3^+ + He \rightarrow H^+ + H_2 + He$
Δ $H_3^+ + He \rightarrow H_2^+ + H + He$
(STORAGE ION SOURCE)
RELATIVE CROSS SECTION (arb. units)
0
4
8
12
16
ION KINETIC ENERGY (lab), eV
0
2
4
6
8
10
ION KINETIC ENERGY (CM), eV

Fig. 2.

APPENDIX C.

Measurement of the Branching Ratio for the Dissociative Recombination of $H_3^+ + e$

J. B. A. Mitchell, J. L. Forand, C. T. Ng, D. P. Levac, R. E. Mitchell, P. M. Mul,[a] W. Claeys,[b] A. Sen, and J. Wm. McGowan

Department of Physics and the Center for Chemical Physics, University of Western Ontario, London, Ontario N6A 3K7, Canada

(Received 19 October 1982)

The dissociative recombination of H_3^+ with electrons can have two exit channels, namely $e + H_3^+ \rightarrow H + H + H$ (channel I), and $e + H_3^+ \rightarrow H_2 + H$ (channel II). A new technique has been developed which has been used to determine the relative contributions of channels I and II to the overall recombination process. Over the energy range from 0.01 to 0.05 eV it has been found that channel I dominates.

PACS numbers: 34.80.Gs, 82.30.Lp

The identification of the products of dissociative recombination is of vital importance not only to our understanding of electron-ion recombination mechanisms and the structure of the molecular system under study but also to complement the modeling of the chemistry of ionized systems. For example, many reaction schemes have been proposed to explain the presence of large organic molecules such as polyacetylenes in interstellar space[1,2] or to explain the energy balance of the Jovian atmosphere.[3,4] These depend critically upon the branching ratios for the final channels of dissociative recombination.

Peart and Dolder[5,6] have measured the cross sections for ion pair ($H^+ + H^-$, $H_2^+ + H^-$) formation during the recombination of electrons with H_2^+ and H_3^+ ions, and the excitation states of atomic products formed during dissociative recombination have been measured for H_2^+ and D_2^+,[7,8] for O_2^+,[9] for Xe_2^+, Kr_2^+, and Ar_2^+,[10-12] and for NO^+.[13]

Kinetic modeling of pulse radiolysis experiments with organic gases[14-16] has been used to predict the major dissociation channels for a variety of organic ions, while Herbst[17] has used a statistical phase-space theory to estimate the neutral-product branching ratios for $HCNH^+$, H_3O^+, CH_3^+, and NH_4^+.

In this paper we have successfully used a technique which follows from a suggestion of Berkner *et al.*[18] in 1971, which allows us to identify the individual exit channels for the dissociative recombination of H_3^+ with electrons. This is the first direct measurement of neutral-product branching ratios for polyatomic-ion recombination.

For the measurements we have used the merged electron-ion beam apparatus (MEIBE-I) which has been described in detail previously.[19,20] Briefly, H_3^+ ions, formed in an rf ion source at a pressure 0.1 Torr of hydrogen gas, are accelerated and interact with an electron beam which is made to merge with the ion beam. By matching the electron and ion velocities, very low center-of-mass interaction energies can be obtained. The neutral products formed in the interaction region are detected with an energy-sensitive surface-barrier detector.

The main reactions which occur in the interaction region are as follows:

$$\text{signal} \quad e + H_3^+ \rightarrow H + H + H, \qquad \text{(I)}$$

$$\rightarrow H_2 + H; \qquad \text{(II)}$$

$$\text{background} \quad H_3^+ + X \rightarrow H^+ + (H + H) + X, \qquad \text{(III)}$$

$$\rightarrow H_2^+ + H + X, \qquad \text{(IV)}$$

$$\rightarrow (H + H) + H + X^+. \qquad \text{(V)}$$

(Recombination to H_3^* requires radiative stabilization which is very slow and so can be neglected.)

Following these dissociation reactions, the resulting fragments continue to move with approximately the same velocity as the primary beam. Therefore the kinetic energy of the initial ions is divided between the neutral fragments according to their mass.

The surface-barrier detector used to detect the neutrals is energy sensitive. The output pulse-height spectrum for the signal plus background neutral products from an H_3^+ beam interacting with the electron beam and the background gas is shown in Fig. 1(a). An example of the signal distribution is given in Fig. 1(b).

H atoms from Reaction IV arrive at the detector with one-third of the total energy. H_2 molecules or 2H atoms from Reaction III carry two-thirds of the energy while Channels I, II, and V which yield all neutral hydrogen products give rise to pulses whose energy corresponds to the total

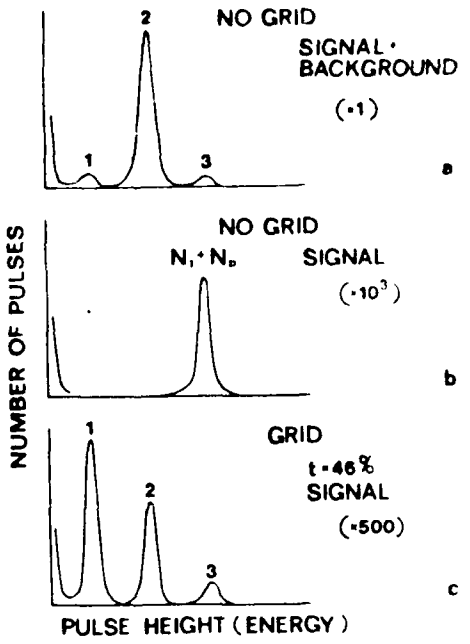

FIG. 1. Pulse-height distributions of detector pulses for (a) H_3^+ beam, no grid, signal plus background. (b) H_3^+ beam, no grid, signal only. (c) H_3^+ beam, 46% transmission grid, signal only.

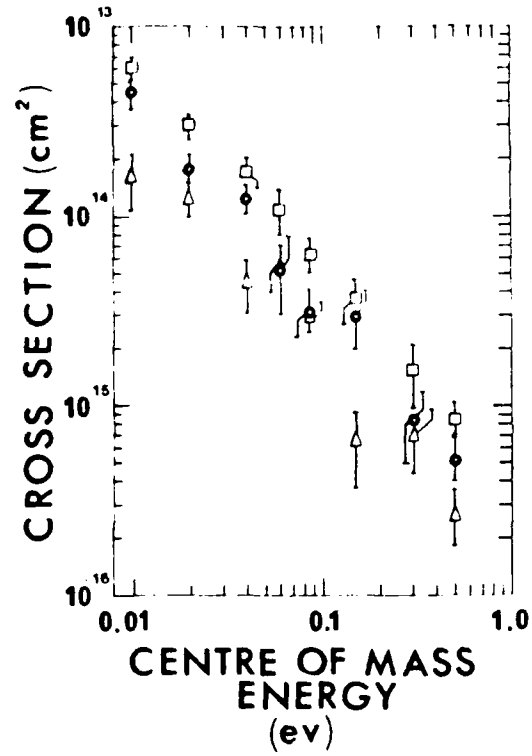

FIG. 2. Cross sections for the dissociative recombination of $H_3^+ + e$ leading to H + H + H (circles), H_2 + H (triangles), and total cross section (squares).

beam energy. This is because the products *arrive at the detector almost simultaneously and* so are indistinguishable from a single full-energy mass-3 neutral, which incidentally is not expected to exist.

For low energies I and II are the only electron-ion processes which can occur.[21] Hence when the background is subtracted out, the pulse-height distribution at the detector is as shown in Fig. 1(b).

If a grid with known transmission t is placed in front of the detector then the probability that all three particles from Channel I will reach the detector is no longer the same as for the two particles from Channel II. This can be used to separate out the contributions from these two channels. If $N_{\rm I}$ and $N_{\rm II}$ are the number of neutral counts arising in a given time from Channels I and II respectively and if N_1, N_2, and N_3 are the number of counts under peaks 1, 2, and 3, then it is easily shown that

$$N_3 = t^3 N_{\rm I} + t^2 N_{\rm II}\,, \tag{1}$$

$$N_2 = 3t^2(1-t)N_{\rm I} + t(1-t)N_{\rm II}\,, \tag{2}$$

$$N_1 = 3t(1-t)^2 N_{\rm I} + t(1-t)N_{\rm II}\,. \tag{3}$$

This is illustrated in Fig. 1(c) which shows the signal pulse-height distribution with a 46% grid in place.

Equations (1)–(3) can be rearranged to yield three sets of expressions for $N_{\rm I}$ and $N_{\rm II}$, namely ($t \neq 0, 1$),

$$N_{\rm I} = \frac{tN_2 - (1-t)N_3}{2t^3(1-t)}\,, \tag{2a}$$

$$= \frac{(1-t)N_3 - tN_1}{t^2(4t-3)(1-t)}\,, \quad t \neq 0.75\,, \tag{2b}$$

$$= \frac{N_1 - N_2}{3t(1-t)(1-2t)}\,, \quad t \neq 0.5\,, \tag{2c}$$

and

$$N_{\rm II} = \frac{3(1-t)N_3 - tN_2}{2t^2(1-t)}\,. \tag{3a}$$

These equations can be used to calculate the respective cross sections for Reactions I and II.

A most important parameter in Eqs. (2) and (3) is the transmission t. This must be known to very high accuracy. Two methods were used to determine t. One was an optical measurement of the ratio of open area to total area of the grid using a calibrated microscope. This yielded a value of $t = (45 \pm 5)\%$. The second method exploits the redundancy of information in Eqs. (2) and (3) where three experimentally measured variables N_1, N_2, and N_3 are used to determine two quanti-

ties $N_{\perp}$ and $N_{\parallel}$. Because of this redundancy t can be treated as a variable and a self-consistent analysis performed to find a value of t which gives the closest agreement between all the equations. This analysis yielded a value of $t = (44 \pm 2)\%$ which was finally adopted for evaluating $N_{\perp}$ and $N_{\parallel}$.

Figure 2 shows our experimental results for $\sigma_{\perp}$, $\sigma_{\parallel}$, and $\sigma_{\perp} + \sigma_{\parallel}$ versus center-of-mass energy. The error bars shown represent the neutral counting statistics, the uncertainty in ion and electron currents, and the uncertainty in the measurement of the grid transmission t. Other systematic errors due to the determination of the form factor and other experimental parameters though not shown contribute an additional overall uncertainty in the magnitude of the cross-section curve of ±15%.

It can be seen that over the measured energy interval from 0.01 to 0.50 eV, the channel leading to three hydrogen atoms dominates over the one leading to $H_2^* + H$. Also, the data suggest that the ratio $(H_2 + H)/3H$ may be electron-energy dependent. The exact dependence will be determined in subsequent experiments.

Recent theoretical calculations by Kulander and Guest[22] have indicated that if the sum of the internal energy of the H_3^+ ions and the kinetic energy of the electrons is greater than about 1 eV above the ground vibrational state of H_3^+, then the dominant dissociation channel will lead to $H_2(^1\Sigma_g^+) + H(2s \text{ or } 2p)$. For energies less than this, indirect recombination via capture into Rydberg levels of the neutral model is predicted to dominate leading to dissociation into three hydrogen atoms.

An estimate of the distribution of vibrational states in our H_3^+ beam can be obtained by comparison with studies by Blakly, Vestal, and Futrell,[23] who used an electron-impact ion source to produce H_3^+ ions. By examining low-energy ion-molecule reactions they were able to demonstrate that at a source pressure of 0.1 Torr, more than 75% of their beam was vibrationally excited. Our rf source, being larger (diameter 2.5 cm), has a longer mean residence time and at 0.1 Torr, their analysis indicates that about 65% of the H_3^+ ions are excited. Approximately 10% have internal energies in excess of 1 eV.

Given this analysis it would appear that there is at least qualitative agreement between our findings and the theoretical predictions of Kulander and Guest although their analysis does not include contributions due to dissociation to $H_2 + H(1s)$.

A consideration of the vibrational modes of H_3^+[24] shows that A and E states are fairly evenly populated. The A states perform symmetric stretch vibrations which are likely to couple to states dissociating to 3H atoms. E states are degenerate with one mode favoring dissociation to 3H atoms and another favoring $H_2 + H$. Hence given a highly vibrationally excited H_3^+ beam, it is perhaps not surprising that the dominant mode of dissociative recombination would lead to 3H atoms.

The excellent technical assistance of I. Schmidt, H. Chen, P. Frank, and D. Miko is gratefully acknowledged. This work was supported by the Natural Sciences and Engineering Research Council of Canada and the U. S. Department of Energy.

---

[a]Present address: Philips International Institute, Eindhoven, The Netherlands.

[b]Permanent address: Institut de Physique, Universite de Louvain, Louvain-la-Neuve, Belgium.

[1]G. F. Mitchell, W. T. Huntress, and S. S. Prasad, Astrophys. J. 233, 102 (1979).

[2]S. Green, Annu. Rev. Phys. Chem. 32, 103 (1981).

[3]J. J. Olivero, J. N. Bass, and A. E. S. Green, J. Geophys. Res. 78, 2812 (1973).

[4]M. G. Heaps, J. N. Bass, and A. E. S. Green, Icarus 20, 297 (1973).

[5]B. Peart and K. T. Dolder, J. Phys. B 8, 1570 (1975).

[6]B. Peart and K. T. Dolder, J. Phys. B 12, 3441 (1979).

[7]M. Vogler and G. H. Dunn, Phys. Rev. A 11, 1983 (1975).

[8]R. A. Phaneuf, D. H. Crandall, and G. H. Dunn, Phys. Rev. A 11, 528 (1975).

[9]E. Zipf, Geophys. Res. Lett. 6, 881 (1979).

[10]Y. J. Shiu and M. A. Biondi, Phys. Rev. A 17, 868 (1978).

[11]Y. J. Shiu and M. A. Biondi, Phys. Rev. A 16, 1817 (1977).

[12]Y. J. Shiu, M. A. Biondi, and D. P. Sipler, Phys. Rev. A 15, 494 (1977).

[13]D. Kley, G. M. Lawrence, and E. J. Stone, J. Chem. Phys. 66, 4157 (1977).

[14]R. E. Rebbert and P. Ausloos, J. Res. Natl. Bur. Stand. Sect. A 76, 329 (1972).

[15]R. E. Rebbert and P. Ausloos, J. Res. Natl. Bur. Stand. Sect. A 77, 109 (1973).

[16]R. E. Rebbert, S. G. Lias, and P. Ausloos, J. Res. Natl. Bur. Stand. Sect. A 77, 249 (1973).

[17]E. Herbst, Astrophys. J. 222, 508 (1978).

[18]K. H. Berkner, T. J. Morgan, R. V. Pyle, and J. W. Steams, in *Proceedings of the Seventh International*

Conference on the Physics of Electronic and Atomic Collisions, Amsterdam, 1971. Abstracts, edited by J. Kistemaker (North-Holland, Amsterdam, 1971), p. 422.

[18]D. Auerbach, R. Cacak, R. Caudano, T. D. Gaily, C. J. Keyser, J. Wm. McGowan, J. B. A. Mitchell, and S. F. J. Wilk, J. Phys. B 10, 3797 (1977).

[20]C. J. Keyser, H. R. Froelich, J. B. A. Mitchell, and J. Wm. McGowan, J. Phys. E 12, 316 (1979).

[21]B. Peart and K. T. Dolder, J. Phys. B 7, 1567 (1974).

[22]C. Kulander and M. F. Guest, J. Phys. B 12, L501 (1979).

[23]C. R. Blakley, M. L. Vestal, and J. H. Futrell, J. Chem. Phys. 66, 2392 (1977).

[24]G. D. Carney and R. N. Porter, J. Chem. Phys. 65, 3547 (1976).

J. Phys. E.: Sci. Instrum., Vol 18, 1985. Printed in Great Britain

Triatomic molecular dissociation: a method for measuring individual decay channel cross sections

J L Forand†, J B A Mitchell and J Wm McGowan‡
Department of Physics and Centre for Chemical Physics, The University of Western Ontario, London, Ontario, Canada N6A 3K7

Received 19 October 1984, in final form 31 January 1985

Abstract. Mathematical details concerning a method for identifying individual dissociation channels of a triatomic molecule are presented. The technique utilises a transmission grid in front of a particle detector to limit the probability of dissociation products from reaching the detector.

1. Introduction

Recent experiments in this laboratory (Mitchell *et al* 1983) have yielded the first direct measurements of the branching ratio for the dissociative recombination of a polyatomic ion. Individual cross sections were measured for the two decay channels of the dissociative recombination of H_3^+ with electrons, namely:

$$e + H_3^+ \rightarrow H + H + H \qquad (A)$$

$$\rightarrow H_2 + H \qquad (B)$$

using a technique which is described in this paper.

The merged electron–ion beam experiment (MEIBE-I) (Auerbach *et al* 1977) was used for this measurement. In this apparatus a fast beam of electrons is made to merge with a fast molecular ion beam from a 400 keV van de Graaff accelerator. The merging is accomplished using an axial magnetic field and a well defined transverse electric field to cause the electrons to move from their initial path to one superimposed on the ion beam.

*The major advantage of this technique is that very low colli*sion energies in the centre of mass frame can be achieved by matching the velocities of the two beams. The large laboratory energies of the beams however facilitate their handling and the subsequent detection of neutral products.

The neutrals, resulting both from the recombination and from collisions of the ion beam with the background gas in the apparatus, are detected using an energy sensitive surface barrier detector. By modulating the electron beam and counting the detector pulses in and out of phase with the modulation, the recombination signals can be distinguished from the background effects.

Figure 1(*a*) shows the pulse height spectrum of the output from the surface barrier detector when H_3^+ ions are used. Since the break-up fragments continue to move with the same velocity as the primary ion beam their kinetic energy is determined by their relative masses. Thus a single hydrogen atom will leave the collision centre with one third of the energy of the H_3^+ parent ion while an H_2 molecule will carry away two thirds.

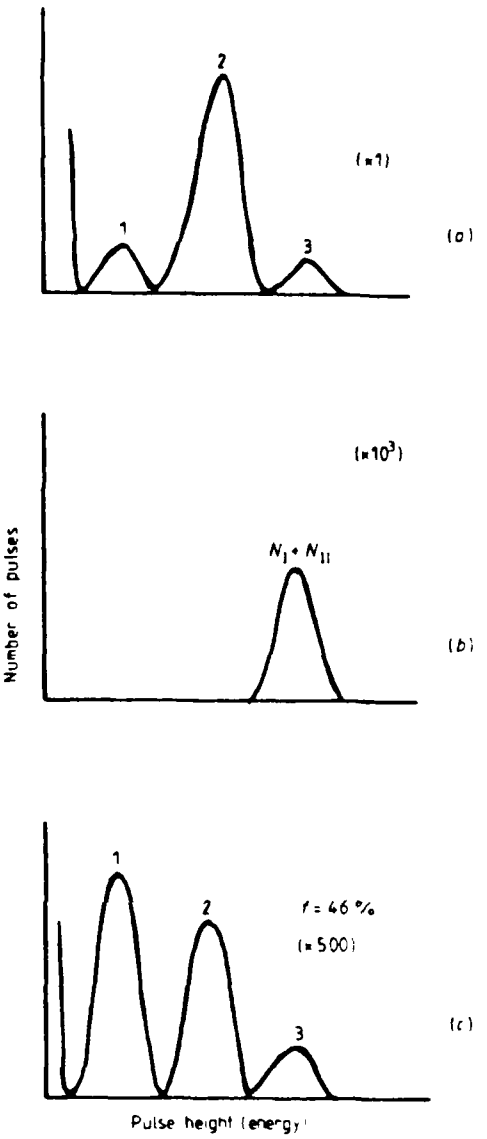

Figure 1. Pulse height distributions from surface barrier detector. (*a*), H_3^+ beam, no grid, signal plus background shown (*b*), H_3^+ beam, no grid, background removed. (*c*), H_3^+ beam, 46% transparency grid, background removed.

The timing resolution of the counting system is insufficient to distinguish between individual particles arising from a single recombination event so that the three hydrogen atoms from channel (A) and the H_2 + H pair from channel (B) both appear as a single full energy signal, i.e. they are indistinguishable

The one third and two thirds energy peaks in figure 1(*a*) are due to the beam background gas reactions

$$H_3^+ + X \rightarrow H_3^{+*} + H + X$$

$$\rightarrow H_2 + H^{+*} + X$$

$$\rightarrow H^{+*} + H + H + X$$

while the reaction

$$H_3^+ + X \rightarrow (H + H) + H + X^*$$

gives background signals in the full energy peak.

† Present address: Department of Physics, University of Windsor, Windsor, Ontario, Canada.

‡ Present address: Director, National Museum of Science and Technology, 1867 St. Laurent Blvd., Ottawa, Ontario K1A 0M8, Canada.

Single channel analysers can be used to select the individual energy peaks so that each channel can be counted separately. The pulse height spectrum following subtraction of the signal plus background and background cycles of the modulated counting scheme is shown in figure 1(*b*), since the recombination signals do not cancel. Thus the total cross section for dissociative recombination can be determined. It can be seen that only one peak, due to the products from both channels A and B remain.

A technique has been developed in this laboratory (based on an earlier idea by Berkner *et al* (1971)) which allows us to separate the contributions from channels A and B. This technique involves placing a grid of known transmission, t, in front of the surface barrier detector. Since the probability of one particle passing through the grid is t, that for two particles is t^2, and for three particles, t^3. This has the effect of distributing the particles from channels A and B into the other peaks in the pulse height spectrum. This is shown in figure 1(*c*). Since the redistribution differs for each channel they become distinguishable. The mathematical formalism for determining the relative contributions from each channel (and hence their respective cross sections) for a triatomic ion of form X_3^+ was discussed in our previous publication (Mitchell *et al* 1983).

Here we extend the formalism to deal with the more complete case of a triatomic of the form X_2Y^+ so as to be able to deal with the isotopes of X_3^+.

2. Mathematical development

The dissociative recombination of X_2Y^+ with electrons can be represented as follows:

$$X_2Y^+ + e \rightarrow X + X + Y \qquad \text{(I)}$$

$$\rightarrow X_2 + Y \qquad \text{(II)}$$

$$\rightarrow XY + X. \qquad \text{(III)}$$

$m(X)$ and $m(Y)$ are the respective masses of atoms X and Y where

$$m(Y) = am(X) \qquad a > 0. \qquad (1)$$

The transmission probability of the grid is t where $(0 \leqslant t \leqslant 1)$.

During a given experiment the number of recombinations which decay via channels I, II and III are denoted as N_I, N_{II} and N_{III} respectively.

When a transmission grid is installed in front of the detector, three, four or five signal peaks are observed (figure 1(*c*)). The grid makes it less likely that all the recombination products will reach the detector and so incomplete families of products will show up as lower energy peaks.

The cross sections for the individual channels can be calculated if the projectile flux target density and collision geometry are known and if N_I, N_{II} and N_{III} can be determined. For example, in the case of MEIBI experiments the cross section for channel C is given by

$$\sigma_c = \frac{N_c e^2}{I_i I_e L} \left| \frac{v_i - v_e}{v_i - v_e} \right| F$$

where e is the electronic charge, v_i, v_e, I_i, I_e are the ion and electron velocities and currents, L is the length of the interaction region and F is the effective collision area (Keyser *et al* 1979).

Since all the products leave the collision centre with essentially the same velocity in the laboratory frame as the parent molecular ion, they share the parent's kinetic energy in proportion to their mass. Hence peaks will appear in the detector pulse height spectrum corresponding to masses $m(X)$, $m(Y)$, $2m(X)$, $m(X) + m(Y)$ and $2m(X) + m(Y)$. Substituting for Y using equation (1) this can be represented as follows:

$$1m(X),\ am(X),\ 2m(X),\ (1+a)m(X) \text{ and } (2+a)m(X)$$

When $a = 2$ only four peaks appear and this is reduced to three when $a = 1$.

The number of counts in each of the five peaks can be denoted as: N_1, N_a, N_2, $N_{(1+a)}$ and $N_{(2+a)}$ respectively. In addition the number of particles which fail to reach the detector, being stopped by the grid, is represented as N_0.

If the transmission coefficients of the grid is t then the probabilities of one, two and three particle traversing the grid are t, t^2 and t^3 respectively. The probability of a particle not traversing the grid is $(1-t)$. Using these facts and taking account of the effects of identical particles one can determine how the particles will be shared between the various peaks in the pulse height distribution.

Three individual cases must be considered. These are discussed in the following.

2.1. Case I ($a \neq 1$ or 2)

An example of this is the ion D_2H^+.

The relevant equations for this case are

$$N_0 = (1-t)^3 N_I + (1-t)^2(N_{II} + N_{III})$$

$$N_1 = 2t(1-t)^2 N_I + t(1-t)N_{III}$$

$$N_2 = t^2(1-t)N_I + t(1-t)N_{II}$$

$$N_a = t(1-t)^2 N_I + t(1-t)N_{II}$$

$$N_{(1+a)} = 2t^2(1-t)N_I + t(1-t)N_{III}$$

$$N_{(2+a)} = t^3 N_I + t^2(N_{II} + N_{III}).$$

Rearranging these equations allows us to solve for N_I, N_{II} and N_{III}. These can then be used to calculate the individual cross sections for channels I, II and III. Some of the solutions are as follows

$$N_I = \frac{N_1 - N_{(1+a)}}{2t(1-t)(1-2t)}$$

$$= \frac{N_a - N_2}{t(1-t)(1-2t)} \qquad (t \neq 0, 0.5, 1)$$

$$N_{II} = \frac{(1-t)N_2 - tN_a}{t(1-t)(1-2t)}$$

$$= \frac{2(1-t)(1-2t)N_{(2+a)} + t^2 N_1 + t(3t-2)N_{(1+a)}}{2t^2(1-t)(1-2t)}$$

$$(t \neq 0, 0.5, 1)$$

$$N_{III} = \frac{(1-t)N_{(1+a)} - tN_1}{t(1-t)(1-2t)}$$

$$= \frac{(1-t)N_{(2+a)} - tN_2}{t^2(1-t)} \qquad (t \neq 0, 0.5, 1).$$

2.2. Case II ($a = 2$)

An example of this is the ion H_2D^+. Here the equations are

$$N_0 = (1-t)^3 N_I + (1-t)^2(N_{II} + N_{III})$$

$$N_1 = 2t(1-t)^2 N_I + t(1-t)N_{III}$$

$$N_2 = [t^2(1-t) + t(1-t)^2]N_I + 2t(1-t)N_{II}$$

$$N_3 = 2t^2(1-t)N_I + t(1-t)N_{III}$$

$$N_4 = t^3 N_I + t^2(N_{II} + N_{III})$$

and $N_{\rm I}$, $N_{\rm II}$ and $N_{\rm III}$ are given by

$$N_{\rm I} = \frac{N_1 - N_3}{2t(1-t)(1-2t)}$$

$$= \frac{4(1-t)(1-2t)N_4 - 2t(1-2t)N_2 + t(4t-1)N_1 + t(4t-3)N_3}{4t^3(1-t)(1-2t)} \qquad (t \neq 0, 0.5, 1)$$

$$N_{\rm II} = \frac{2(1-2t)N_2 - (N_1 - N_3)}{4t(1-t)(1-2t)}$$

$$= \frac{2(1-t)(1-2t)N_4 + t^2N_1 + t(3t-2)N_3}{2t^2(1-t)(1-2t)} \qquad (t \neq 0, 0.5, 1)$$

$$N_{\rm III} = \frac{(1-t)N_3 - tN_1}{t(1-t)(1-2t)}$$

$$= \frac{4(1-t)N_4 + t(N_1 - N_3) - 2tN_2}{4t^2(1-t)} \qquad (t \neq 0, 0.5, 1)$$

Again there are other solutions for $N_{\rm I}$, $N_{\rm II}$ and $N_{\rm III}$.

2.3. Case III ($a = 1$, $X = Y$)

Examples of this case are the ions H_3^+ and D_3^+. Only two channels are open here, namely

$$e + X_3^+ \rightarrow X + X + X \qquad \text{I}$$

$$\rightarrow X_2 + X \qquad \text{II}$$

and the equations for the number of counts in each peak are

$$N_0 = (1-t)^3N_{\rm I} + (1-t)^2N_{\rm II}$$

$$N_1 = 3t(1-t)^2N_{\rm I} + t(1-t)N_{\rm II}$$

$$N_2 = 3t^2(1-t)N_{\rm I} + t(1-t)N_{\rm II}$$

$$N_3 = t^3N_{\rm I} + t^2N_{\rm II}$$

and $N_{\rm I}$ and $N_{\rm II}$ are given by

$$N_{\rm I} = \frac{tN_2 - (1-t)N_3}{2t^3(1-t)} \qquad t \neq 0, 1$$

$$= \frac{(1-t)N_3 - tN_1}{t^2(4t-3)(1-t)} \qquad t \neq 0, 0.75, 1$$

$$= \frac{N_1 - N_2}{3t(1-t)(1-2t)} \qquad t \neq 0, 0.5, 1$$

$$N_{\rm II} = \frac{3(1-t)N_3 - tN_2}{2t^2(1-t)} \qquad t \neq 0, 1$$

$$= \frac{t^2N_1 - 3(1-t)^2N_3}{t^2(4t-3)(1-t)} \qquad t \neq 0, 0.75, 1$$

$$= \frac{(1-t)N_2 - tN_1}{t(1-t)(1-2t)} \qquad t \neq 0, 0.5, 1.$$

Here, all the solutions have been presented.

3. Discussion

As mentioned in the introduction, this technique has already been used to measure the branching ratio for the two exit channels for the dissociative recombination of H_3^+ (Mitchell *et al* 1983). Individual cross sections for channel A ($H + H + H$) and B ($H_2 + H$) were determined by analysing the signals in the three product energy channels as discussed in case III. A 44% transparency grid was used for this study. It was found that the cross section for channel A exceeded that for channel B by a factor of two. The sum of the cross sections determined by this method agree well with measurements for the total cross section for H_3^+ recombination made without the grid (Mitchell *et al* 1984). This serves to confirm the efficacy of the technique in that it shows that there is no overall loss of signal.

An interesting feature of the analysis is the redundancy of the solutions. For example for case III there are three equations but only two unknowns. This fact can be used to perform internal consistency tests. By using the transmission t as an adjustable parameter, the value of t which gives the closest agreement between all the solutions can be determined. For the H_3^+ measurement the value of t obtained in this way was found to agree with that determined by direct measurement using a microscope, to within 3% (Forand 1983). This shows that the effects of glancing collisions of particles with the sides of the grid are minimal.

Fundamental to the success of the technique is the requirement that the particles be spatially uncorrelated. In other words the probability equations are only valid provided that the probability of two or more particles going through the same grid opening is negligible. This obviously is determined by the size of the grid opening and by the spatial distribution of the dissociation products. An analysis of this situation with reference to the measurement of dissociation reactions in the MEIBI experiment is given in the appendix and it is shown that spatial correlation can be neglected in this apparatus.

It should be noted that not all values of the transmission are valid. In particular the cases of $t = 0$ or 1 are trivial, corresponding to no grid and an opaque grid respectively. Furthermore, it can be seen that values of $t = 0.5$ and 0.75 should be avoided in some cases. This is because these values can lead to a reduction in the amount of information available. For example for case I, if $t = 0.5$ then N_1 and $N_{(1+3)}$ will be equal. Thus the simultaneous equations for these two quantities reduce to one and there is insufficient information to solve for both $N_{\rm I}$ and $N_{\rm III}$.

In addition to dissociative recombination, this technique can be used to study other dissociation processes. Recently Abraham *et al* (1984) have used a transmission grid technique to investigate the collisional dissociation of D_3^+ ions in gases. Furthermore other triatomics such as CH_3^+, NH_3^+, C_2H^+ and H_2O^+ can be studied provided that the energy resolution of the detector is sufficient to resolve the various peaks in the pulse height distribution.

Appendix

When a molecule dissociates there is inevitably some release of internal energy which is shared among the dissociation products in the form of internal excitation or kinetic energy. Conservation of momentum ensures that the products will move away from each other and the dissociation centre so that a homogeneous distribution of products will form in the interaction region. In the MEIBI experiment, the product detector is situated at a distance of 1 m from the interaction region. The size of the sphere containing the collision products can then be determined from the product kinetic energy release and the primary beam energy. The kinetic energy is shared among the products according to their mass.

For the case of H_3^+ dissociative recombination, 5 eV of internal energy is released in dissociation to the $H + H + H$ channel. 9 eV is released for the $H_2 + H$ channel. If we consider the former channel then each H atom will carry away 1.67 eV of kinetic energy. This means that it will move away from the dissociation centre with an extra velocity of 1.8×10^4 m s^{-1}. The primary H_3^+ ions having an energy of 400 keV will have an axial velocity of 5.0×10^6 m s^{-1}.

The fragments which leave the dissociation centre at right angles to the primary beam direction will have moved a distance of 3.5 mm by the time they reach the detector. This is the radius

of the spherical product distribution. The grid used in the experiment of Mitchell *et al* (1983) had a measured grid opening of $(1.7 \pm 0.08) \times 10^{-2}$ mm. The probability of two particles going through the same opening is given by the ratio of the opening area to the cross sectional area of the spherical distribution. For the above example this ratio is 7.5×10^{-6}. The error introduced by this is negligible compared with other uncertainties associated with the measurement.

References

Abraham S, Nir D and Rosner B 1984 Measurement of the branching ratio for the dissociative recombination of $H_3^+ + e$ *Phys. Rev.* A **29** 3122

Auerbach D J, Cacak R, Caudano R, Gaily T D, Keyser C J, McGowan J Wm, Mitchell J B A and Wilk S F J 1977 Merged electron–ion beam experiments I. Method and measurements of $(e-H_2^+)$ and $(e-H_3^+)$ dissociative–recombination cross sections *J. Phys. B: At. Mol. Phys.* **10** 3797

Berkner K H, Morgan T J, Pyle R V and Stearns J W 1971 *Proc. 7th ICPEAC, Amsterdam, 1977* ed. J Kistemaker (Amsterdam: North-Holland) p 422

Forand J L 1983 *MSc. Thesis* University of Western Ontario

Keyser C J, Froelich J R, Mitchell J B A and McGowan J Wm 1979 Beam-scanning system for determination of beam profiles and form factors in merged-beam experiments *J. Phys. E: Sci. Instrum.* **12** 316

Mitchell J B A, Forand J L, Ng C T, Levac D P, Mitchell R E, Mul P M, Claeys W, Sen A and McGowan J Wm 1983 Correlation between channel probabilities in collisional dissociation of D_3^+ *Phys. Rev. Lett.* **51** 885

Mitchell J B A, Ng C T, Forand L, Janssen R and McGowan J Wm 1984 Total cross sections for the dissociative recombination of H_3^+, HD_3^+ and D_3^+ *J. Phys. B: At. Mol. Phys.* **17** L909

APPENDIX D.

To appear in: "The Physics of Electron - Ion and Ion - Ion Collisions". NATO ASI Han-sur-Lesse,Belgium 1985. (eds. F. Brouillard and P. Defrance) Plenum Press, NY, 1986.

DISSOCIATIVE RECOMBINATION OF MOLECULAR IONS

J.B.A. Mitchell

Dept. of Physics and Centre for Chemical Physics

The University of Western Ontario

London, Ontario, Canada. N6A 3K7

INTRODUCTION

The dissociative recombination of molecular ions with electrons plays a central role in the physics and chemistry of ionized systems. Although simple in concept it displays an underlying complexity which has frustrated many attempts to obtain a clear understanding of its nature. In fact almost without exception it is impossible to say with confidence that the recombination of any molecular species is well understood. The problem lies partially within the inherent complexity of molecular systems with their infinite series of excited rydberg states which play an important role in the mechanism for recombination. An additional concern is the fact that as yet no absolute demonstration of the predicted mechanisms for recombination has been performed. Many experimental measurements relating to recombination have been made. All however have either inherent uncertainties concerning the identity of initial and final excitation states or have been performed on systems where recombination can proceed through a variety of channels so that no individual one can be singled out.

A number of reviews on molecular ion recombination have been published. Bardsley and Biondi (1970), Bardsley (1979), Berry and Leach (1981), Maruyama et al (1981), Eletskii and Smirnov (1982), Mitchell and McGowan (1983), McGowan and Mitchell (1984). This current review will concentrate upon a comparison of theoretical and experimental studies and in particular developments since the last NATO ASI on the Physics of Electron-Ion and Ion-Ion Collisions will be highlighted.

The recombination of small molecular ions generally proceeds via a mechanism in which the resulting electron-ion compound state dissociates into neutral fragments. This is called dissociative recombination. Energy has to be imparted to a molecule to ionize it. During recombination at least part of this energy must be removed and for dissociative recombination excess energy is carried away in the forms of kinetic energy and internal energy of the dissociation products. In this way the recombination process is stabilized so that the system does not become reionized. The initial electron-ion compound state formed when the electron is first captured, has a potential energy greater than the ionization limit of the

molecule so it can autoionize within a typical time of 10^{-13} secs. For the stabilization of the recombination to be efficient it must have a characteristic time of the same order or smaller than this. The time for the electron-ion state to dissociate into neutral fragments is typically comparable to the lifetime against auto-ionization so dissociative recombination can be a very efficient process. For atomic ions, stabilization occurs via radiative emission of photons with a characteristic time of $\sim 10^{-9}$ secs. This process does not compete very effectively with auto-ionization and so atomic ions have very small probabilities for recombination.

Bates and Massey (1947) first proposed the mechanism for dissociative recombination in order to explain the diurnal variation of the electron density in the earth's ionosphere. Earlier proposals based upon atomic ion recombination proved to have too long a timescale since predicted recombination rates were small. The much more efficient dissociative recombination mechanism allows molecular ions, formed via photoionization during the daytime, to act as an efficient sink for electrons at night.

Bates and Massey's mechanism for dissociative recombination can be understood with reference to figure 1. This shows the ground electronic state of a diatomic molecular ion AB^+. The latter is intersected by a repulsive doubly excited state of the neutral, AB_1^{**} and this dissociates to the limit $A^* + B$. Consider an electron with kinetic energy Ee approaching the ion AB^+. The total energy of the electron-ion system is then equal to the potential energy of AB^+ plus Ee. It can be seen from figure 1 that this energy is degenerate with the energy of AB_1^{**} for any value of Ee provided that AB_1^{**} intersects AB^+ in the vicinity of its minimum.

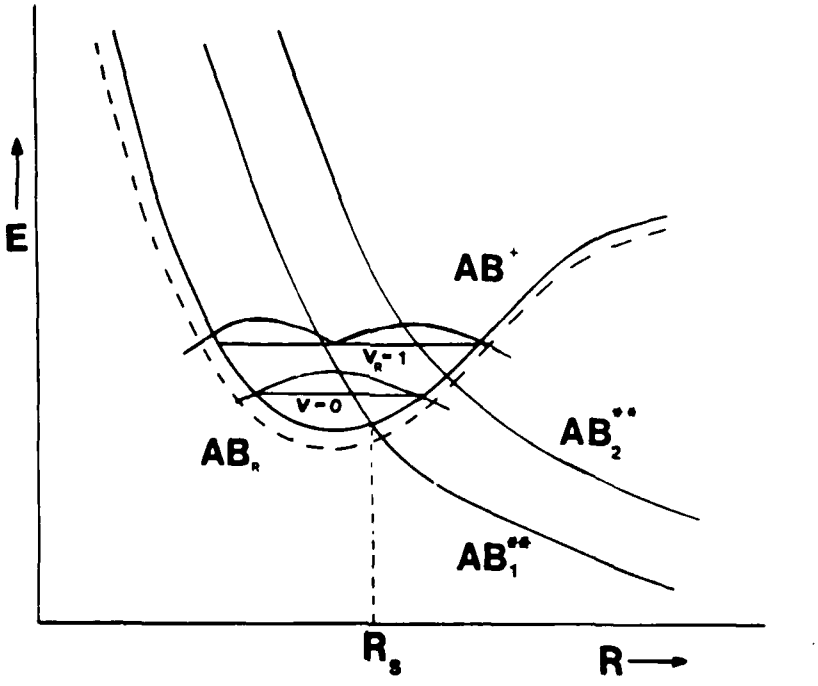

Fig. 1 Schematic representation of the states involved in the dissociative recombination of molecular ions.

It is possible then for the system to make a transition

$$e + AB^+ \rightarrow AB_i^{**}$$

i.e. a compound state can be formed. Since however this state lies above the ionization limit, it can decay back to AB^+ and a free electron. This is called autoionization. AB_i^{**} is repulsive however and so A^* and B will move rapidly apart. As they do their kinetic energy increases and so the potential energy of the system decreases. When their separation is greater than Rs, then AB_i^{**} can no longer autoionize and the recombination is stabilized. AB_i^{**} then continues towards dissociation

$$AB_i^{**} \rightarrow A^* + B$$

The above model presupposes however, that a state such as AB_i^{**} exists and that there is a good overlap between the nuclear wavefunctions of the AB^+ and AB_i^{**}.

It can be seen from figure 1 that if the ion is vibrationally excited then the overlap between the nuclear wavefunctions of AB^+ and AB_i^{**} is small. In this case there is a small probability of the initial electron capture occurring except for high energies. Note that the electron capture proceeds via a vertical, Franck-Condon transition between AB^+ and AB_i^{**}.

On the other hand, if the only available dissociating state is AB_2^{**} then the reverse is true. Ground state ions will not recombine with low energy electrons via this mechanism whereas vibrationally excited states will.

Experimental techniques.

The probability of electron-ion recombination is commonly quantified in terms of a rate coefficient $\alpha(cm^3s^{-1})$ defined by:

$$\frac{dNo}{dt} = \alpha N_i N_e \qquad \text{--- (1)}$$

where N_e, N_i and N_o are the number of electrons, ions and recombined neutrals in a given system. The term α is related to the collision cross section $\sigma(cm^2)$ by

$$\alpha = \int v_e \sigma(v_e) f(v_e) dv_e \qquad \text{--- (2)}$$

where v_e is the electron velocity of the reaction products and $f(v_e)$ is the velocity distribution. For most ionized media $f(v_e)$ is a Maxwellian distribution.

A wide variety of experimental techniques have been used to study molecular ion recombination. Essentially they fall into two categories, those which measure the disappearance of ions or electrons due to recombination and those where the neutrals thus formed are detected directly. Intersecting beam techniques such as Merged (Auerbach et al 1977), Inclined (Peart and Dolder 1974), crossed beams (Phaneuf et al 1975, Vogler and Dunn 1975) and laser induced fluorescence (Zipf 1980a,b) belong to the latter category. Microwave afterglow (Mehr and Biondi, 1969, Shiu et al 1977, Oskam and Mittelstadt 1963), Shock tube (Cunningham & Hobson 1969), Pulse radiolysis (Rebbert & Ausloos 1972) Maier & Fessenden (1975), Flame studies (Hayhurst and Telford 1971, Burdett and Telford 1979), Flowing afterglow langmuir probe (Alge, Adams and Smith 1983), Trapped ion (Walls and Dunn 1974, Mathur et al 1978) belong to the former.

Details and characteristics of these techniques have been discussed elsewhere (Mitchell and McGowan, 1983, McGowan and Mitchell 1984) and only the three techniques which are currently most active will be discussed here.

Microwave Afterglow

The afterglow technique was used to provide the first measurements of dissociative recombination more than thirty years ago and is still actively pursued. In the experiments, fig. (2) a glow discharge plasma is formed in a reaction vessel and when the exciting mechanism is turned off the decay of the plasma electrons is observed as a function of time by studying the reflection of low energy microwaves. The change in the electron density is given by:

$$\frac{\partial N_e}{\partial t} = \Sigma P_i - \Sigma L_i - \nabla.\Gamma_e \qquad \text{--- (3)}$$

where P_i = formation rate

L_i = Loss rate due to atomic processes

$\nabla.\Gamma_e$ = Loss rate due to diffusion.

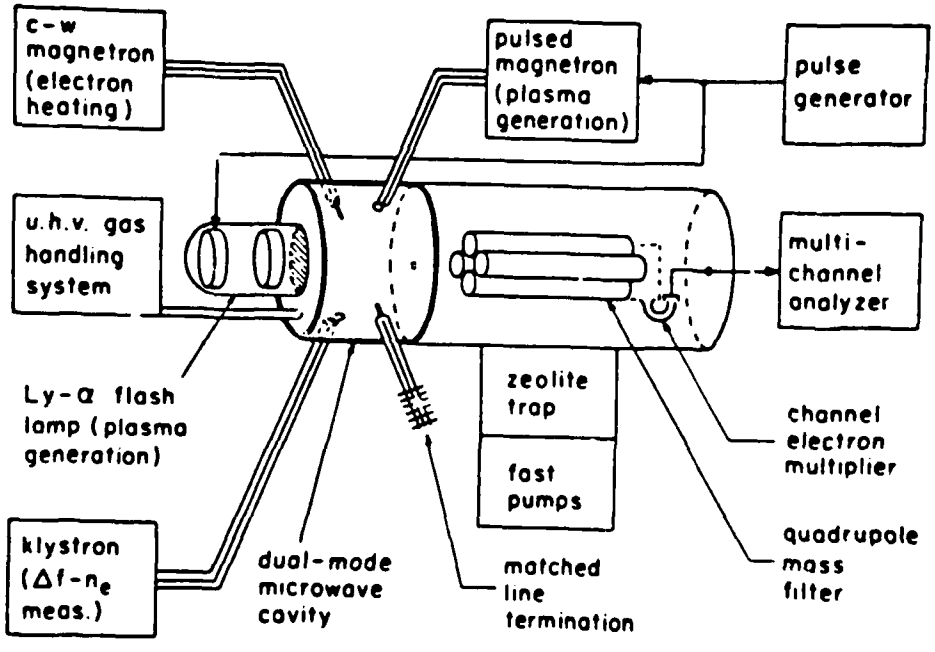

Fig. 2 Schematic Diagram of Biondi's Microwave Afterglow Apparatus. (Mehr and Biondi, 1969).

Care has to be taken to make sure that all contributions to each of the three terms on the RHS of equation (3) are taken account of. For example, metastable collisions can give rise to associative ionization thus increasing P_i; if the pressure is too high then three body effects contribute to L_i. One must also consider the importance of electron heating processes such as superelastic collision of electrons with excited atoms and molecules.

Ambipolar diffusion losses are usually minimized by using an appropriate buffer gas. Under ideal conditions:

$$\Gamma P_i = 0$$

$$\nabla . \Gamma_e = 0$$

$$L_i = \alpha N_i N_e$$

$$N_i = N_e$$

Then

$$\frac{dN_e}{dt} = - \alpha N_e^2 \qquad \text{--- (4)}$$

and so

$$\frac{1}{N_e}(r,t) = \frac{1}{N_e}(r,o) + \alpha t \qquad \text{--- (5)}$$

Hence the rate coefficient α can be determined from the slope of the $1/N_e$ vs. t plot. In practice, however, ambipolar diffusion giving rise to non-uniform electron distributions cannot be ignored requiring computer generated solutions of equation (3). Under normal conditions, $T_e = T_i = T_{gas}$, that is, the system has time to thermalize. It is possible however, to raise T_e, the electron temperature by microwave heating and so study the temperature dependance of the dissociative recombination rate coefficient. In this case T_i remains equal to T_{gas}.

The major problems associated with this technique are concerned with the identification of the ion under study and its excitation state. Clustering processes occur in the plasmas under certain conditions and these give rise to species such as $H_3O^+.(H_2O)_n$, $(N_4)^+$, etc. which compete for electrons in the plasma with the primary ion under study in the recombination process. The use of a mass spectrometer for the monitoring of plasma conditions is mandatory for the proper measurement of individual recombination rates of the various ion species.

A more complete description of a microwave afterglow apparatus employing mass spectrometric sampling may be found in Mehr and Biondi (1969). Determination of the state of excitation of the ion under study, is a major problem in recombination measurements. The problem lies in the fact that molecular ions can be electronically, vibrationally and rotationally excited. These states are often long lived compared to the lifetime of the ion in the system. In the past most experimenters have inferred the presence or absence of excitation by studying the rate coefficient for the recombination as the experimental conditions are varied. For example inert buffer gases are used in the plasma afterglow technique and the pressure of these gases can determine the rate of vibrational relaxation of the ion under study.

Recently Zipf (1980 a,b) however has introduced the use of laser induced photofluorescence for the determination of initial ion excitation in afterglow measurements. In this technique, a 1 MW tuneable dye laser is used to excite a particular transition from a given initial vibrational state (e.g. v = 0) and the fluorescence arising from the relaxation of the upper state is measured. Since the absolute laser flux entering the cavity is known then the population of the state under study can be determined directly.

Both Zipf (1980a,b) and Shiu et al (1977a,b,78) have further extended the afterglow technique to the examination of the excitation states of the dissociation products by measuring the light emitted when these states relax. Measurements such as these are vital to our eventual understanding of the mechanisms for dissociative recombination. Unfortunately, however, plasma techniques are capable of measuring rate coefficients only, because the observations are averaged over the electron velocity distribution of the plasma. They are therefore not as sensitive as the intersecting beam methods capable of measuring cross sections.

INTERSECTING BEAM EXPERIMENTS

These are experiments in which a beam of electrons is made to collide with a beam of ions and the products of the recombination are subsequently measured. Three variations have been used, namely crossed beams, inclined beams and merged beams.

Comprehensive reviews of intersecting beam techniques have been given by Harrison (1966), Dolder (1969), Brouillard and Claeys (1983) and Auerbach et al (1977).

Considering the case of a monenergetic ion beam with energy E_i intersecting a monoenergetic electron beam of energy E_e at some angle θ, then the collision energy in the centre of mass frame for this system is given by:

$$E_{cm} = \tfrac{1}{2}\mu(\bar{v}_i - \bar{v}_e)^2 = \mu[E_i/m_i + E_e/m_e - 2(E_i E_e/m_i m_e)^{\frac{1}{2}} \cos\theta] \qquad \text{--- (6)}$$

where m_i, m_e, are the ion and electron masses.

$$\mu = m_e m_i/(m_e + m_i) = m_e$$

μ = the reduced mass of the system.

v_r = relative velocity of the ion and the electron.

We can define a quantity called the reduced ion energy E_+:

$$E_+ = \frac{m_e}{m_i} \cdot E_i \qquad \text{--- (7)}$$

so that equation (6) becomes simplified to:

$$E_{cm} = E_+ + E_e - 2(E_+ E_e)^{\frac{1}{2}} \cos\theta. \qquad \text{--- (8)}$$

When θ is small, this reduces to

$$E_{cm} \simeq (E_+^{\frac{1}{2}} - E_e^{\frac{1}{2}})^2 + (E_+ E_e)^{\frac{1}{2}}\theta^2 \qquad \text{--- (9)}$$

Hence when $E_+ = E_e$, the minimum achievable centre of mass energy is limited by the value of θ.

By differentiating equation (6) with respect to E_i, E_e and θ one can obtain the following expression for the energy resolution ΔE_{cm}. (Assuming Gaussian distributions for ΔE_i, ΔE_e, and $\Delta\theta$).

$$\Delta E_{cm} = \left[\left(\left[1-(E_+/E_e)^{\frac{1}{2}} \right] \Delta E_e \right)^2 + \left(\left[1-(E_e/E_+)^{\frac{1}{2}} \right] \Delta E_+ \right)^2 + \left[2(E_e E_+)^{\frac{1}{2}} \theta \Delta\theta \right]^2 \right]^{\frac{1}{2}} \quad \text{--- (10)}$$

When $E_+ \simeq E_e$ the contributions due to ΔE_e and ΔE_i become negligible and the energy resolution is dominated by the angular term. This enables one to achieve very high resolution in the merged beam case provided θ can be made small.

Three groups have used intersecting beams for the study of dissociative recombination. Dunn, at JILA, used a crossed beam experiment for the study of the formation of D(2p) and D(n=4) atoms during e + D_2^+ recombination in the energy range from 0.6 - 7eV. Dolder, at Newcastle upon Tyne extended the energy range down to 0.3eV by using the inclined beam technique and measured total cross sections for e + D_2^+, H_2^+ and H_3^+ collisions. The most extensive beam studies of dissociative recombination have been performed at the University of Western Ontario, using a merged beam apparatus. To date more than 30 different species have been studied. McGowan and Mitchell (1984).

In Dunn's experiments, the recombination was measured by detecting the photons emitted during the decay of the excited dissociation products. This is technically difficult to do but detailed information concerning the decay channels of the process can be obtained in this way.

The other experiments both depend on measuring the number of neutrals formed as a result of the electron ion recombination. Because space does not permit detailed description of each of the apparatuses, only a brief outline of the MEIBE I (Merged Electron Ion Beam Experiment) at the University of Western Ontario will be given here.

Ions are produced in an rf ion source mounted in the terminal of a 400 Kev Van de Graaff accelerator. After focussing and mass analysis, the ion beam enters the ultra high vacuum experimental chamber where after being offset electrostatically to remove neutrals it passes through the interaction region. After collision with the electrons, the ion beam is analysed electrostatically to remove neutrals formed as a result of both electron-ion and background collisions and the primary ions are collected in a Faraday cup. The neutrals are allowed to strike a surface barrier detector and are subsequently counted.

The electron beam is formed in a Pierce type electron gun and is subsequently merged with the ion beam using a trochoidal analyser. This device operates by having a magnetic field axial to the electron beam and an electric field perpendicular to it. The electrons undergo a precise spiralling motion in the analyzer and when they emerge, if the correct conditions are present, the input and output vectors of the beam will be identical but the axis of the beam will be shifted to a new axis offset from the original. This new axis is made to coincide with the axis of the ion beam so that merging occurs.

After the interaction with the ion beam, the electrons are then "demerged" using a second trochoidal analyzer before being collected in a Faraday cup. A schematic diagram of the apparatus is given in Fig. (3).

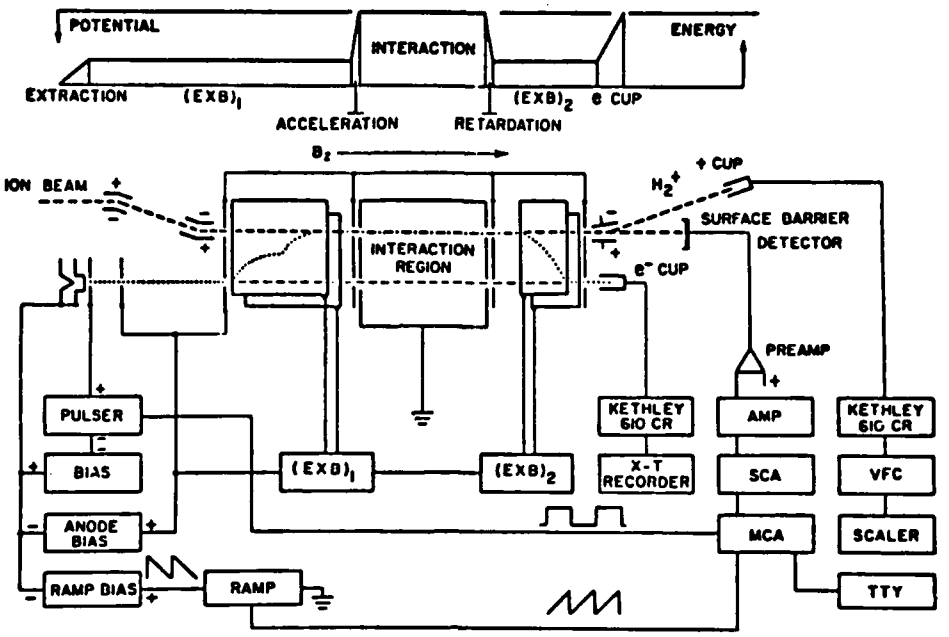

Fig. 3 Schematic diagram of the Merged Electron-Ion Beam Experiment (MEIBE I) at The University of Western Ontario. (Auerbach et al 1977).

The recombination cross section may be obtained using the following expression:

$$\sigma(E_{cm}) = \frac{C_n e^2 F}{I_e I_i L}\left|\frac{\bar{v}_i \cdot \bar{v}_e}{\bar{v}_i - \bar{v}_e}\right| \simeq \frac{C_n e^2 F}{I_e I_i L}\left|\frac{v_i v_e}{[(v_i - v_e)^2 + v_i v_e \theta^2]^{\frac{1}{2}}}\right| \qquad \text{--- (11)}$$

where C_n = neutral count rate

I_e, I_i = Electron and Ion beam currents

v_e, v_i = Electron and Ion beam velocities

θ = intersection angle

L = intersection length

$$F = \left[\iiint i_e(x,y)\, dxdy \iint i_i(x,y) dxdy\right]\left[\iiint i_e(x,y) . i_i(x,y) dxdy\right]^{-1} \qquad \text{--- (12)}$$

The form factor F is determined by measuring the beam density distributions and overlap at three places along the intersection length (Keyser et al 1979) and so absolute cross sections may be obtained using this apparatus.

A major reduction in background noise levels can be achieved by exploiting the energy resolving properties of the surface barrier detector. Neutral atoms arising from dissociative collisions of the primary beam with the background gas giving ion-atom pairs, arrive with only a fraction of the beam energy and so can be distinguished from other processes such as dissociative recombination and dissociative charge exchange where the resulting neutrals carry the total beam energy. Separation of these latter two processes is then accomplished by modulating the electron beam and counting the neutrals in and out of phase with the modulation using gated scalers.

The merged beam technique represents a very significant advance over previous methods for studying dissociative recombination. Some of its advantages and disadvantages are outlined in table (I).

TABLE I

ADVANTAGES

1. Absolute cross sections can be measured over a very wide energy range, a few meV to many eV.

2. Collision energy is accurately known since nearly monoenergetic beams are used, the only uncertainty coming from the uncertainty in θ. Furthermore, energy de-amplication during conversion from the laboratory to the centre of mass frame of reference makes very high resolution measurements possible (Few meV). Lower limit is determined primarily by intersection angle.

3. Signal to background ratio higher than for inclined beam experiments.

4. Use of nuclear counting techniques allows the neutral products to be studied. Measurement of final state excitation and branching ratios are possible by improving the energy resolution of the counting system and exploiting the energy amplification upon transforming from the centre of mass to the laboratory frame of reference.

FLOWING AFTERGLOW LANGMUIR PROBE

This technique has been used recently to measure a number of dissociative recombination rate coefficients. (Alge et al 1983, Adams et al 1984). It has been described in detail in the review by Smith and Adams (1983) at the previous NATO ASI on the Physics of Ion-Ion and Electron-Ion Collisions.

Briefly a helium carrier gas is introduced into a stainless steel flow tube and is made to pass through the tube under the action of a Roots pump. The gas is excited upstream using a microwave cavity and He^*, He^+ and electrons are generated Fig. (4). Typical carrier gas pressures in the range 0.6-1.0 Torr are used and electron densities up to $7 \times 10^{10} cm^{-3}$ are produced.

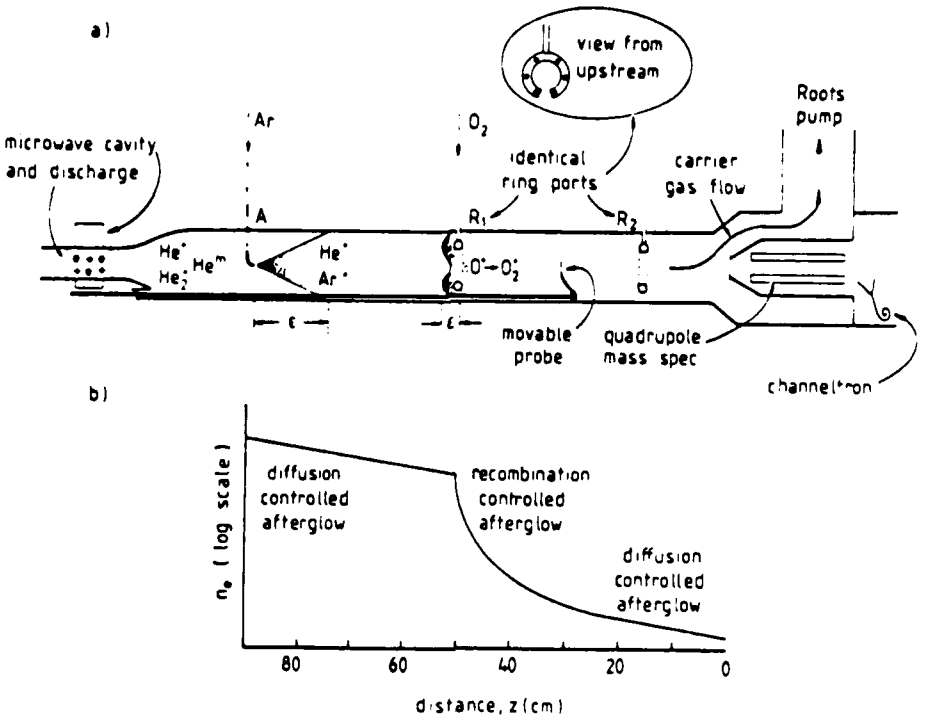

Fig. 4 The FALP experiment showing details of the gas inlet ports, diagnostic instruments, etc. Also shown is a typical electron density profile along the flow tube during recombination studies. (Alge et al, 1983).

A moveable langmuir probe is used to measure absolute ion and electron densities. Argon is introduced at port A and this serves to remove the metastable Helium atoms through the reaction:

$$He^* + Ar \rightarrow He + Ar^+ + e$$

Reactant gas is introduced via ports R_1 or R_2 and this is ionized via charge exchange collisions with He^+ ions. The electron density is measured as a function of distance along the tube (fig. (4b) and the rate coefficient for molecular ion recombination is determined from the equation

$$\frac{\partial Ne}{\partial t} = D_a \nabla^2 N_e - \alpha Ne \cdot N_i$$

where D_a is the ambipolar diffusion coefficient. By operating at high helium pressures, the diffusion term becomes negligible so that recombination dominates. A quadrupole mass spectrometer is used to identify the reactant ions.

The FALP apparatus can be operated at a range of temperatures from 80-600K by cooling or heating the tube. At lower temperatures, the formation of cluster ions becomes a problem.

The ions are believed to be de-excited to their vibrational and rotational ground states because of thermalizing collisions with both the reactant and carrier gases.

To date the ions O_2^+, NO^+, NH_4^+, HCO^+, N_2H^+, CH_5^+ have been studied using this apparatus but the most significant study has been of H_3^+ recombination. The FALP study has indicated that this process has a very small rate coefficient. More will be said of the significance of this result later.

THEORETICAL STUDIES

(i) Potential Energy Curves

Calculation of the cross section for dissociative recombination begins with the determination of the relevant potential energy curves for the system. The normal potential curves for a diatomic molecule represent stationary states which are "adiabatic" in form. That is, they represent the energy that the molecule would have in a given electronic configuration for a range of inter-nuclear separations if the atoms were at rest with respect to each other. These permanent states can be observed directly by means of optical spectroscopy and so their energies can be measured experimentally with great accuracy. The molecule can exist not only in its ground state but also in a host of excited states representing configurations where one or both of the electrons is excited.

The energies of these states may be calculated from the Schrodinger equation:

$$H\Psi = E\Psi \qquad \text{--- (1)}$$

where H is the Hamiltonian, Ψ the wavefunction and E the total energy of the complete system, i.e. nuclei and electrons. H can be written in the form:

$$H = H_e + T_R \qquad \text{--- (2)}$$

where T_R is the nuclear kinetic energy operator.

$$T_R = -\left[\hbar^2/2M\right]\nabla_R^2 \qquad \text{--- (3)}$$

M being the reduced mass of the two nuclei [$M = m_A m_B/m_A+m_B$] and R is the internuclear separation. H_e is called the electronic Hamiltonian and represents the kinetic and potential energy of the electrons plus the potential energy of the nuclei due to their electrostatic repulsion.

$$H_o = \sum_{i=1}^{N}\left[-(\hbar^2/2m)\nabla_i^2 - \frac{Z_A e^2}{r_{iA}} - \frac{Z_B e^2}{r_{iB}} + \sum_{j=i+1}^{N}\frac{e^2}{r}\right] + \frac{Z_A Z e_B^2}{R} \qquad \text{--- (4)}$$

where the sum is over N electrons, m is the electron mass, r_{iA} and r_{iB} are the distances between the electron i and the nuclei A and B and r_{ij} is the distance between electron i and another electron j. Z is the nuclear charge. The total wavefunction for the system can be expanded in terms of electron wave functions $\phi_i(r,R)$ and nuclear wavefunctions

$$\Psi = \sum \phi_i(r,R)\,\chi_i(R) \qquad \text{--- (5)}$$

This would seem to be a major stumbling block. However the fact is that this rule does not apply to states ϕ_i which do not diagonalize H_e. It is possible to choose wavefunctions ϕ_i which do not diagonalize the electronic Hamiltonian H_e but which when combined with suitable nuclear wavefunctions χ_i do diagonalize the total Hamiltonian. This is of course necessary for the states to have definite energies. Such states are referred to as diabatic states and are discussed very lucidly by O'Malley (1971) from which most of the preceding discussion has been taken. The main point to notice is that for these states, the right hand side of equation (7) is no longer zero and so there is coupling between different states which allows non-optical transitions between different states to occur.

For the case of dissociative recombination or attachment, the most suitable set of wavefunctions ϕ_i is one containing potential scattering terms and terms which describe the resonant electron-ion compound state.

Calculation of the energies of these diabatic states is beyond the scope of this lecture and the interested reader is referred to the reviews of Guberman 1983, Michels 1981, and O'Malley 1969. The results and consequences of such calculations for individual systems will be discussed later.

(ii) Calculation of the Cross Section

Once the intermediate AB^{**} state has been identified then calculations of the cross section for dissociative recombination can proceed. The overall problem is to determine the probability of a transition from an electron-ion scattering continuum to an atom-atom dissociation continuum. In practice this involves calculating the probability of the capture of a free electron into a doubly excited resonance state AB^{**} followed by the determination of the probability of dissociation of this state. Thus the dissociative recombination cross section is often represented:

$$\sigma_{DR} = \sigma_{CAP} \times S_P$$

where S_P, the survival factor has a value of unity or less and represents the dissociation probability. The coupling between the initial scattering state, the intermediate resonance and the final dissociation continuum is complicated by the presence of an infinite number of Rydberg states of the neutral molecule whose potential energy curves lie beneath that of the molecular ion ground state. Initially we shall ignore these and consider only direct dissociative recombination which only involves the three states already alluded to.

This problem has been treated by O'Malley 1966, 1971, 1981, Bardsley 1968a,b, Bottcher 1976.

The dissociative recombination cross section is given by:

$$\sigma = \left\{\frac{4\pi^3}{k^2}\right\} g |T|^2 \qquad \text{--- (10)}$$

where $k = p/\hbar$ is the electron wave number (p is the momentum), g is the spin-weighting factor, the ratio of the statistical weights between the two states $\hbar = h/2\pi$ where h is Planck's constant and T is given by

Multiplying equation (1) on the left by ϕ_i^* and integrating over all electronic co-ordinates allows a set of coupled equations for the nuclear wavefunction to be written down. Upon rearranging terms:

$$\left[T_R + T''_{ii} + V_{ii}(R) - E\right] \chi_i(R) = \sum_{j\neq i}^{N} \left[V_{ij} + T'_{ij} + T''_{ij}\right] \chi_j(R) \qquad \text{--- (6)}$$

where $V_{ab} = \langle \phi_a | H_e | \phi_b \rangle$

T' and T" result from the term $\nabla^2 \phi\, \chi$

Since $\nabla^2 \phi\, \chi = \phi \nabla^2 \chi + 2 \nabla\phi . \nabla\chi + \chi \nabla^2 \phi$

then $T'_{ij} = -2(\hbar^2/2M) \langle \phi_i | \nabla_R | \phi_j \rangle . \nabla_R$

$$T''_{ij} = -(\hbar^2/2M) \langle \phi_i | \nabla_R^2 | \phi_i \rangle$$

Because of the huge difference in mass between the nuclei and the electrons, the nuclei can essentially be assumed to be at rest when compared with the electronic motion. The Born-Oppenheimer approximation involves neglecting the T' and T" terms which are much smaller than the other terms in equation (6) which then reduces to

$$\left[T_R + V_{ii}(R) - E\right] \chi_i(R) = - \sum_{j\neq i}^{N} V_{ij} \chi_j \qquad \text{--- (7)}$$

Note that in this equation, the V_{ab} terms contain the potential energies of the nuclear motion together with electronic coupling terms for given ϕ's. The problem then is to find suitable ϕ functions so that V may be evaluated. It should be remembered that for stationary solutions the Ψ functions must diagonalize the total Hamiltonian H.

If we take ϕ_i to be the stationary eigenvalue of H_e, i.e. the solution to:

$$H_e \phi_i = V_{ii} \phi_i \qquad \text{--- (8)}$$

then equation (7) is considerably simplified

since $\langle \phi_i | H_e | \phi_j \rangle = V_{ii} \delta_{ij}$

where $\delta_{ii} = 1 \quad \delta_{ij} = 0$

These ϕ_i states are referred to as adiabatic states.

Equation (7) becomes

$$\left[T_R + V_{ii} - E\right] \chi_i = 0 \qquad \text{--- (9)}$$

The essential feature of this equation is that the states χ_i are uncoupled, i.e. there are no coupling terms between different states so that they are permanent states. These are the normal molecular states observed by optical spectroscopy.

The problem with these states from the point of view of describing dissociative recombination is that the non-crossing rule of Von Neumann and Wigner (1929) states that two potential energy curves V_{ii} and V_{jj} may not cross if they have the same symmetry (spin, parity and angular momentum).

$$T = \exp(i\rho) \langle \chi_i | V_a | \chi_d \rangle$$

Here χ_i is the vibrational wave function of the initial ion AB^+

χ_d is the vibrational wavefunction of the resonance state and V_a is the electronic matrix element

$$V_a = \langle \phi_i | H_e | \phi_r \rangle$$

The resonance width Γ_a is given by

$$\Gamma_a = 2\pi |V_a|^2$$

where the lifetime of the resonance against autoionization is $\hbar/\Gamma a$.
ρ is the complex phaseshift for the resonance AB^{**}. The square of the $e^{i\rho}$ term is the survival factor.
Equation (10) can be written in an alternative form.

$$\sigma = \text{const.} \frac{\Gamma_a}{E} \times FC \times SP$$

where Γ_a is the autoionization width of the resonance

E is the energy of the incoming electron

FC, the Frank-Condon factor is the overlap integral between the vibrational wavefunctions of the initial and resonant states and SP is the survival factor.

It is interesting to note that if there is a good overlap, then the cross section should vary as E^{-1}.

The case of $e\text{-}H_2^+$ recombination is of particular importance since it may be approached by ab initio techniques and a number of studies of direct dissociative recombination have been performed for this ion. Bauer and Wu (1956), Wilkins (1966), Bottcher (1976), Zhdanov & Chibisov (1978) Rai Dastidar & Rai Dastidar (1979), Derkits et al (1979), Zhdanov (1980), Schneider et al (1985).

Generally, it is accepted that the lowest repulsive state, the $^1\Sigma_g^+ \; 1\sigma_u^2$ state dominates the electron capture and accurate calculations of the energy and wavefunctions of this state have been performed. The results of Guberman (1983) are shown in fig. (5) and they indicate a curve crossing at the v=1 level. This generally agrees with calculations of Hazi et al (1983). Although the earlier studies of Bottcher & Docken (1974) predicted a curve crossing in the vicinity of the v=2 level.

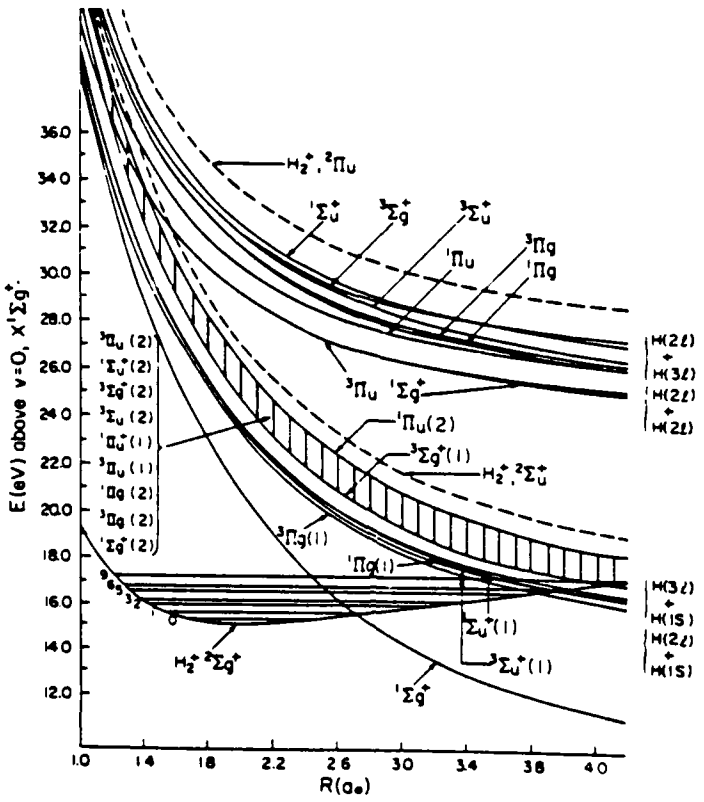

Fig. 5 Potential energy curves for H_2^+ and H_2 as calculated by Guberman, 1983.

The most recent calculation by Schneider et al (1985) actually predicts a curve crossing in the vicinity of v=0 although the authors point out that they treat the state as a rydberg state which it is not. The validity of this calculation is therefore suspect.

Other calculations, Zhdanov and Chibisov (1978), Derkits et al (1979), Zhdanov (1980) and Schneider et al (1985) have considered contributions due to higher repulsive states of the form $1\sigma_u$ nl which are rydberg states of the $^2\Sigma_u^+$ $1\sigma_u$ state of H_2^+. These states probably play an important role for higher electron energies and for vibrationally excited ions.

The results of Derkits et al (1979) for the recombination cross section through the $1\sigma_u 3s$ $^1\Sigma_u^+$ and $^3\Sigma_u^+$ states of H_2 for H_2^+ ions in various vibrational states are shown in fig. (6). It can be seen that these cross sections clearly reflect the Franck-Condon overlap between the repulsive state wavefunction and that of the various vibrational states of the H_2^+ ion.

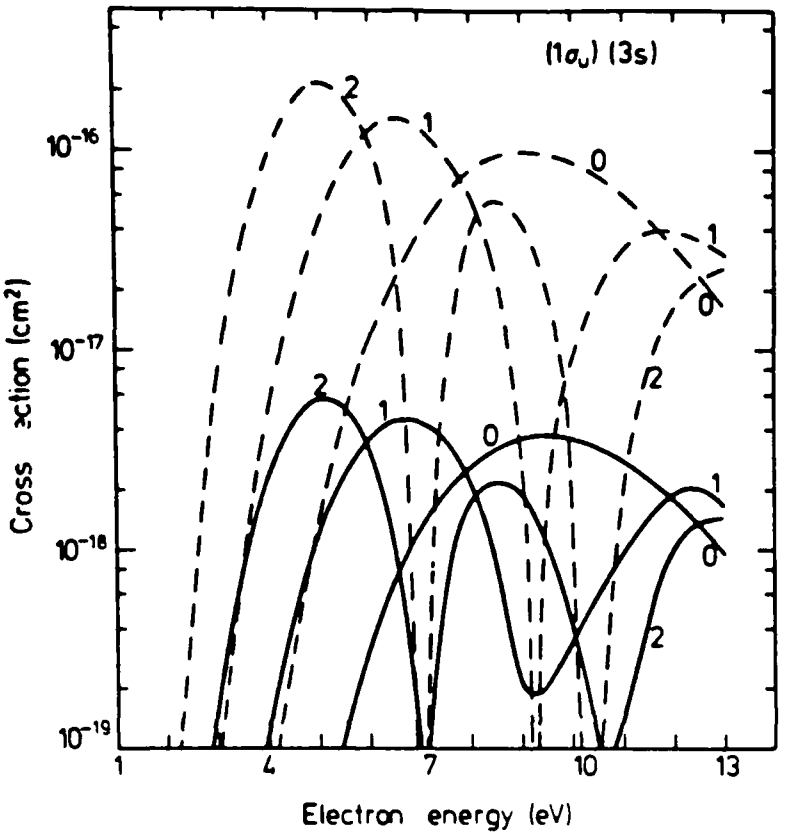

Fig. 6 Cross sections for recombination of electrons with H_2^+ in various initial vibrational states. ——, calculated with allowance for autoionization - - -, calculated without allowance for autoionization. (Derkits et al, 1979).

The Influence of Rydberg States

As mentioned earlier the transition from the electron-ion continuum to the dissociation continuum is complicated by the presence of Rydberg states of the neutral molecule which lie just below the H_2^+ ground state or potential curve See fig. (1). These states affect both the initial electron capture process and the subsequent dissociation.

Vibrationally excited levels of high lying rydberg states can lie above the ionization limit of the molecule and can therefore autoionize. The influence of such states upon the ionization thresholds of simple molecules has been amply demonstrated by the high resolution spectroscopic studies of Dehmer and Chupka (1976).

It is conceivable therefore that the reverse of autoionization, namely electron capture can occur via these states. In other words the electron is first captured into a vibrationally excited Rydberg state which can subsequently decay either via autoionization or via predissociation through the diabatic AB^{**} state discussed previously. Since the electron can only be captured when its energy coincides with the energy difference between the vibrational levels of the Rydberg and ion states this process is essentially resonant.

Our understanding of the influence of these Rydberg states on the recombination process has matured considerably since the indirect mechanism was first proposed. The early studies of Bardsley (1968a,b) treated the direct and indirect processes separately but recent work by Giusti (1980), O'Malley (1981) and Giusti et al (1983) have used a combined formalism allowing the interference between the two processes to be studied.

Giusti-Suzor et al (1983) have studied the recombination of H_2^+ in the ground and excited vibrational states using both configuration interaction and MQDT approaches.

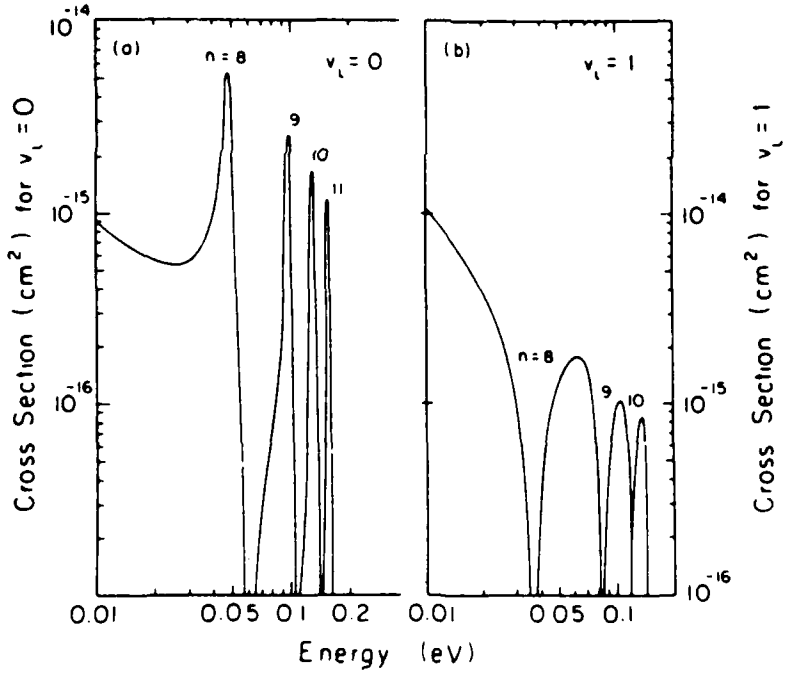

Fig. 7 Cross section for dissociative recombination of H_2^+ computed using the configuration interaction method and a hypothetical resonance curve. (a) for ions with v=0. (b) For v=1. Dips in (b) arise from Rydberg states with v=2. Each series should extend to n=∞ at the vibrational excitation threshold (close to 0.27 eV).

Fig. (7) shows their results for H_2^+ in v=0 and v=1 levels recombining through a hypothetical state which crosses the H_2^+ state at R=2.8A, i.e. well away from the Franck-Condon region of the v=0 level. It can be seen that for $H_2^+(v=0)$, indirect recombination gives rise to peaks while for $H_2^+(v=1)$ it leads to dips in the total cross section. The predicted resonances are typically, a few meV in width. This work is discussed in more detail by Giusti in this volume.

O'Malley (1981) has used an alternative approach in his analysis of the effects of Rydberg states on dissociative recombination. He neglected electron capture via Rydberg states which gives rise to narrow resonance structure but treated the coupling between the dissociating AB^{**} state and low n value Rydberg states AB_R. This coupling is very important as it determines the final states of the neutral recombination products. Fig. (8) shows how transitions will occur between the states AB^{**} and AB_D.

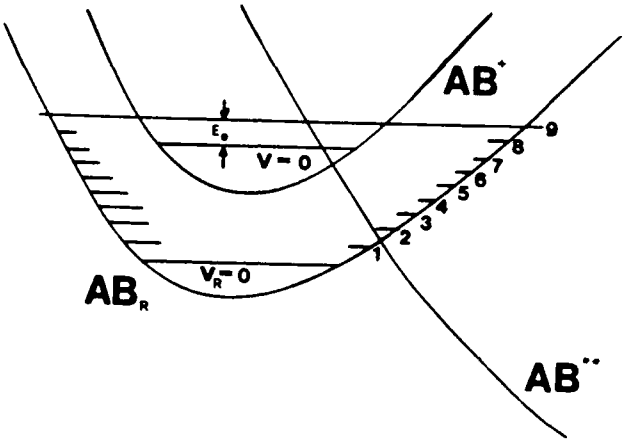

Fig. 8 Schematic illustrating the resonant aspects of the crossing of the dissociating curve responsible for the initial electron capture with low lying Rydberg states.

Now since energy is conserved this means that a transition will satisfy the condition:

$$(V_{**_{AB}} + KE_{**_{AB}}) = (V_{AB_R} + KE_{AB_R})$$

Thus a transition is most likely for the condition that AB^{**} and AB_R both start out with the same potential energy. This can only occur for discrete values of VAB_R corresponding to vibrational levels. Since these vibrational levels can themselves decay via autoionization or dissociation they can be treated as resonances and so resonance formalism (Lippmann and O'Malley 1970) can be used to describe the coupling between AB^{**} and AB_R.

O'Malley has shown that introduction of this coupling serves to modulate the zeroth order cross section (neglecting coupling) close to the resonance energy so that

$$\sigma = \sigma_o\left[\cos \eta_\gamma + e^{-\rho}\sin \eta_\gamma\right]^2$$

where $\eta_r = \tan^{-1}\left[\tfrac{1}{2}\Gamma_r/(E_r - E_e)\right]$

Γ_r is the resonance width given by:

$$\Gamma_r = 2\pi|V_r|^2 \quad \text{and} \quad V_r = \langle \chi_{AB_r} | V_{dr} | \chi_{AB}^{**} \rangle$$

where V_{dr} represents the coupling between the two states. E_r is the energy of the resonance (above AB^+) and E_e is the electron energy. The term $e^{-\rho}$ is the survival factor which is unity for the case of the resonance being completely stable against autoionization and equal to zero if the resonance is fully autoionizing. The ratio of σ/σ_o is plotted against η_r, i.e. against E_e in the vicinity of the resonance, in Fig. (9). It can be seen that for the case of $e^{-\rho} = 0$, the coupling between the states leads to a dip in the cross section the width of which is estimated by O'Malley to be 30-50meV. If the resonance does not autoionize then it displays a Fano-Beutler profile (Fano 1961), i.e. giving rise to both a local increase and decrease of σ, due to interference between the directly and indirectly dissociating channels.

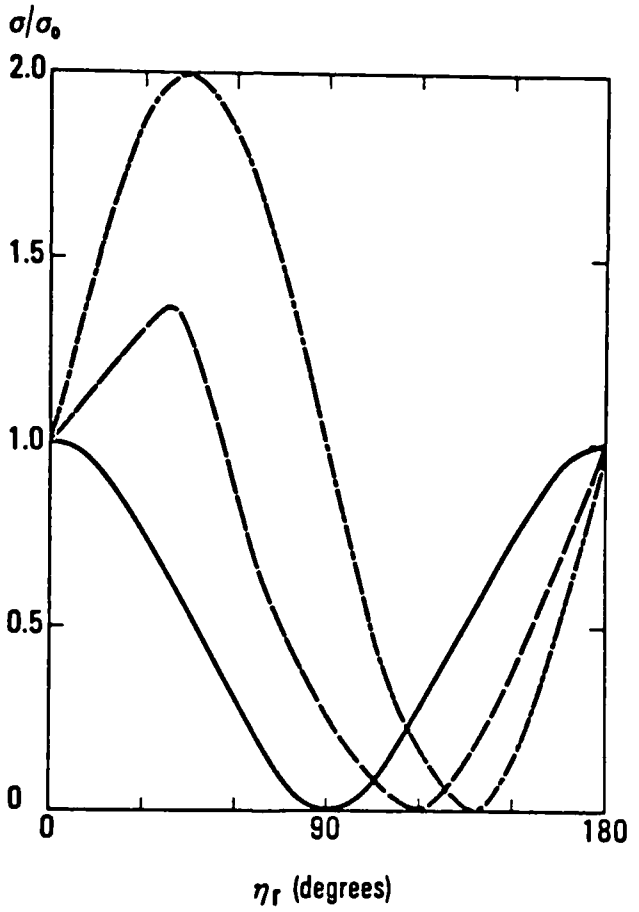

Fig. 9 The ratio of the cross section for dissociative recombination including Rydberg state interaction to that without plotted against η_r.

(——) $e^{-\rho} = 0$. (- -) $e^{-\rho} = 0.5$.

(- · -) $e^{-\rho} = 1.0$.

H_2^+ Studies

Much of the impetus for this work came from the work of Auerbach et al (1977) who discovered a host of resonant structures in the cross sections for e + H_2^+ and e + H_3^+ recombination. Subsequent studies however, (D'Angelo 1979, Ng, 1982, Sen 1985) intended to reproduce these resonances have revealed only minimal structure. Following the measurements of Auerbach et al modifications were made to the MEIBE apparatus which although successful in improving the signal to background ratio, may possibly have deteriorated the energy resolution. In addition recent studies of vibrational population control, Sen (1985), have shown that the rf source used in the original measurements is less than suitable because of the short residence time of the ions within the source.

Clearly before the theoretical calculations can be properly compared with actual measurements a much improved experiment incorporating well defined vibrational populations and improved energy resolution will have to be performed. Planning for this is underway.

An aspect of dissociative recombination that has received more attention experimentally that theoretically is the identity of the final products. In particular Phaneuf et al (1975) and Vogler and Dunn (1975) have measured the partial cross section for the recombination of D_2^+ leading to $D^*(n=4)$ and $D^*(2p)$ respectively. In each case they found that the measured partial cross section accounted for only about 10% of the total cross section for e + D_2^+ recombination (Peart & Dolder 1973).

The measurements were however made for energies greater than 0.6eV and no attempt was made to alter the vibrational population of the D_2^+ ions. A variety of exit channels leading to higher n states was therefore available.

For low energy collisions involving vibrationally cold ions only the dissociational limit giving n=2 atoms is energetically available. Peart and Dolder (1975) have studied the cross section for ion pair formation following dissociative recombination of H_2^+, i.e.

$$e + H_2^+ \rightarrow H^+ + H^-$$

They found that the cross section was small, less than 0.1% of the total cross section (Peart and Dolder, 1974). This is interesting since the dissociating state involved in the electron capture actually tends to a limit of $H^+ + H^-$ at large R. (O'Malley, 1969).

The fact that neutrals are the dominant product of dissociative recombination indicates that curve crossings between the resonant dissociating state and the low n Rydberg states play a vital role in the recombination process. (O'Malley 1981).

Recent developments at UWO have opened up new opportunities for the study of H_2^+. As mentioned earlier, the H_2^+ formed by electron impact ionization of molecular hydrogen has all 19 available vibrational states populated. (Von Busch & Dunn 1972). It is in principle possible to selectively remove many of the excited vibrational levels by suitable manipulation of ion source chemistry.

Chupka et al (1968) have shown that the reactions:

$$H_2^+(v) + He \rightarrow HeH^+ + H$$

$$H_2^+(v) + Ne \rightarrow NeH^+ + H$$

are endothermic. Vibrational excitation of the H_2^+ ions corresponding to v>2 and v>1 respectively allows the reactions to proceed rapidly. By mixing helium or neon with the hydrogen gas in the ion source, it is in principle possible to react out the excited levels. Therefore the H_2^+ beams extracted under these conditions should have only the v=0,1,2 or v=0, 1 levels populated. This was tried by Auerbach et al (1977) and it was observed that the measured cross section changed by about a factor of 2 for a hydrogen/helium mixture and by a further factor of 1.6 for a neon/hydrogen mixture. Recent modelling calculations by Sen (1985) however suggest that the reasonably short residence time for ions in the rf source used by Auerbach et al precluded the complete de-excitation. Indeed Sen's analysis indicates that states up to and including v=6 remain populated under normal source conditions.

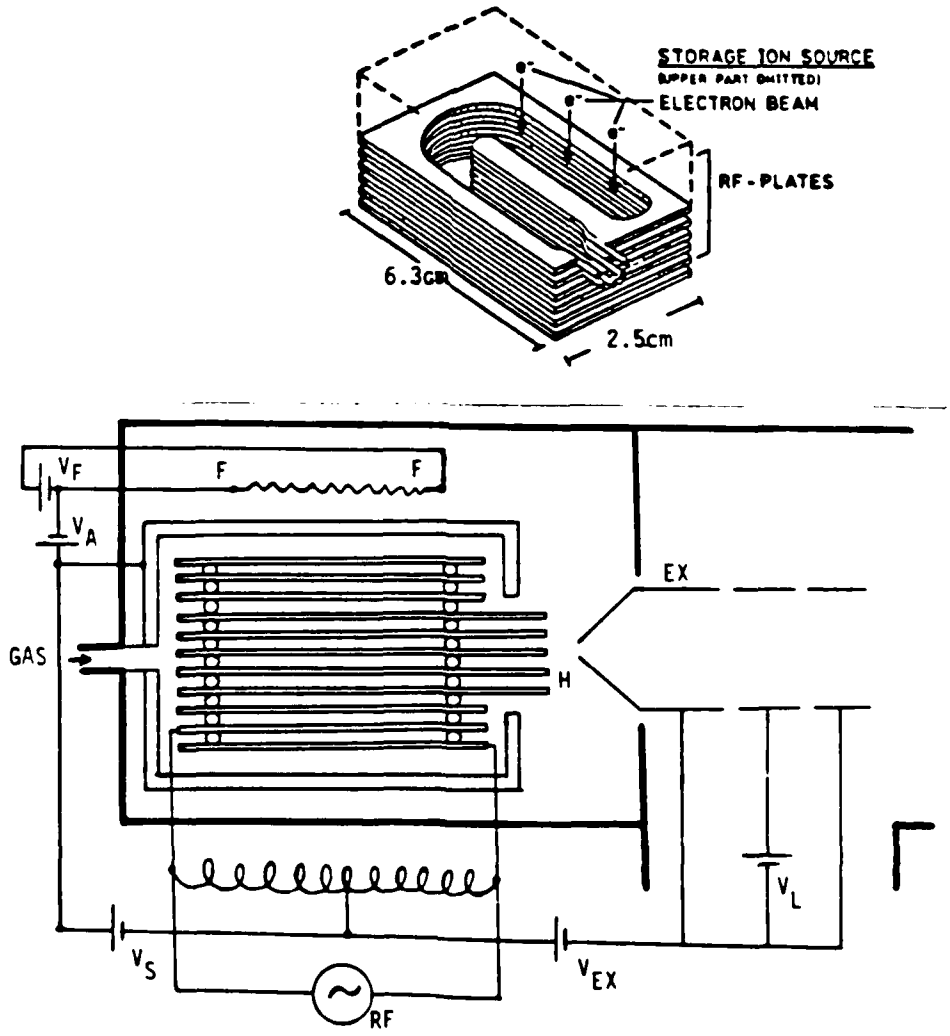

Fig. 10 The Teloy storage ion source showing the arrangement of the plates with the U-holes and the octupolar exit geometry.
FF: Filament, H: Octupolar exit hole, EX: Extractor, RF: Radiofrequency source, V_F: Filament voltage; V_A: Electron accelerating voltage; V_S: Suppressor voltage: V_{EX}: Extraction voltage; V_L: Lens voltage. (Sen, 1985).

A radio frequency storage ion source has been constructed at UWO following a design by Teloy & Gehrlich (1974). In this source, ions are formed by electron impact and are confined in a potential well formed by an oscillating electric field applied to a stack of electrodes Fig. (10). Ions diffuse along the U-shaped channel before eventually being extracted through the hexapolar extraction lens. Residence times of several milliseconds can be achieved in this source.

Sen et al (1985) have examined the excitation state of ions extracted from this source by using a low energy crossed beams apparatus to study the collisional dissociation of molecular ions in collision with a beam of helium atoms. Fig. (11) shows the relative cross section for the formation of H^+ from H_2^+ + He collisions for ions formed under different source conditions. It can be seen that for low pressures and pure hydrogen source gas, the process exhibits a low reaction threshold indicating the presence of vibrationally excited H_2^+ ions. When neon is added and the source is operated at elevated pressures, then the excited states are quenched leaving only v=0 and 1 as predicted. Similar results were found for helium except that the observed threshold indicated the presence of v=2 ions in the beam. Fig. (12).

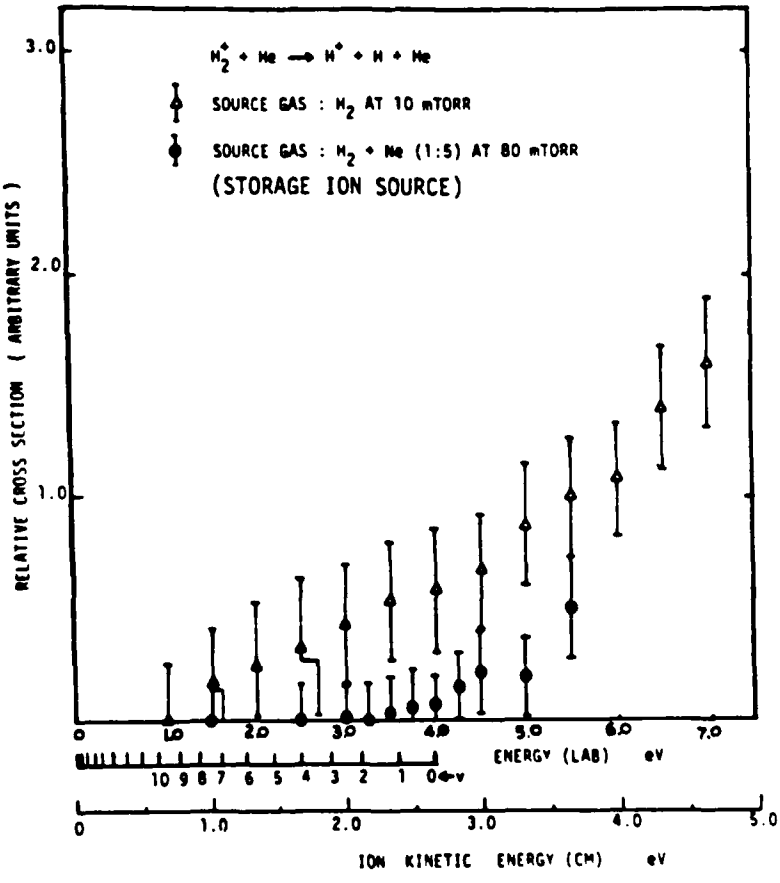

collisional induced dissociation of H_2^+ ions formed in the storage ion source with pure hydrogen gas and with a mixture of hydrogen and neon, (1:5). Threshold energies for the different vibrational levels of H_2^+ are also shown. (Sen et al, 1985).

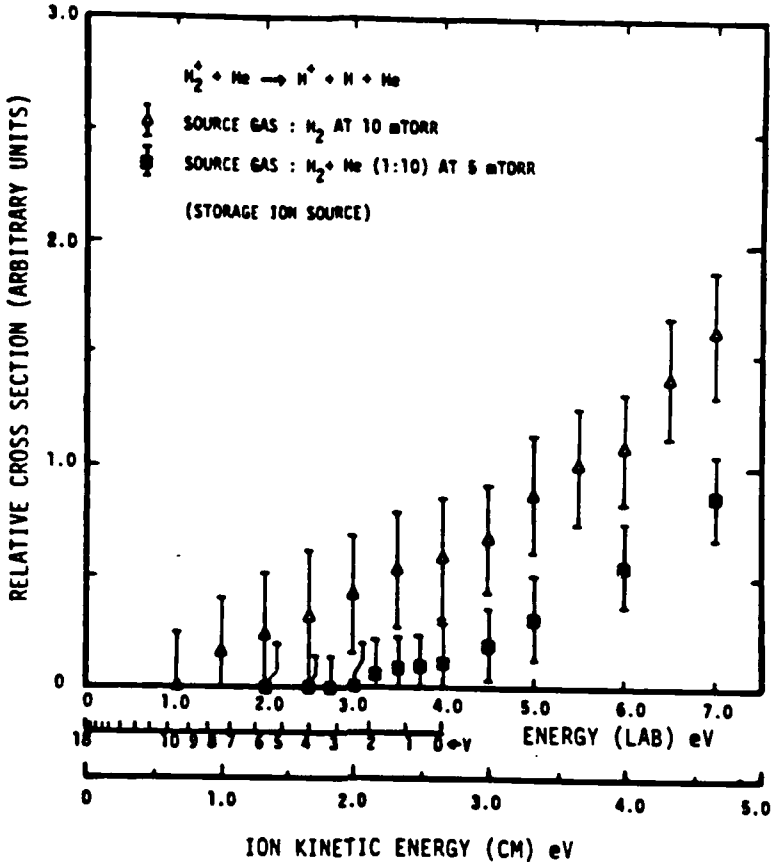

Fig. 12 Relative cross sections for the collisional induced dissociation of H_2^+ ions formed in a storage ion source with pure hydrogen gas and with a mixture of hydrogen and helium, (1:10). Threshold energies for the different vibrational levels of H_2^+ are also shown. (Sen et al, 1985).

It is intended to install this source in the MEIBE apparatus and to use it to investigate $H_2^+(v=0,1)$ and $H_2^+(v=0,1,2)$ recombination. In particular it will be interesting to see if the Franck-Condon signature on the collision cross section will be observed, i.e. a deviation from a simple E^{-1} dependance.

Another experiment which is especially important to our understanding of the relative roles of direct and indirect recombination is the search for the predicted resonances in the cross section. Auerbach et al (1977) apparently observed a rich structure in the cross section. Subsequent experiments however, D'Angelo 1979, Ng 1982, Sen 1985, have failed to reproduce the earlier results although in fact some structure is visible in their data.

Currently the energy resolution of the MEIBE apparatus is estimated to be ~40 meV and this is due mainly to electrons leaving the cathode with transverse thermal velocities. Since they are travelling in an axial magnetic field, they perform a spiralling motion with a diameter given by $(D = 67.4V_{\perp}^{\frac{1}{2}}/B)$mm and a pitch of $(212V_{\perp\perp}^{\frac{1}{2}}/B)$mm (B in Gauss, $V_{\perp}$ and $V_{\perp\perp}$ are kinetic energies associated with perpendicular and parallel velocities, in eV) Taylor et al (1974). Given the operating conditions of MEIBE I this translates to ~2 mm and ~8cms respectively.

Because of the spiralling it is possible for electrons with large transverse velocities to wriggle through thin, small apertures and so remain in the beam. Plans are underway to build a new electron gun with thick diaphragms with small diameter/length ratios which will trap spiralling electrons allowing axially moving electrons to pass unhindered. Such guns have been designed and used in H. Brongersma's laboratory (Private Communication 1985).

This should greatly improve the resolution of the MEIBE apparatus. With good resolution and well defined ion beams the search for the resonances stands a much better chance for success.

H_3^+ Studies

The simplest polyatomic ion is of course H_3^+ which is a major component of hydrogen plasmas. In fact when molecular hydrogen gas is ionized to form H_2^+, the reaction

$$H_2^+ + H_2 \rightarrow H_3^+ + H$$

rapidly displaces the H_2^+ ion.

Several experimental measurements of the dissociative recombination of H_3^+ have been performed. Leu et al (1973), Peart & Dolder (1974b), Auerbach et al 1977, MacDonald et al (1984) Mathur et al (1978) and Mitchell et al (1984). There is fairly good agreement about the general nature of the cross section as measured in these experiments. The most recent study however Smith et al (1984), Adams et al (1984) performed using the FALP technique has indicated that in fact H_3^+ has a cross section much smaller than previously measured. This finding agrees with theoretical predictions concerning H_3^+. In particular Michels & Hobbs (1984) have found that not only does H_3^+ not have a suitable curve crossing for the direct dissociative recombination of ground state ions, it does not have a large probability for indirect recombination either (Fig. 13). This apparent agreement between theory and experiment has caused a considerable stir particularly because of the great importance of H_3^+ recombination.

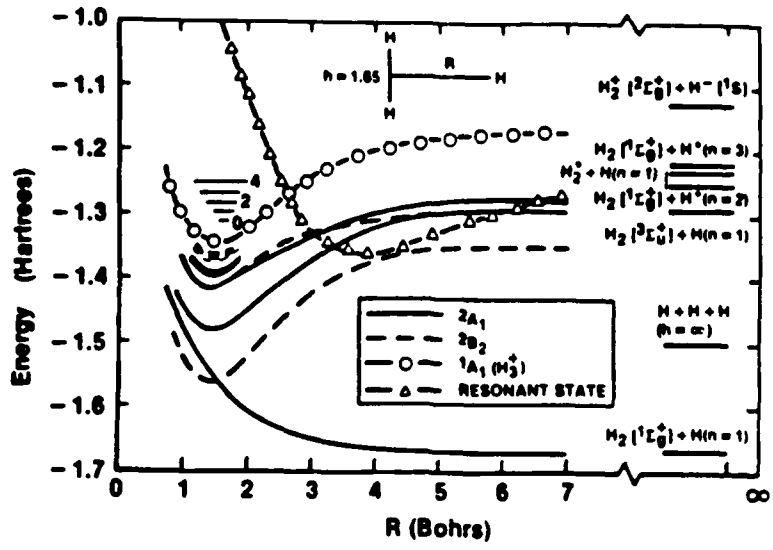

Fig. 13 Potential energy curves for H_3^+ and H_3 showing the intersection with the dissociative curve responsible for e-H_3^+ recombination. (Michels and Hobbs, 1984).

Plans at U.W.O.

Sen and Mitchell (1985) have demonstrated that H_3^+ ions with very small internal energies can be produced using the rf storage ion source. This source will again be used with the MEIBE I apparatus to re-examine the e+H_3^+ cross section. The wide energy range available with the merged beam technique should allow a definitive measurement to be made. The cross section may indeed be small at low energies but for E_{cm}>1.0eV it should be observed to rise to much larger values as the crossing states become accessible. This experiment should be performed within the coming year.

BRANCHING RATIOS FOR DECAY CHANNELS

Much of the modelling of interstellar chemistry relies on having a clear understanding of the branching ratios for the various decay channels following the dissociative recombination of polyatomic molecular ions. Until recently however very little information has been available on this subject. Modelling of processes occurring during the pulse radiolysis of methane and acetylene have allowed estimates of the main decay channels for the dissociative recombination of CH_4^+ and $C_2H_2^+$ to be obtained. (Rebbert et al. 1972, 1973a,b). On the theoretical side, Herbst (1978) has used a statistical phase space theory to predict branching ratios for $HCNH^+$, H_3O^+, CH_3^+ and NH_4^+ while Kulander and Guest (1979) have studied the decay of H_3^+ following recombination.

In 1983 the first direct measurements of the branching ratio for a polyatomic ion recombination were made using the MEIBE I apparatus at the University of Western Ontario, (Mitchell et al 1983). The process studied was:

$$e + H_3^+ \rightarrow H + H + H \text{ --- I}$$

$$\rightarrow H_2 + H \text{ --- II}$$

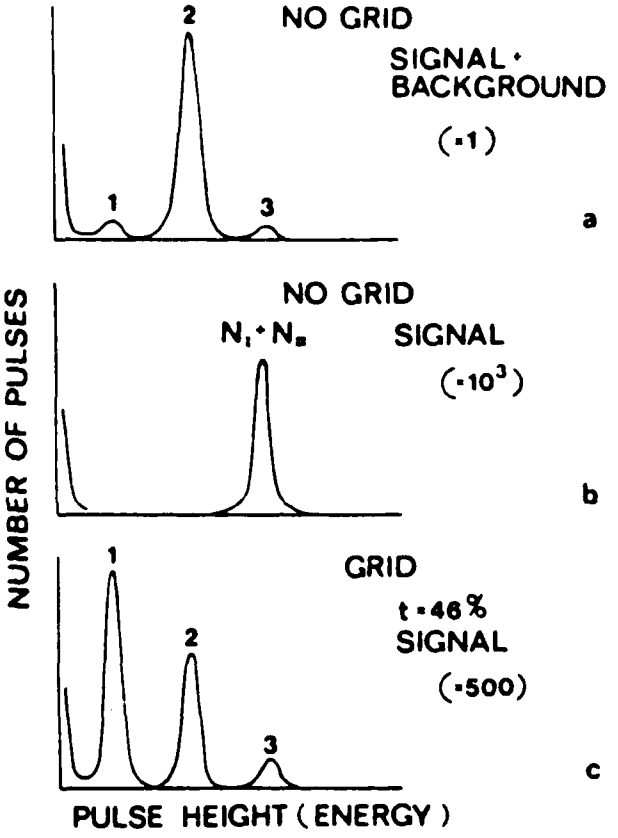

Fig. 14 Pulse height distributions of detector pulses for

(a) H_3^+ beam, no grid, signal plus background.
(b) no grid, signal only
(c) 46% transmission grid, signal only.

To understand the measurement it is necessary to understand the response of a surface barrier detector to dissociation products. When H_3^+ dissociates, its kinetic energy is shared among the dissociation products according to their mass. Therefore a 300 KeV H_3^+ ion will give rise to three hydrogen atoms each with 100 KeV or a 200 KeV H_2 molecule and a 100 KeV H atom. Since all the products arrive at the detector essentially simultaneously, they yield the same pulse height as a single 300 KeV particle. Hence under normal circumstances channels I and II are indistinguishable. Fig. (14) shows the output from the surface barrier detector for H_3^+ in the MEIBE apparatus. The peaks coresponding to 100 and 200 and 300 KeV particles are populated by neutrals arising from interactions with the background gas:

$$H_3^+ + X \rightarrow H + H_2^+ + X$$

$$H_3^+ + X \rightarrow (H + H) + H^+ + X$$

$$H_3^+ + X \rightarrow (H + H) + H + X^+$$

The 300 KeV peak at low centre of mass energy will also contain a contribution due to dissociative recombination. At higher centre of mass energies, the 100 and 200 KeV peaks will contain contributions from dissociative excitation. (See later). Background signals are separated from electron-ion signals by modulating the electron beam and counting neutrals in and out of phase with the modulation.

If a metallic grid of known transmission probability t is placed in front of the detector, then the probability of two particles traversing the grid is proportional to t^2 and of three particles to t^3. Taking account of the probability for a particle not to pass through the grid being 1-t then it is easily shown that the number of counts in each of the channels is given by

$$N_{100} = 3t(1-t)^2N_I + t(1-t)N_{II}$$

$$N_{200} = 3t^2(1-t)N_I + t(1-t)N_{II}$$

$$N_{300} = t^3N_I + t^2N_{II}$$

where N_I and N_{II} are the number of recombination events decaying to channel I and II respectively. By using single channel analysers, N_{100}, N_{200} and N_{300} can be individually determined and so N_I and N_{II} can be found by solving these equations. Hence the partial cross sections for recombination to channel I and II can be calculated separately. Fig. (15) shows the results that were obtained using H_3^+ ions that were produced in an rf ion source. It has been estimated using a model by Blakely et al (1977) that only 35% of these ions were in the ground state. It can be seen that over the measured energy range, channel I dominates channel II by about a factor of 2:1. Kulander and Guest (1978) predicted that for ground vibrational state H_3^+ and low electron energies only channel I is available for decay. For H_3^+ ions with more than 1 eV

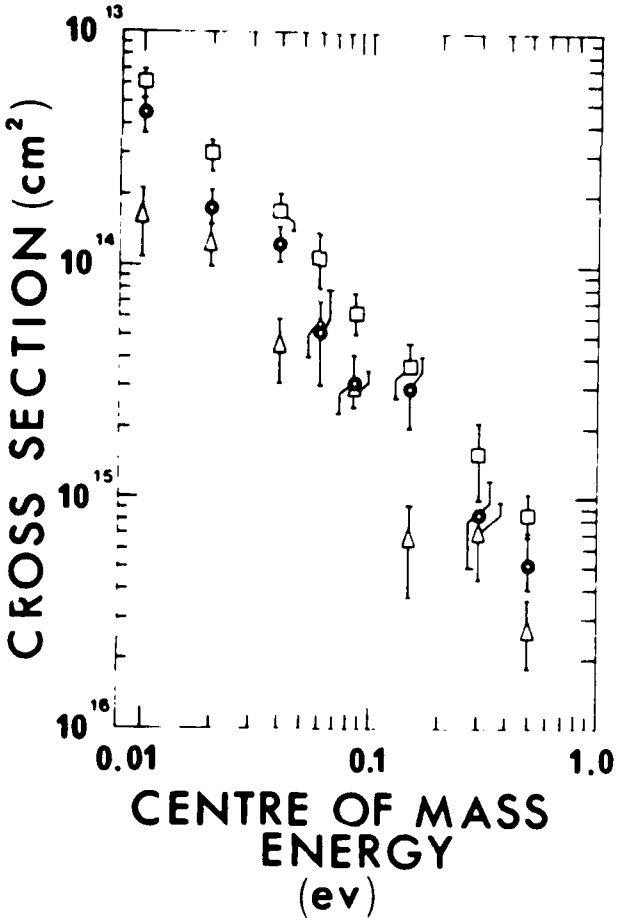

Fig. 15 Cross sections for the dissociative recombination of H_3^+ + e leading to H+H+H (circles) and to H_2+H (triangles). Total cross section also shown, (squares). (Mitchell et al, 1983).

of internal energy then channel II should dominate. Thus given that the ions used in this study had a range of internal energies, there is qualitative agreement between the experimental and theoretical studies.

It will be particularly interesting to repeat these studies using ground state H_3^+ ions from the Teloy source.

Further details concerning this technique together with the analysis for more complex triatomic ions such as H_2D^+ or HD_2^+ has been published recently. (Forand et al 1985).

DISSOCIATIVE EXCITATION

Peart and Dolder (1974c, 1975b) have studied the electron impact dissociation or dissociative excitation of H_3^+ and by comparing the experimentally measured threshold for this reaction with the theoretical predicted threshold, they concluded that their H_3^+ ions were de-excited. Their results are shown in fig. (17). This is a very useful measurement as it employs exactly the same experimental configuration as that used for the dissociative recombination measurement. Peart and Dolder examined the reaction

$$e + H_3^+ \rightarrow H^+ + (H + H) + e$$

They did not have sufficient energy resolution in their detector to allow the other dissociation process:

$$e + H_3^+ \rightarrow H + H_2^+ + e$$

to be examined. The measurement was performed by counting the H_2 molecules or pairs of H atoms resulting from the dissociation. This is done by using a single channel analyser to select out the $H_2/2H$ channel from the pulse height distribution [see Fig. (14)].

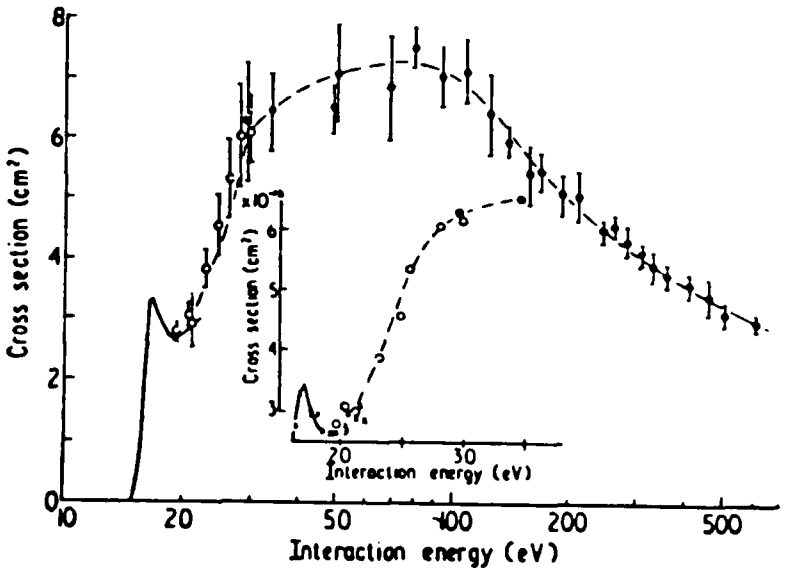

Fig. 16 Measured cross sections for the production of protons by collisions between electrons and H_3^+ ions. (Peart and Dolder 1974c, 1975b).

The main source of error in the interpretation of the results lies in the accuracy of the theoretical prediction for the threshold.

Dissociative excitation proceeds via an electronic transition from a bound electronic state of the ion to an excited repulsive state. Usually the initial state is the ground electronic state which may be vibrationally or rotationally excited.

For H_3^+ this state represents a configuration where in equilibrium the three hydrogen atoms are located at the vertices of an equilateral triangle of side 1.65 - 1.66 Bohr. The total energy of this state, below the threshold for dissociation to $H^+ + H^+ + H^+$, is estimated to be -1.34 to -1.35 Hartrees (-36.46 to -36.72 eV) (Kawaoka and Borkman 1971). The vibrational levels of this state have been calculated by Carney and Porter (1976), Carney (1980).

H_3^+ can also exist in excited triangular or linear configurations. We shall neglect the latter for the purposes of the following discussion. The molecule can vibrate either symmetrically or assymmetrically and in these modes it will remain invariant under a number of symmetry operations. (Reflection about axis, rotation etc.) For a full discussion see for example Herzberg (1966), Bright Wilson et al (1955). Group theory can be used to describe molecules in particular conditions which display sets of vibrational modes characteristic of those conditions.

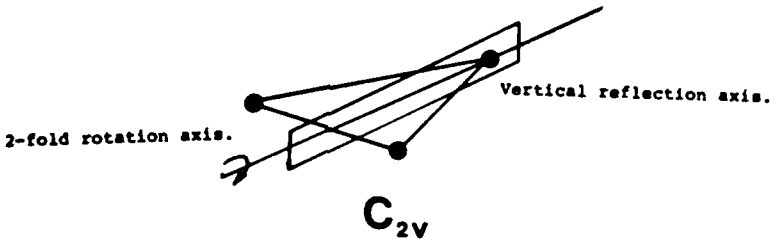

Fig. 17a C_{2v} symmetry group.

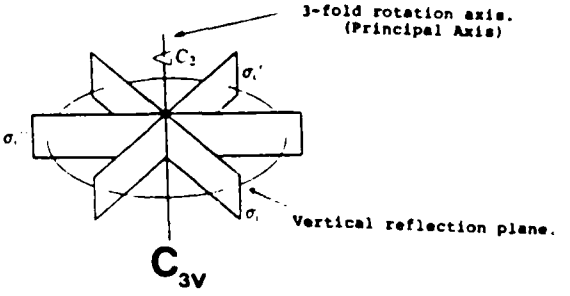

C_{3v}

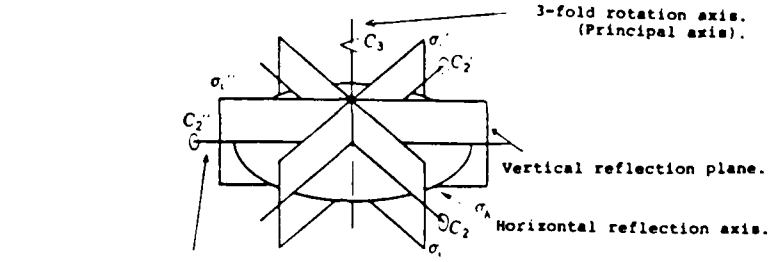

D_{3h}

Fig. 17b C_{3v} and D_{3h} symmetry groups.

Thus for H_3^+ vibrating in an asymmetric (or isoceles) mode, it can be described via the C_{2v} symmetry group. See Fig. (17). H_3^+ vibrating in a symmetrical (equilateral) mode is described by D_{3h} symmetry. Now it should be noticed that these two symmetry groups are not isolated from each other, they do overlap. They are said to be degenerate. A molecule which is vibrating in an asymmetric fashion does pass through a configuration in which it is equilateral [see Fig. (18)].

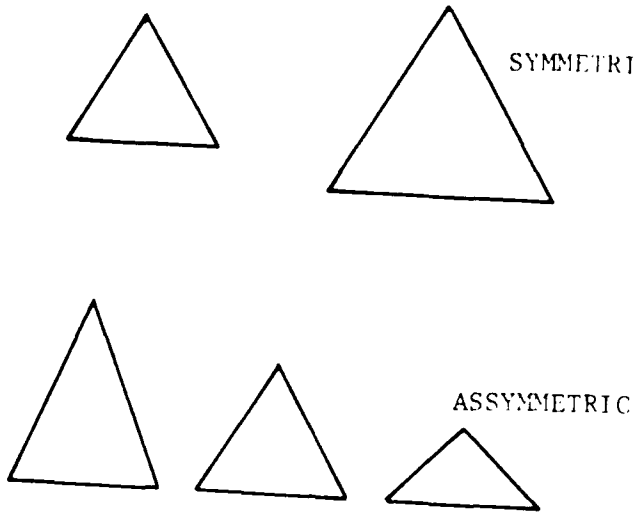

Fig. 18 Vibrational modes for a triangular molecule.

H_3^+ in a D_{3h} configuration has electronic states designated as follows:

$$A_1', A_1'', A_2', A_2'', E', E''$$

which can be either singlet or triplet. E states are degenerate. Possible electronic states in the more restricted C_{2v} symmetry are designated:

$$A_1, A_2, B_1, B_2$$

again singlet or triplet.

Because D_{3h} and C_{2v} symmetries are degenerate under some configurations then there are equivalences between these states. These are shown in Table (II).

D_{3h}	C_{2v}
A_1'	A_1
A_2'	B_2
E'	A_1, B_2
A_1''	A_2
A_2''	B_1
E''	A_2, B_1

The final and perhaps most important point to make here is that a symmetrical vibrational mode will go to an asymptotic dissociation limit of:

$$H + H + H^+$$

while an asymmetric vibration will yield

$$H + H_2^+$$

or $$H_2 + H^+$$

A number of calculations of the potential energy surfaces for H_3^+ have been performed. Fig. (19) shows the results of Kawaoka and Borkman (1971) who calculated the energies of the ground $^1A_1$ and excited states in D_{3h} symmetry. R is the internuclear separation which for an equilateral configuration is independant of which atoms are examined. Of course it is also possible for the atoms to move asymmetrically and so the energies of these states should also be calculated in C_{2v} symmetry as well. This has been done by Conroy (1969) and by Bauschlicher et al 1973.

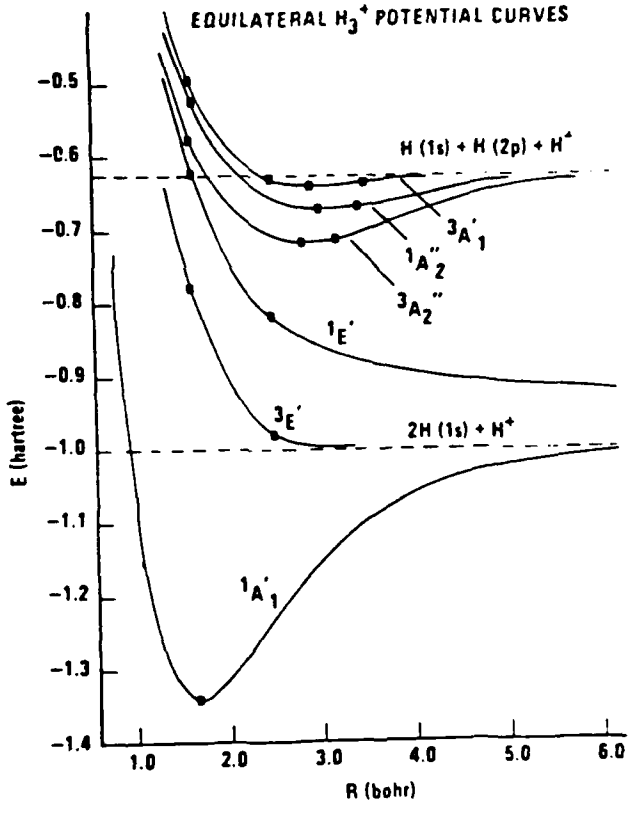

Fig. .. ...ential energy curves for the ground and excited states of H_3^+ in D_{3h} symmetry. (Kawaoka and Borkman, 1971).

For example the lowest $^1E'$ state of Kawaoka and Borkman (1971) translates to $^1A_1$ and $^1B_2$ states in C_{2v} symmetry. The $^1A_1$ state is shown in fig. (21). Note the difference in the meanings of r and R which are explained in the diagram. It can be seen that when R is large, the $^1A_1$ state is bound with respect to dissociation of the H_A, H_B pair. In this case the third hydrogen atom Hc is essentially separate so that the molecule is really a complex of H_2^+ + H. As H_C approaches the other two however, the potential energy of the minimum rises until in the equilateral configuration the state is unbound. At this point the $^1A_1$ state in C_{2v} and the $^1E'$ state in D_{3h} are essentially the same state. The situation is perhaps more clearly seen in Fig. (21) which shows three dimensional plots of the ground and excited $^1A_1$ states. (Bauschlicher et al 1973).

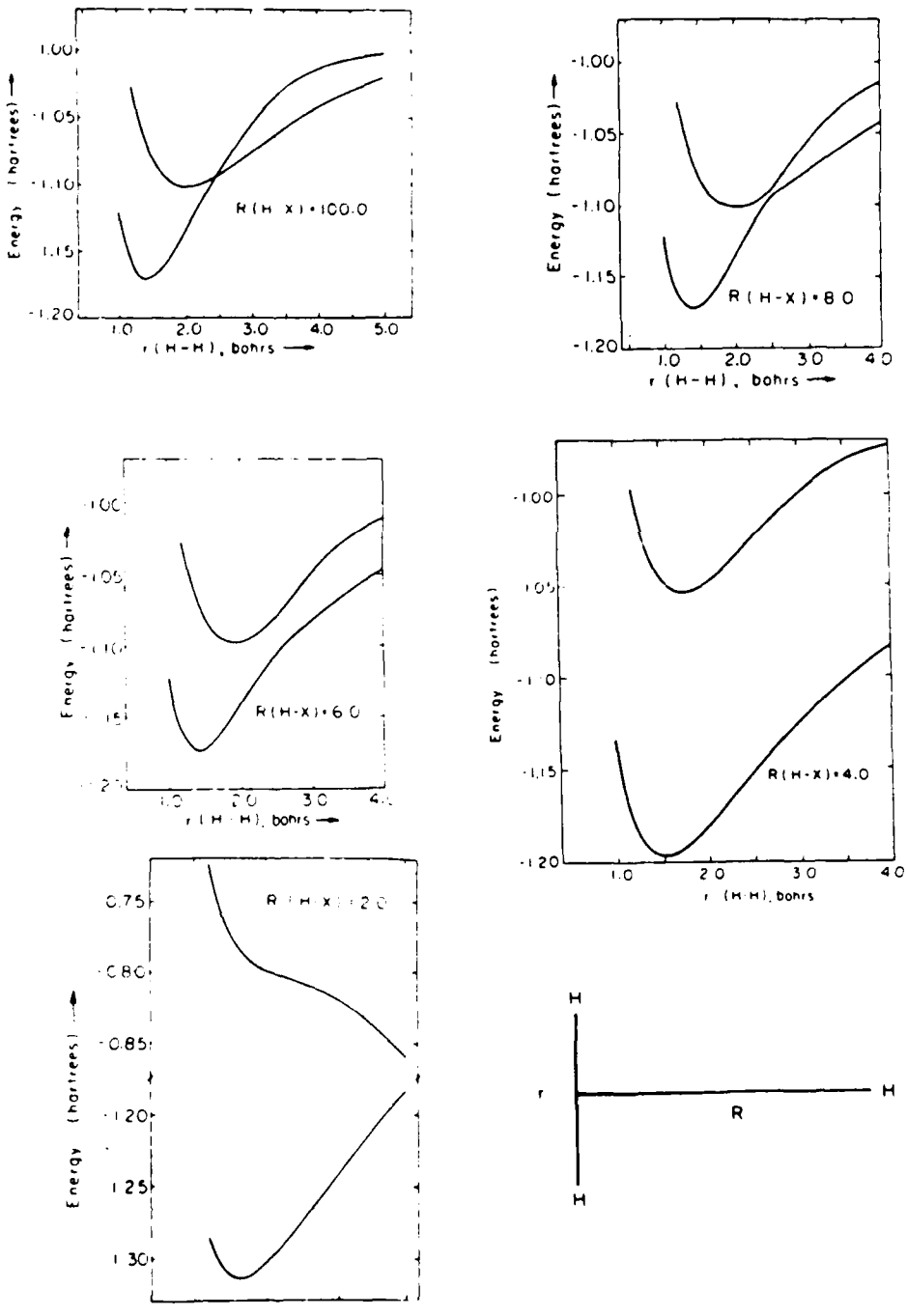

Fig. 20 Potential energy curves for the ground and excited $^1A_1$ states of H_3^+. (Bauschlicher et al, 1973).

For the $^1B_2$ component, Conroy (1969) has shown that this is weakly stable with respect to dissociation to $H_2^+(^2\Sigma_g)$ + H(2p) and less so to $H_2(^1\Sigma_u)$ + H^+. Fig. (22). The H_2 ($^1\Sigma_u$) state is however repulsive so it in turn would dissociate to H(1S) + H(1S). The $^1B_2$ component is unstable with respect to dissociation to $H_2^+(^2\Sigma_u)$ + H(1S) but again the H_2^+ state is unstable and will further dissociate to H(1S) + H^+. Hence all transitions leading to the $^1B_2$ component are likely to give rise to dissociation via the H + H + H^+ channel.

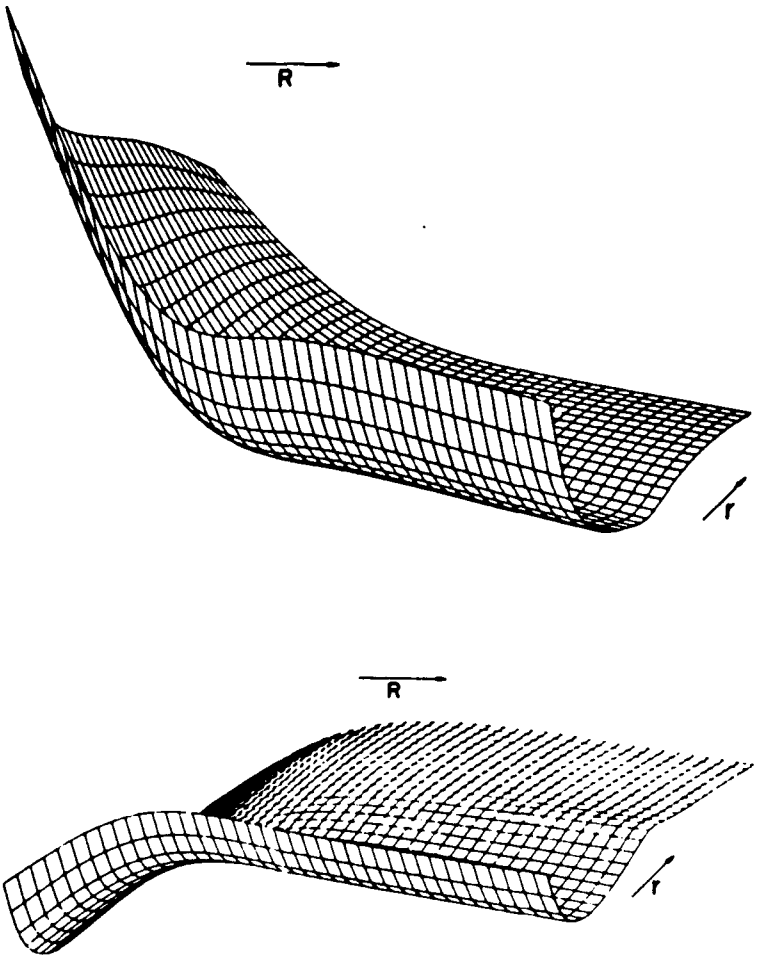

Fig. 21 Perspective plots of the lowest and first excited $^1A_1$ states of H_3^+. (Bauschlicher et al, 1973).

Now let us consider the case of electron impact on H_3^+. The case for photon impact has been examined by Kulander and Bottcher (1978). Electronic transitions between these two states occur in a time very much less than typical vibrational periods so that such transitions occur vertically i.e. they are Franck-Condon transitions. Thus from Fig. (19) it can be seen that an energy of ~19 eV is required for an H_3^+ ion in its electronic and vibrational ground state (symmetrical) to be excited to the $^1E'$ state. Note this energy takes account of the energy of the ground vibrational level above the minimum of the $^1A_1{}'$ ground state (0.54 eV - Carney and Porter 1976).

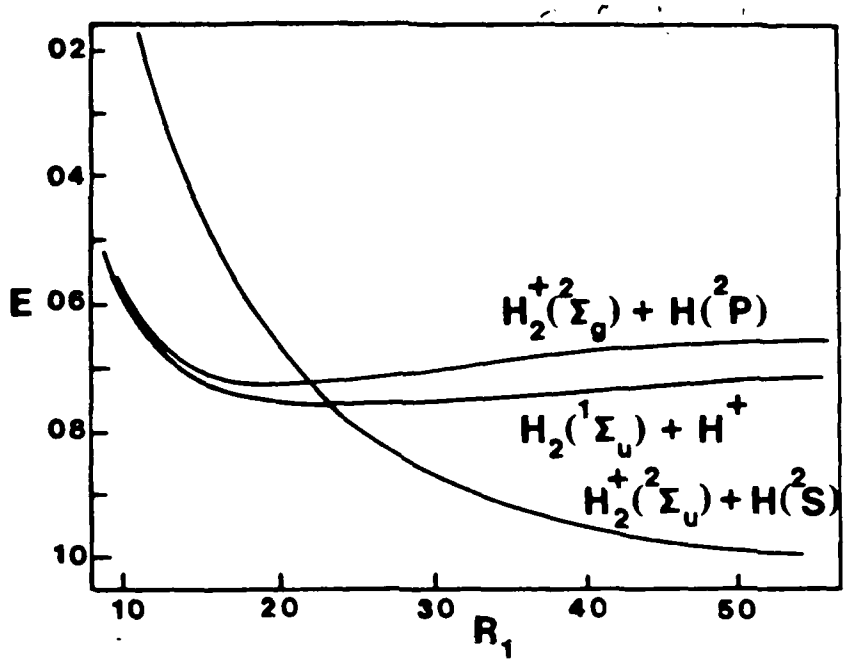

Fig. 22. Potential energy curves for the $^1B_2$ states of H_3^+. (Conroy, 1969).

Once excited then the molecule can either dissociate into H + H + H^+, i.e. R and r → ∞ or into H_2^+ + H, R → ∞, r remains finite. Kulander and Bottcher (1978) point out that there is a ridge on the $^1E'$ ($^1A_1$) surface which tends to make the H + H + H^+ channel more favoured provided the initial H_3^+ ion is not too excited. Their calculation treated the states adiabatically so that an avoided crossing occurs leading to the distortion of the potential surface. A subsequent calculation, Kulander and Heller (1978) used diabatic states so that no avoided crossing occurred. This means that dissociation of H_2^+ + H might then be favoured due to the steeper gradient. Which of these two scenarios is more accurate is not yet known due to lack of experimental evidence.

Dipole allowed transitions involve transitions between states with similar spins and so a transition to the $^3E'$ state Fig. (19) is forbidden for photon impact. For electron impact however, exchange of the projectile and target electrons will permit such a transition to occur. In C_{2v} symmetry, this state translates to $^3A_1$ and $^3B_2$ states. These states dissociate to $H_2^+(^2\Sigma_g^+)$ + H(1S) and to $H_2^+(^2\Sigma_u^+)$ + H(1S) respectively, the latter dissociating further to H^+ + H(1s) + H(1s). In its symmetric $^3E'$ form it dissociates to H(1s) + H(1s) + H^+.

For transitions from the ground vibrational state of H_3^+ the energy required to reach the $^3E'$ state is 14.76eV. [Kawaoka & Borkman (1971), Carney & Porter (1976)].

An interesting feature of the dissociative excitation of H_3^+ is the fact that exchange processes are only effective over a narrow energy range and so the transition to the $^3E'$ state appears as a narrow peak in the cross section at threshold. See Fig. (16). The transition to the $^1E'$ state however is allowed and so it rises to broad maximum far above the transition threshold.

Acknowledgements

I should like to acknowledge the many useful discussions which I have had with Bill McGowan, Norman Bardsley, Tom O'Malley, Chris Bottcher, Anik Giusti-Suzor, Ken Kulander and Harvey Michels. The assistance of co-workers listed in the references has been highly valued. Special thanks are also due to the Canadian National Science and Engineering Research Council, the U.S. Department of Energy and the U.S. Air Force Office of Scientific Research for their support of the merged beam program at U.W.O.

References

1. N.G. Adams, D. Smith and E. Alge. J. Chem. Phys. 81, 1778, 1984.
2. E. Alge, N.G. Adams and D. Smith. J. Phys. B, 16, 1433, 1983.
3. D. Auerbach, R. Cacak, R. Caudano, T.D. Gaily, C.J. Keyser, J. Wm. McGowan, J.B.A. Mitchell, S.F.J. Wilk. J. Phys. B. 10, 3797, 1977.
4. J.N. Bardsley and M.A. Biondi. Adv. At. Mol. Phys. (eds. D.R. Bates and I. Estermann). Vol. 6. Academic Press, NY, 1970, p.1.
5. J.N. Bardsley. Symp. Electron-Molecule Collisions. Invited Papers (ed. I. Shimamura and M. Matsuzawa) (U. of Tokyo, 1979), p.121.
6. J.N. Bardsley, J. Phys. B, 1, 349, 1968.
7. J.N. Bardsley, J. Phys. B, 1 365, 1968.
8. D.R. Bates and H.S.W. Massey, Proc. Roy. Soc. A192, 1, 1947.
9. E. Bauer and T.Y. Wu, Can. J. Phys. 34, 1436, 1956.
10. C.W. Bauschlicher, S.W. O'Neill, R.K. Preston, H.F. Schaefer III and C.F. Bender. J. Chem. Phys. 59, 1286, 1973.
11. R.S. Berry and S. Leach. Adv. Electron. Electron Phys. 57 1, 1981.
12. C.R. Blakeley, M.L. Vestal and J.H. Futrell, J. Chem. Phys. 66, 2392, 1977.
13. C. Bottcher and K. Docken, J. Phys. B. 7, L5, 1974.
14. C. Bottcher. J. Phys. B, 9, 2899, 1976.
15. E. Bright-Wilson, J.C. Derius and P.C. Cross. Molecular Vibrations Dover Pub. Inc., New York, 1955.

16. N.A. Burdett and A.N. Hayhurst. Comb. Flame 34, 119, 1979.
17. F. Brouillard and W. Claeys in Physics of Ion-Ion and Electron Ion Collisions (eds. F. Brouillard and J. Wm. McGowan), (NATO ASI, Baddeck, Nova Scotia), Plenum, NY. p.415, 1983.
18. G.D. Carney and R.H. Porter. J. Chem. Phys. 65, 3547, 1976.
19. G.D. Carney. Mol. Phys. 39, 923, 1980.
20. A. Carrington and R.A. Kennedy. J. Chem. Phys. 81, 91, 1984.
21. H. Conroy. J. Chem. Phys. 51, 3979, 1969.
22. W.A. Chupka and M.E. Russell. J. Chem. Phys. 49, 5426, 1968.
23. A.J. Cunningham and R.M. Hobson. J. Res. NBS A76, 329, 1972.
24. V. D'Angelo. MSc Thesis, University of Western Ontario, 1979.
25. C. Derkits, J.N. Bardsley and J.M. Wadehra. J. Phys. B, 12, L529, 1979.
26. P.M. Dehmer and W.A. Chupka. J. Chem. Phys. 65, 2243, 1976.
27. K.T. Dolder in Case Studies in Atomic Collision Physics, Vol. 1 (ed. E.W. McDaniel and M.R.C. McDowell) (North-Holland, Amsterdam) p.249, 1969.
28. A.V. Eletskii and B.M. Smirnov. Sov. Phys. Usp. 25, 13, 1982.
29. U. Fano. Phys. Rev. 124, 1866, 1961.
30. L. Forand, J.B.A. Mitchell and J. Wm. McGowan. J. Phys. E, 18, 623, 1985.
31. S.L. Guberman. J. Chem Phys. 78, 1404, 1983.
32. S.L. Guberman, in Physics of Ion-Ion and Electron-Ion Collisions (eds. F. Brouillard and J. Wm. McGowan) (NATO ASI Baddeck, Nova Scotia), Plenum New York, p.167, 1981.
33. A. Giusti. J. Phys. B, 13, 3867, 1980.
34. A. Giusti-Suzor, J.N. Bardsley and C. Derkits. Phys. Rev. A, 28, 682, 1983.
35. M.F.A. Harrison. Brit. J. Appl. Phys. 17, 371, 1966.
36. A.N. Hayhurst and N.R. Telford. Proc. Roy. Soc. A322, 1999, 1974.
37. A. Hazi. Phys. Rev. A27, 1751, 1983.
38. E. Herbst. Ap. J. 222, 508, 1978.
39. G. Herzberg. Electronic Spectra of Polyatomic Molecules. Van Nostrand Reinhold Co., New York, 1966.
40. K. Kawaoka and R.F. Borkman. J. Chem. Phys. 54, 4234, 1971.
41. C.J. Keyser, H.R. Proelich, J.B.A. Mitchell and J.Wm. McGowan, J. Phys. E12, 316, 1979.
42. K.C. Kulander and C. Bottcher. Chem Phys. 29, 141, 1978.
43. K.C. Kulander and E.J. Heller. J. Chem. Phys. 69, 2439, 1978.
44. K.C. Kulander and M.F. Guest. J. Phys. B, 12, L501, 1979.
45. M.T. Leu, M.A. Biondi and R. Johnsen. Phys. Rev. A8, 413, 1973.
46. B.A. Lippman and T.F. O'Malley. Phys. Rev. A2, 2115, 1970.
47. J. MacDonald, M.A. Biondi and R. Johnsen. Planet. Space Sci. 32, 651, 1984.
48. T. Maruyama, Y. Ichikawa, R.M. Hobson, S. Teii, T. Kaneda and J.S. Chang. IEE, Japan. Proc. Symp. 2, 1, 1981.
49. H.N. Maier and R.W. Fessenden. J. Chem. Phys. 62, 4790, 1975.
50. D. Mathur, S.U. Khan and J.B. Hasted. J. Phys. B11, 3615, 1978.
51. F.J. Mehr and M.A. Biondi. Phys. Rev. 181, 264, 1969.
52. J. Wm. McGowan and J.B.A. Mitchell, in Electron-Molecule Interactions and their Applications, Vol.II, ed. L.G. Christophoron. Academic Press, NY, 1984.
53. H.H. Michels, in The Excited State in Chemical Physics. Adv. Chem. Phys., Vol.XLV (ed. J. Wm. McGowan), Wiley Interscience, NY, p.225, 1975.
54. H.H. Michels and R.H. Hobbs. Ap. J. 286, L27, 1984.

55. J.B.A. Mitchell, J.F. Forand, C.T. Ng, D.P. Levac, R.E. Mitchell, P.M. Mul, W. Claeys, A. Sen and J. Wm. McGowan. Phys. Rev. Lett. 51, 885, 1983.
56. J.B.A. Mitchell and J. Wm. McGowan, in Physics of Ion-Ion and Electron-Ion Collisions (eds. F. Brouillard and J. Wm. McGowan) (NATO ASI, Baddeck, Nova Scotia), Plenum, New York, p.279, 1983.
57. J.B.A. Mitchell, C.T. Ng, L. Forand, R. Janssen and J. Wm. McGowan. J. Phys. B, 17, L909, 1984.
58. C.T. Ng. MSc Thesis, University of Western Ontario, 1982.
59. T.F. O'Malley, Phys. Rev. 150, 14, 1966.
60. T.F. O'Malley, J. Chem. Phys. 61, 322, 1969.
61. T.F. O'Malley in Adv. At. Mol. Phys., Vol.7 (Eds. D.R. Bates and I. Estermann), Academic Press, NY, p.223, 1971.
62. T.F. O'Malley, J. Phys. B, 14, 1229, 1981.
63. H.J. Oskam and V.R. Mittelstadt. Phys. Rev. 132, 1445, 1963.
64. B. Peart and K.T. Dolder. J. Phys. B, 6, L359, 1973.
65. B. Peart and K.T. Dolder. J. Phys. B, 7, 236, 1974a.
66. B. Peart and K.T. Dolder. J. Phys. B, 7, 1948, 1974b.
67. B. Peart and K.T. Dolder, J. Phys. B, 7, 1567, 1974c.
68. B. Peart and K.T. Dolder. J. Phys. B, 8, 1570, 1975a.
69. B. Peart and K.T. Dolder. J. Phys. B, 8, L143, 1975b.
70. R.A. Phaneuf, D.H. Crandall and G.H. Dunn. Phys. Rev. A11, 1983, 1975.
71. K. Rai Dastidar and T.K. Rai Dastidar. J. Phys. Soc. Japan, 46, 1288, 1979.
72. R.E. Rebbert and P. Ausloos. J. Res. NBS A76, 329, 1972.
73. R.E. Rebbert and P. Ausloos. J. Res. NBS A77, 109, 1973.
74. R.E. Rebbert, S.G. Lias and P. Ausloos. J. Res. NBS A77, 249, 1973.
75. I. Schneider, I.N. Mihailescu, L. Nanu and I Iovil-Popescu. J. Phys. B18, 791, 1985.
76. A. Sen, J.B.A. Mitchell and J. Wm. McGowan. Abstracts of Papers, XIV, ICPEAC, 1985, p.667.
77. A. Sen and J.B.A. Mitchell. Abstracts of Papers XIV ICPEAC, 1985, p.600.
78. A. Sen. Ph.D. Thesis, University of Western Ontario, 1985.
79. Y.J. Shiu, M.A. Biondi and D.P. Sipler. Phys. Rev. A15, 494, 1977a.
80. Y.J. Shiu and M.A. Biondi. Phys. Rev. A16, 1817, 1977b.
81. Y.J. Shiu and M.A. Biondi. Phys. Rev. A17, 868, 1978.
82. D. Smith and N.G. Adams in Physics of Ion-Ion and Electron-Ion Collisions (eds. F. Brouillard and J. Wm. McGowan) (NATO ASI, Baddeck, Nova Scotia), Plenum, NY, p.501, 1983.
83. D. Smith and N.G. Adams. Ap. J. 284, L13, 1984.
84. P.O. Taylor, K.T. Dolder, W.E. Kauppila and G.H. Dunn. Rev. Sci. Inst. 45, 538, 1974.
85. E. Teloy and D. Gehrlich. Chem. Phys. 4, 417, 1974.
86. M. Vogler and G.H. Dunn. Phys. Rev. A11, 1983, 1975.
87. F. Von Busch and G.H. Dunn. Phys. Rev. A5, 1726, 1972.
88. J. Von Neumann and E.P. Wigner. Phys. Z. 30, 467, 1929.
89. F.L. Walls and G.H. Dunn. J. Geophys. Res. 79, 1911, 1974.
90. R.L. Wilkins. J. Chem. Phys. 44, 1884, 1966.
91. E. Zipf. J. Geophys. Res. 85, 4232, 1980a.
92. E. Zipf. Geophys. Res. Lett. 7, 645, 1980b.
93. V.P. Zhdanov and M.I. Chibisov. Sov. Phys. JETP 47, 38, 1978.
94. V.P. Zhdanov. J. Phys. B, 13, L311, 1980.

PHYSICS

The University of

Western Ontario